Iowa State University
Electric Power Research Center

Fifty-Sixth Annual Report

of the

Electric Power Research Center

May 2019

For more information:
Phone: 515-294-7678
FAX: 515-294-4263
e-mail: akimber@iastate.edu

IOWA STATE UNIVERSITY
Electric Power Research Center

1111 Coover Hall
Ames, IA 50011-3060
515-294-7678
FAX: 515-294-4263

Table of Contents

EPRC 56th Annual Meeting May 21-23, 2019

Research Reports

Poster Abstracts

IOWA STATE UNIVERSITY
Electric Power Research Center

1111 Coover Hall, Ames, IA 50011
Anne Kimber, Director
akimber@iastate.edu
515-294-7678
515-291-4378 (cell)

Electric Power Research Center (EPRC)

Overview: EPRC is a catalyst for collaboration among ISU faculty, the power industry, state agencies, national labs, federal agencies and national trade associations, on research and technology transfer to solve the most challenging problems of the electric grid. EPRC power industry members jointly select and fund projects of common interest to the group. EPRC and members also participate in DOE and NSF grants, as well as grants from non-profits and state agencies.

History: EPRC began in 1963 as the Power Affiliate Research Program, founded to advance education and research in electric power systems, and strengthen industry ties to the ISU power program.

Governance and Budget: EPRC is advised by a Technical Advisory Committee (TAC) of industry members. Its budget comes from member fees, grants and continuing education courses. Funds are used primarily to fund graduate student research and develop professional education for technology transfer.

Meetings: EPRC meets with its members twice a year to provide research updates and choose new projects.

Membership: Full Membership is an annual contribution of $25,000 or more and allows the member to appoint a representative to the TAC with one full vote per $25,000 block. A Contributing Membership level is flexible, typically at least $5,000. A Contributing Member has a representative at the TAC meetings and has a fractional vote proportional to their level of contribution.

Current Members: EPRC has nine industry members: Alliant Energy, the Central Iowa Power Cooperative, the City of Ames, the City of Bloomfield, the City of Cedar Falls, Corn Belt Power Cooperative, ITC Midwest, MidAmerican Energy, and the Midcontinent Independent System Operator (MISO).

Research teams: include faculty from Electrical and Computer Engineering (power engineering and cyber security), Industrial and Manufacturing Systems Engineering, Materials Science and Engineering, Mechanical Engineering, Civil, Construction and Environmental Engineering, Statistics, Economics, and Geological and Atmospheric Sciences. Industry advisors participate in developing and reviewing projects.

Research topics: Research reflects challenges arising from a rapidly changing power industry and changes in standards and markets. Recent projects include development of new tools to improve grid reliability and security, optimization of generation resource planning focusing on renewable integration, studies of risk management in wholesale and retail power markets, improvement of meteorological models for wind forecasting, design of new aluminum composite conductor, the impact of smart grid developments on markets and transmission planning, development of condition-based maintenance tools, and resiliency planning for distribution systems.

EPRC-funded Projects 2010-2019

Power System Operation and Planning

2010-2011	Generation Expansion Planning: Portfolio Optimization
2010-2012	Analysis of very low frequency oscillations
2010-2011	Optimal allocation of dynamic VAR sources for enhancing power system dynamic security
2010-2011	Embedded sensor network and decision algorithms for robust power system
2011-2013	Optimal online control strategies to maintain high voltage security in large scale power systems
2012-2014	Measuring stress across an area of a power system with area angles
2013-2015	PMU-based real time short term stability monitoring transmission planning and defense plans
2014-2016	Fast monitoring of voltage collapse and cascading outages with PMUs
2015-2017	Opportunities and Benefits for Deploying VSC-Based HVDC
2015-2017	Development of integrated software to study impact of distributed generation on grid reliability
2015-2018	Real-time monitoring and control of long-term voltage stability with high wind penetration via local linear regression
2016-2018	Power Grid Resilience: Assessment, Enhancement and Outage Management

Ongoing projects FY19

2015-2019	*Assessing the impacts of geomagnetic disturbances on Midwest transmission system reliability*
2017-2019	*Impacts of power transformer overload ratings on transformer reliability and life*
2018-2019	*Coordinating Conventional Voltage Control Devices with Smart Inverters in Rural Distribution Networks with DER Penetration.*
2018-2019	*High-Fidelity Performance/Degradation Modelling of Utility-Scale Battery Energy Storage Systems*

Markets

2010-2012	Financial and Operational Risk Management for Restructured Wholesale Markets
2010-2012	Forecasting sales of PHEVs and PHEV users' recharging behavior
2010-2013	Integrated retail and wholesale power system operation with smart-grid functionality
2012-2014	Risk assessment of unit commitment cost under uncertainty
2015-2016	Integrated Distribution and Transmission Effects of Demand-Response Initiatives

Wind modeling

2010-2011	Impact of wind power on control performance standards and frequency regulation contributions of DFIG wind generators
2010-2011	Design of a meteorological model ensemble forecasting system for improved wind energy forecasting
2011-2013	Resource to backbone transmission design for very high wind penetration
2013-2015	Wind turbine generator and wind power plant modeling
2014-2016	Leveraging a geographic information system in high wind penetration transmission design

Ongoing project FY19

2016-2018	*Functional assessment of DFIG and PMSG-based wind turbines for grid support applications.*

Materials

2011-2013	Developing high conductivity, ultralight hi-strength aluminum composite conductor.
2013-2015	Phase 2 development of a stronger, lighter, more conductive high voltage transmission conductor material.

Impact of Power Transformer Overload Ratings on Transformer Reliability and Life

Farzad Azimzadeh Moghaddam and James D. McCalley

farzadam@iastate.edu, jdm@iastate.edu

May 2019

ABSTRACT

Power transformers are usually operated within their nameplate MVA rating, as identified by the transformer manufacturer. There are, however, conditions under which a transformer may experience loading beyond which it was originally intended, a situation that drives consideration of alternative responses of either making capital investments, employing operational constraints, or operating the unit beyond its rating. This project aims to define guidelines and criteria to support such decision-making, identifying power transformer loadings that achieve good balance among economics, reliability, and transformer life while considering the influence of increased renewable penetration in the network and the influence of geomagnetic disturbances on transformer performance. In order to address the project objectives, a system called the "Transformer Management Tool (TMT)," is under development; this system will be described. The current focus of the project is on addressing issues raised by Cedar Falls Utilities (CFU); CFU project objectives are presented. Also, a proposed procedure for processing dissolved gas analysis test results is provided.

1.0 Introduction

In this report, first, the project objectives are presented. Afterwards, a brief description of the TMT, a system under development to address issues raised by the Iowa State University (ISU) Electric Power Research Center (EPRC) member companies, is provided. In Section 4, CFU project objectives are described. Section 5 is dedicated to a proposed approach for dissolved gas analysis (DGA) test data processing. And finally, in Section 6, this report is concluded.

In order to evaluate the performance of the TMT, transformer data, especially from failed units (if available) would be of significant importance. Utilizing cause and effect relationship from already failed units for performance testing of the TMT, would be a very effective approach to analyze functionality of different modules within this system.

2.0 Project objectives

The project objectives are as follows:

1. Develop a decision-making tool that assists EPRC member companies in:
    a. Transformer purchasing (proper selection and sizing of transformers considering factors, such as load growth, integration of renewables, and harmonics);
    b. Identification of acceptable transformer loading levels considering aging, risk involved, and economic implications;
    c. Prediction of transformer lifetime;
    d. Transformer replacement
2. Identify causes of gassing problem in wind turbine transformers and potential mitigation measures.

3. Develop a thermal assessment software application for transformers to characterize performance during a geomagnetic disturbance (GMD) event (this would apply to all transformers with high side, wye-grounded and connected to above 200 kV [1]).

The above-mentioned objectives have overlap. For instance, a GMD event might affect a transformer's loading decision; a GMD event can cause overheating in a transformer which would limit the transformer's loading capability; this indicates overlap between objectives 1.b and 3.

3.0 A brief description of the TMT

In this section, an overall outlook of the TMT is presented. It is assumed that the TMT will communicate with a database. It gets input data from the database when data ready flag is raised. When the TMT algorithm is done with calculations, outputs are inserted into the database and output ready flag is raised indicating output generation for transformer owner/operator. Almost all internal algorithms within the TMT will use flags to indicate new updates. The TMT and transformer operator interaction via database is shown in Figure 1.

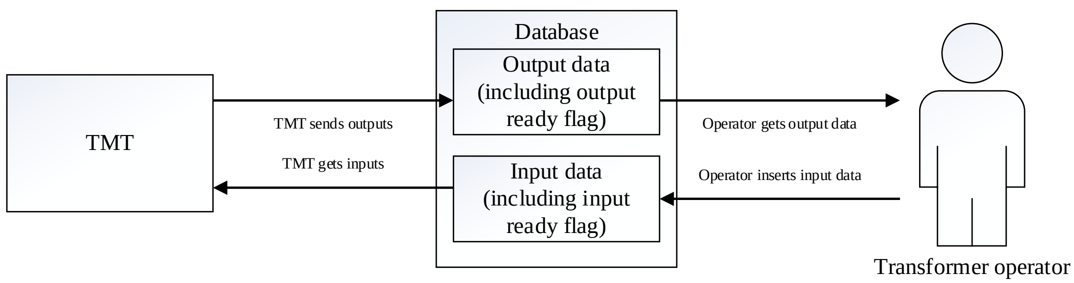

Figure 1: TMT and transformer operator interactions

There are five modules within the TMT; a brief description of each module is provided below:

Input data processing module: Input data is imported from the database. Then these data are validated to make sure they are reasonable. In this step, possible measurement/testing errors are detected. Only validated data are used.

Transformer condition assessment module: Analyzes the available data (transformer tests, loading level, and maintenance information) and expected loading data. And provides a measure of transformer condition and generates a condition flag which indicates if there is currently any problem with the unit or if a problem is expected.

Problem detection module: Problematic component(s) and origin of the problem(s) are detected. Knowledge regarding cause of the problem and impact of the problem is gained in this module.

Risk and economic analysis module: Evaluates when transformer components repair/replacement needs to be done, or when transformer itself is expected to be replaced. Also, risks involved, in case of delay in repair or replacement, are evaluated within this module.

Decision-making/recommendation module: Summarizes all the results achieved from the previous steps of the TMT and provides decision-making guides/recommendations to transformer owner/operator.

Figure 2 presents the operational flowchart of the TMT.

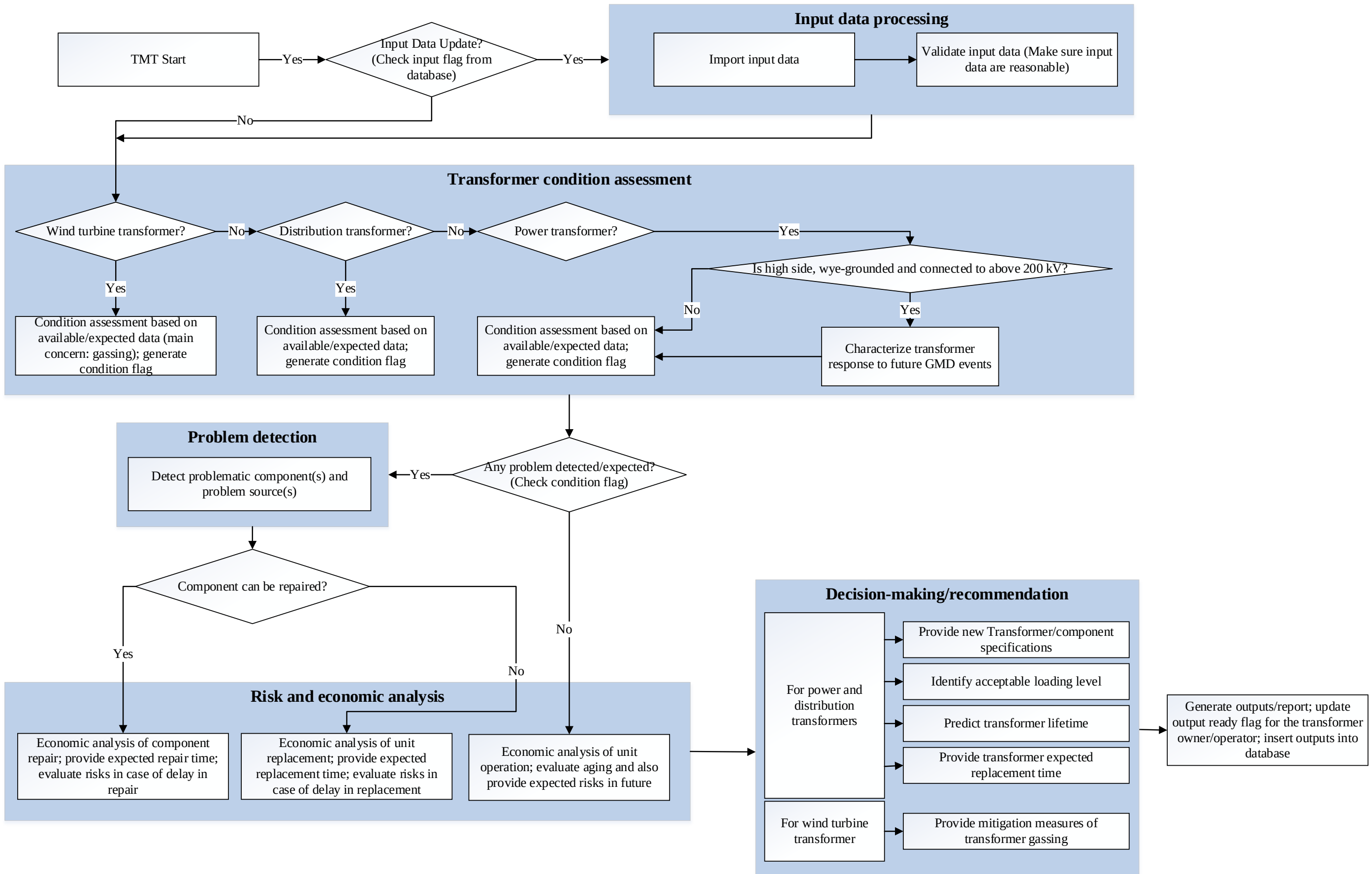

Figure 2: TMT operational flowchart

Table 1 provides a step-by-step description of the TMT operational flowchart. The first column refers to step number; the second column presents step name, and the third column provides a brief description of the respective step. Please note that term “data” in table below refers to all available current and past testing and maintenance data, all available current and past loading data, and also expected future loading levels.

Table 1: Step-by-step description of the TMT

Step #	**Step name**	**Brief description**
1	TMT Start	TMT is activated
2	Checking input flag	Input ready flag is checked. If it is zero, there is no new data update (only old data available), go to step 4. If input ready flag is 1, there is new data update, go to step 3.
3	Input data processing (module)	In this step, new data are imported into the TMT. Then these data are checked to make sure they are valid and reasonable.
4	Transformer condition assessment (module)	This step depends on transformer type and is divided into three categories.

		• If transformer is a wind turbine transformer, assess condition of the unit based on available/expected data. The main issue reported here is gassing. • If transformer is a distribution transformer, assess condition of the unit based on available/expected data. • If transformer is a power transformer: - If transformer high-side, wye-grounded and connected to above 200 kV, first, characterize transformer response to future GMD events. Afterwards, assess **overall** condition of the transformer based on available/expected data. - If GMD is not a concern, assess overall condition of the transformer based on available/expected data. Note: At the end of this step, a condition flag indicating condition of the transformer is generated. Condition flag is used to find out if there is any problem with the unit.
5	Checking condition flag	In this step, condition flag is checked. If it is zero (i.e. no problem detected), go to step 8. If condition flag is 1, this indicates a problem with the unit, go to step 6.
6	Problem detection (module)	This step is to investigate and detect problematic component(s) and source(s) of the problem(s).
7	Evaluating the problem (Component can be repaired?)	This step is to find out if the problematic component can be repaired/replaced (i.e. transformer lifetime can be extended) or if we are stuck with the problem (i.e. transformer itself needs replacement). Note: In either case, the next step is 8, but each situation is handled differently within step 8, risk and economic analysis.
8	Risk and economic analysis (module)	Here, economic calculations are performed, and also possible risks are evaluated. • In case problematic component(s) can be repaired/replaced, provide when repair/replacement needs to be done. Also, evaluate risks involved in case of delay in repair/replacement. • If transformer itself needs replacement, provide expected replacement time, and evaluate risks involved in case of delay in replacement. • If transformer has no problem, still, calculate transformer aging rate and also evaluate expected risks in future.
9	Decision-making/recommendation (module)	All results are summarized and decisions/recommendations are made based on results achieved from previous steps. For instance, here, a new transformer specifications are provided, or a maximum loading level for a transformer is defined.
10	Generate outputs/report	In final step, a report is generated, and output ready flag, indicating availability of new outputs, is updated. All these information are inserted into the database. Hence, transformer owner/operator can utilize the TMT outputs.

4.0 Cedar Falls Utilities transformer project

The TMT will be tested using data provided by CFU. The main CFU concerns and objective are presented below:

Main concerns:

- The load tap changer is the main concern; it is the most maintenance intensive component and has given the most problems.
- CFU has explored feasibility and cost estimates for a Vacuum LTC retrofit for this unit and likely at the same time would replace several other components including gauges, sudden pressure relay, pressure relief device, control wiring, bushings, fans, arresters, and monitoring equipment. The estimated cost for all these upgrades is around $200,000.
- The alternative would be to order a new replacement transformer and take a 2-3 week outage to replace the unit.

CFU Project objective:

- What is the best decision for an aging large power transformer? For example, which is better: Invest $200k into the unit to extend its useful life? Or spend more than twice that for a new unit?

5.0 Proposed procedure for dissolved gas analysis test result processing

DGA test is probably the most performed test by all utilities. DGA test result analysis; however, can be a complex process. In this section, proposed procedure in this project for analyzing DGA test results is briefly presented. The EPRC member company's comments and feedback would be greatly welcomed regarding the proposed procedure. It is intended to test the performance of the proposed approach using DGA data from a DGA lab.

The main idea behind using DGA test for condition assessment of mineral oil-filled transformers is that as faults happen within transformer there would be gas formations. Depending on the type and intensity of the fault, different gases with various concentration levels are generated. In mineral oil-filled transformers gases used for analysis are hydrogen ($\mathrm{H_2}$), methane ($\mathrm{CH_4}$), acetylene ($\mathrm{C_2H_2}$), ethylene ($\mathrm{C_2H_4}$), ethane ($\mathrm{C_2H_6}$), carbon monoxide (CO), carbon dioxide ($\mathrm{CO_2}$). Using these generated gases, different fault types can be detected. For instance, the main gases found in case of electrical arcing would be hydrogen and acetylene.

One of the most critical steps in DGA data analysis is to find out if actually there is a fault in transformer. Some methods such as Duval Triangle 1 will always provide a fault type. So, it is highly important to not diagnose a transformer as faulty when it is in a normal condition. In order to detect unusual operating condition using DGA data, different gas concentrations and their rates of increase are compared with their respective typical values/ranges. In case a gas concentration or its rate of increase exceeds its typical value or typical ranges, this needs to be investigated. These typical values/ranges are provided in already available IEEE and IEC standards; however, they need to be more specific. For instance, the typical gas values and rates of gas increase for a wind turbine transformer, which based on reports experiences high gassing rates, need to be different than a power plant transformer.

The **location factor** is critically important; a transformer close to renewable energy resources might see more harmonics, due to switching actions by inverters connecting these resources into the grid, than other transformers. Also, different operational, maintenance, and replacement approaches need to be applied. This is where the main idea for the proposed procedure comes from. It is intended to establish different typical values/ranges for different transformers based on their location in the grid using data from a DGA lab. Figure 3 below provides an overall view of this procedure.

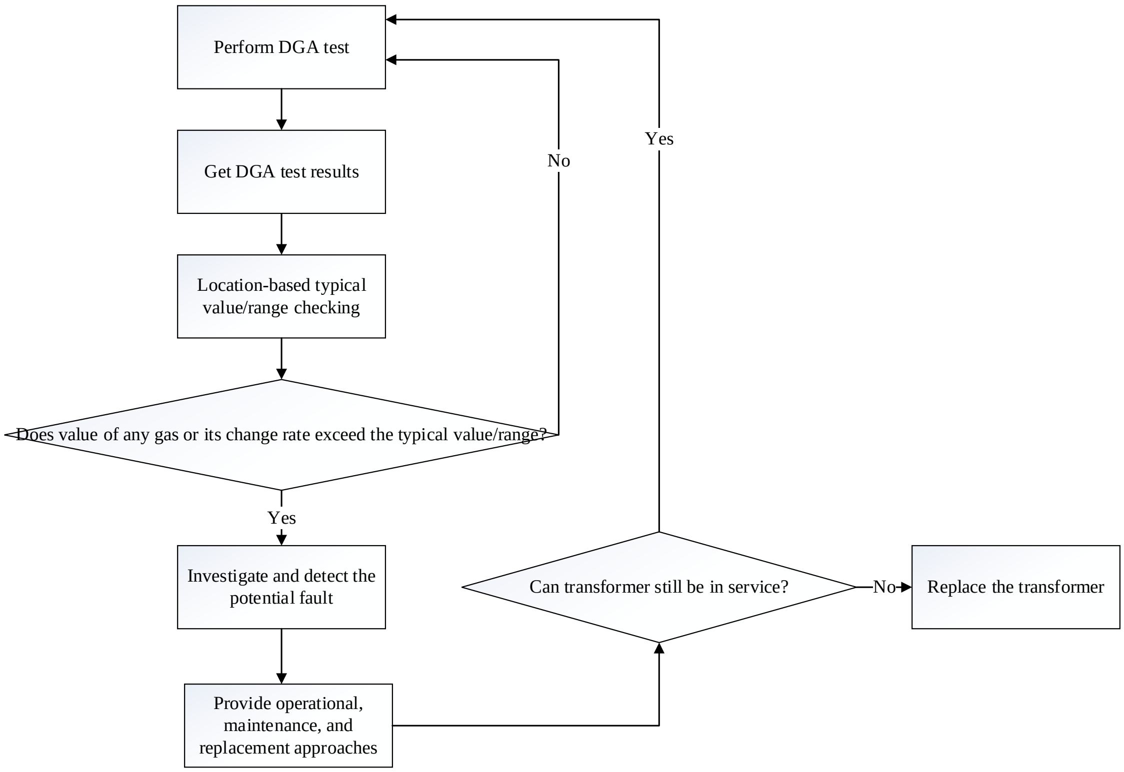

Figure 3: DGA data processing flow chart

Gas concentrations and rates of change are compared with their typical value/ranges based on proposed location-based approach in this project. Then, in case value of any gas or its change rate exceed its typical value/ranges, further investigation is done and potential faults are detected. It is of significant importance to use previous DGA data to detect most recent gas generations. If only test results from one test is available, it would be difficult to find out if this is due to a recent event or it is a cumulative value. Subtracting the latest DGA test gas values from the previous one, it is possible to find out the most recent trend in gas developments. Depending on the DGA test result analysis, operational, maintenance, and replacement approaches are provided to transformer operators.

6.0 Conclusions

In this report, the EPRC transformer project objectives are provided. And a brief description of a system called “Transformer Management Tool (TMT)” is presented; this is realized by providing a flowchart and an accompanying table. The main aim is to provide a high-level, however, clear picture regarding the approach which would be applied to EPRC transformer project in order to address issues raised by member companies. The proposed unit’s performance is intended to be evaluated by applying it to an aged transformer owned by Cedar Falls Utilities (CFU). CFU project objectives are also described. Also, a proposed procedure for DGA data processing is provided. All comments regarding the proposed system (TMT) and procedure for DGA are greatly welcomed.

References

[1] D. Corsi, "NERC TPL-007-1: Geomagnetic Disturbances and What They Mean for Your Large Power Transformers," 5 January 2017. [Online]. Available: https://www.doble.com/nerc-tpl-007-1-geomagnetic-disturbances/. [Accessed 5 December 2017].

Feasibility Study of Combined Heat and Power System for the Iowa Army National Guard Camp Dodge

Summary Report

Aaron Bertram, Song-Charng Kong, Anne Kimber, Iowa State University

Abstract

Combined Heat and Power (CHP) systems achieve high overall system efficiency when normally-wasted heat can be recovered effectively. While CHP systems have commonly been used in industrial settings as well as in utility-scale plants for decades, their use in Microgrids and mission-critical secure applications is much lower. CHP systems offer emissions reductions, efficiency increases, and capacity increases while primarily only adding an increase in capital costs, along with a small footprint of land to move heat. Research questions specific to micro-scale systems (200 kW – 10 MW) are largely related to external demands, such as requirements for storage, additional costs for resilience, and the added value aspects of interactions with other systems. This study uses machine learning models for the facility-wide load, creating a profile from the prior years' data. Engine systems were modeled using public data sets along with expert knowledge and specific engine data sheets to account for efficiency increases or decreases related to ambient conditions. An analysis was performed using the previously-developed engine models and data. While natural gas prices remain low and utility pricing is competitive, with no feasible option to sell excess power, finding value for a CHP system is challenging. This investigation leverages existing assets to balance demand and supply via application of Ground Source Heat Pumps (GSHP) and their installed infrastructure. Issues related to the power system features, i.e., prime mover technology, fuel used, heat recovery type, operational schedule, etc., and their effects on reducing the capital costs of a CHP system are investigated. Analysis shows a typical CHP system near 0.20 $/kWh levelized cost, while the leveraged system could bring the costs nearer to 0.12 $/kWh. When comparing the CHP-based generation system to the utility, a simple economic analysis fails, while comparing to the same power system without CHP, an economic analysis validates the application of CHP.

Progress Summary:

- Preliminary estimates of optimized LCoE ~ 0.10 – 0.20 $/kWh
- Considerations for the GSHP-CHP interactions

The current state of the project is final case analysis to examine how different assumptions and conditions affect the outcomes. Using the model to explore a range of conditions an idea of how CHP can impact all aspects of energy supply including resilience, security, and sustainability.

On-going Work:

- Finalize cost estimates for GSHP-CHP integration
- Prepare reporting with final summary and conclusions.
- Assessing the cost of energy security.

Combining heat pumps with heat recovery is substantial engineering challenge. Fully characterizing the performance of the GSHPs is beyond the scope of this study, however, this study highlights the potential benefits of coupling the GSHP systems with the power generation heat recovery system. CHP systems are well positioned to mitigate the risks associated with GSHPs operating in extremely cold conditions as well as preventing long-term thermal well depletion. As GSHPs are more widely implemented (as a carbon-reduction strategy) the need to address the potential shortfall. GSHP rollout will drive shifts in cold weather from gas to electricity, and potentially, the wintertime peak consumption may exceed the summertime peak. In these scenarios, the load growth from conversion to GSHP can be offset by adding CHP capacity. The GSHP is a mechanism that allows heat from the generation system to directly offset electricity that would be used.

Outlook:

- CHP provides additional security benefits due to the GSHP installations
- Discussion of Natural Gas storage provides the potential to operate the CHP system when the demand for heat is high while leveraging fuel reserves.
- Off-the-shelf Dual fuel solutions provide flexibility and additional resilience but is offset by small efficiency reductions
- CHP systems can be coupled with other heat-producing systems such as biomass reactors/gasifiers, etc. providing increased capacity and resilience with near zero marginal carbon impact
- CHP infrastructure has very high longevity and typical market analysis accounts for only 20-25 years of life while the fundamental components excluding pumps may easily last 50 years or longer.

Conventional energy supply remains less expensive in terms of LCOE, however, several indirect benefits of CHP systems can be realized when coupled with GSHPs and efficient generation systems. Generation systems can achieve 40% efficiency or more, are able to use a wide variety of fuels, and are comparable in terms of cost and maintenance. Conventional piston engines operating on natural gas are the most ideal for CHP as they avoid exhaust “slobber”. At the current time, however, a system which does not interact with the exhaust was used to achieve the lowest possible capital cost.

A modular style CHP installation which fits with the 5- and 10-year growth plans could accommodate load growth through CHP expansion; thus, allowing the same base generation capacity to provide full resilience.

GSHPs will remain an attractive technology qualifying for many “renewable” programs and credits. The proliferation of the GSHPs has created a dramatic shift in the winter-time load makeup. Serious risks exist when weather uncertainties are extreme; magnified with each additional system installed. Buildings which do not remain heated are a massive liability and yet to qualify for the “renewable” the makeup heating apparatus packaged with the GHSPs should not include a gas-fired heater. This conundrum with GSHPs, that they reduce the carbon intensity and increase efficiency but also increase the risk of failure to manage the thermal load of the building.

CHP solutions provide a direct remedy for the lack of heating capacity that GSHPs can experience in extreme weather. Since extreme weather is also commonly associated with damage to power lines it is imperative that a resilient power system be fully capable in all extremes. GSHPs tend to cool more effectively than they heat, as the thermal capacitive well is colder than the desired set point. GSHP proliferation will result in a more efficient cooling profile and a dramatic load shift from carbon-intense gas to electricity. CHP is an easily implemented technology that improves the safety and security of the energy system as a whole.

CHP is flexible and relatively economical; however, modern engines may produce an exhaust gas that is less than ideal for longevity of heat extractors. In many cases this means that titanium and/or stainless steel is used reducing the effectiveness and increasing the costs. The exhaust heat extractor may become caked, blocked, sludged, slagged, etc. Engine operation can be optimized so that the exhaust heat remains optimal for long-term operation, however, this is not the default mode for hardware which is not configured in CHP systems from the manufacturer. As such, adding a full-scale CHP system after the power system is installed may not be advisable. CHP compatible hardware and operating software should be chosen from the outset.

Coordinating Conventional Voltage Control Devices with Smart Inverters in Rural Distribution Networks with DER Penetration

Alok Kumar Bharati
Venkataramana Ajjarapu
Department of Electrical and Computer Engineering
Iowa State University, Ames, IA - 50011

***Abstract*— The project focuses on rural distribution feeders and studying the impact of high penetration of distributed energy resources (DERs) on voltage performance. Voltage performance in power system is closely related to the reactive power & the losses in the system and these have direct impact on the voltage stability of the system. We have found that rural feeders have the tendency to have significantly higher voltage violations depending on the loading conditions due to the longer lines in the network. The amount of unbalance is also not easily controlled and does see some parts of the network being single phase or two-phase causing voltage imbalance in these feeders. This can result in significant load unbalance in the system. IEEE 34-node system is chosen for the setting up of tools and analytical methods as it characterizes most of the rural distribution system features like long lines, lightly loaded and unbalanced system. The sensitivity analysis of the IEEE 34 node system reveals that the voltage regulation devices should be distributed along the feeder to ensure minimum voltage violations. Due to one of the phases being heavily loaded, voltage regulation using 3-phase regulators or capacitor banks tend to cause voltage violations in the other phases while trying to regulate voltage in one phase. The solar PV is a positive impact on the voltage profile in the IEEE 34-node system.**

I. Introduction

Power distribution system is a sub-system of power system that is used to deliver electrical power to the loads that are located at the ends of the radial distribution network. The distribution system is mostly radial in nature and therefore, the voltage decreases as we go further from the substation / root node. Figure 1 shows the decreasing voltage profile in a distribution feeder at 120Volt level.

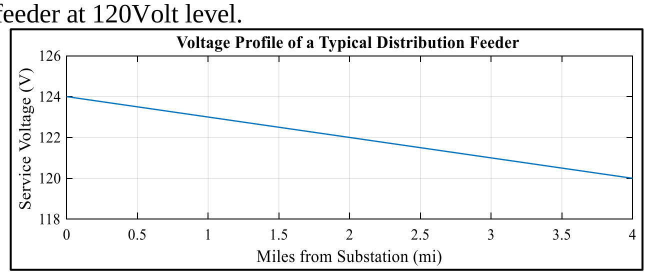

Figure 1: Voltage Profile of a Typical Distrubution Feeder

This decreasing voltage has a greater significance, especially in rural network as the lines are long and system is unbalanced. Due to the long lines, the resistance of the rural distribution lines is higher, and this causes the higher voltage to drop between the substation and the end of the feeder. Voltage regulating devices are used to inject reactive power to ensure the voltages are within acceptable limits.

A. Voltage Regulating Devices

To regulate the feeder voltage several voltage regulating devices are used like on-line tap changers (OLTC), capacitors, voltage regulators, static VAR compensators (SVCs), etc. These devices regulate the voltage to be within the operating limits specified by ANSI standards C84.1 [1]. All these voltage regulating devices have their own merits and demerits. Some of these voltage regulating devices affect the voltage profile locally like capacitors and some affect the lines more remotely like the voltage regulators and help regulating larger parts of the distribution network. Understanding how the different regulating devices work together in a rural distribution system is important. Capacitors and SVCs are discrete devices with fixed rating and reactive power and when connected, they provide a fixed amount of reactive power support to the grid. The voltage regulators and OLTCs have a voltage/ reactive power support range and the deviation from the set-point decides the amount of reactive power being supplied or absorbed, however they all have a saturation point.

B. Smart Inverter for Voltage Regulation

The power distribution system has all the above-mentioned voltage regulating devices that function together in a coordinated way. Each of these voltage regulating devices have a role to play depending on the location of the device in the grid. The modern distribution system is being proliferated by more complex devices like smart inverters that have flexible real and reactive power modulation capability depending on the primary source of power that the inverter is fed from. With solar PV inverters, the ratings of the PV inverter are fixed, and the reactive power modulation capability varies with the amount of real power being supported by the smart inverter. In this project we are exploring the coordination of smart inverters along with

This project is funded by Electric Power Research Center (EPRC), Iowa State University.
Alliant Energy is the utility partner in this project.

the conventional voltage regulating devices in a rural distribution system. Figure 2 shows an example of the droop characteristics that will be used to control the node voltage of the smart inverter locations. Inverter based resources (IBR) like solar PV, battery storage and electric vehicles are integrated to the grid using inverters. The latest IEEE 1547 grid integration standard that governs the integration of various IBR to the grid requires the inverters be rated to allow 44% of the kVA rating for reactive power modulation which means they should be ~10% overrated based on the real power capacity. If the inverters are rated for 100% real power rating, then they will be required to curtail real power to provide the 44% reactive power modulating capability [2].

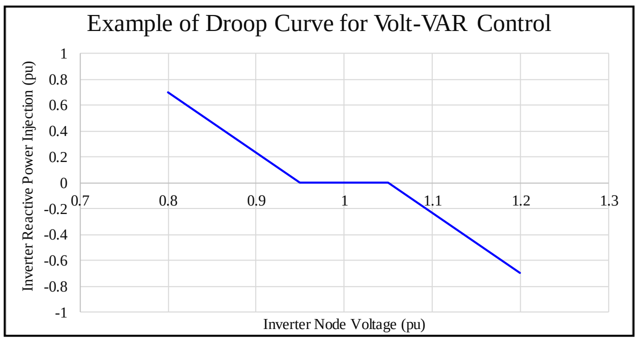

Figure 2: Volt-VAR Droop Curve Example Implemented in a Smart Inverter to Control Node voltage (Acceptable Voltage Range = 0.95 - 1 pu) [3]

The droop curve in Figure 2 shows that if the voltage goes below 0.95 pu, the inverter will inject reactive power into the grid to bring the voltage back within the 0.95 – 1 pu range and if the voltage exceeds 1.05 pu, it will absorb reactive power to maintain the voltage in the range. The ±5% voltage from 1 pu can be reduced to 0% making it strictly follow the voltage set-point. This can be done with various slopes of the voltage control to ensure the control is a stable control to maintain the voltage set-point. The smart inverter control has the potential to provide the required reactive power while supplying the real power from the DERs. We explore the utilization of the smart inverters for voltage control and reduce the usage of the conventional voltage regulating devices and explore the amount of DER penetration required to minimize the tap changes and capacitor switching in the distribution grid.

II. STUDY ON IEEE 34- NODE SYSTEM

The smart inverter-based voltage regulation is done based on the control method called volt/var control which is normally a droop control of the smart inverters where the voltage set-point is decided and the inverter either supplies or absorbs the reactive power to maintain the voltage at the set-point. As mentioned in the previous part of the report, a sensitivity analysis is done to understand the influence of these voltage regulating devices in the rural distribution system. The team has performed the initial study on the IEEE 34-node system. The IEEE 34-node distribution system consists of two voltage regulators, two capacitors and an OLTC for the voltage regulation. It also contains spot and distributed loads and is unbalanced in the three phases. This feeder model characterizes a rural feeder appropriately with its long lines and lightly loaded conditions and is an actual feeder in Arizona [4] and so, is chosen for this study.

The IEEE 34-node system is also characterized with a significant unbalanced load spread across 1-Ø, 2-Ø and 3-Ø lines and loads. The loads are modeled as large spot-loads and many distributed loads along the feeder sections. The distributed loads are modeled with exact-lumped-load model as shown in Figure 3, extracted from reference [5]. The exact lumped load model is used to approximate a uniformly distributed load (UDL) between a feeder section. $\frac{2}{3}$rd of the UDL is lumped at $\frac{1}{4}th$ the feeder length and the rest of the load is lumped at the end of the section. This is done to account for the feeder voltage drop and feeder loss as accurately as possible.

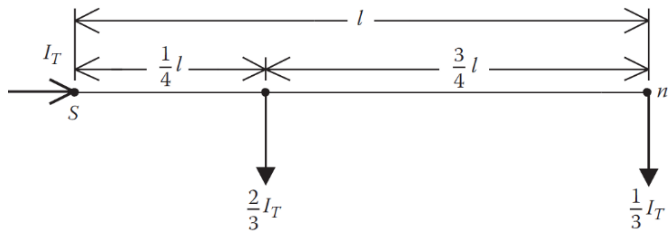

Figure 3: Exact-Lumped-Load Model; extracted from reference [5]

A. *Results of the Sensitivity Study of the Voltage Regulating Devices on the IEEE 34-Node System*

The existing voltage regulating devices on the 34-node system are two capacitors at nodes 848 and 844. There are 2 voltage regulators: one between nodes 814 and 850 and the other between node 852 and 832 as shown in the Figure 4. The voltage profile of the 34-node system without any modification or addition of solar PV inverters is also shown in Figure 4. This is verified with the expected feeder voltage profile provided by IEEE working committee along with the feeder data given in reference [4]. The terminal node 890 is at a lower voltage (0.91 pu) with the regulators and capacitors switched on the grid.

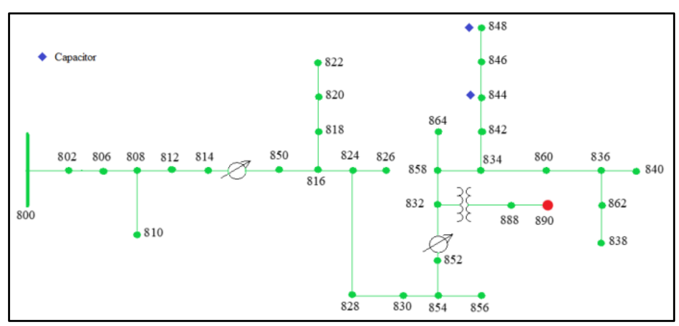

Figure 4: IEEE 34-node Distribution System – base case with voltage violation at node 890

The sensitivity analysis involves the study of voltage profile without any voltage regulation and comparison of the improvement in the voltage profile by individual voltage regulating device in isolation. This analysis results in the identification of critical locations of placement of the voltage regulating devices. At these critical locations, various combinations of the voltage regulating devices will be tested to improve the voltage profile of the entire distribution feeder.

The base case locations and ratings for the regulating devices are chosen for the sensitivity analysis described further in this section.

The Figures 5 and 6 show the parts of the network that has voltage violations (<0.95 pu or >1.05 pu); in this case, the voltages are below the lower limit and are marked in red on the ditribution feeder. It is clear that if the regulator taps are at the maximum ie., maximum reactive power is being pumped into the distribution grid, with and without the capacitor, most of the feeder experiences no voltage violations.

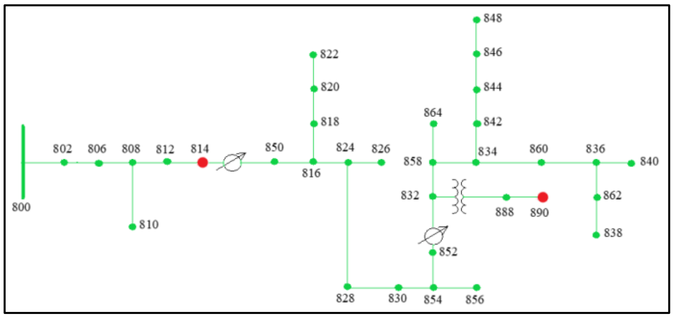

Figure 5: Regulators at maximum Taps and Capacitors Disconnected

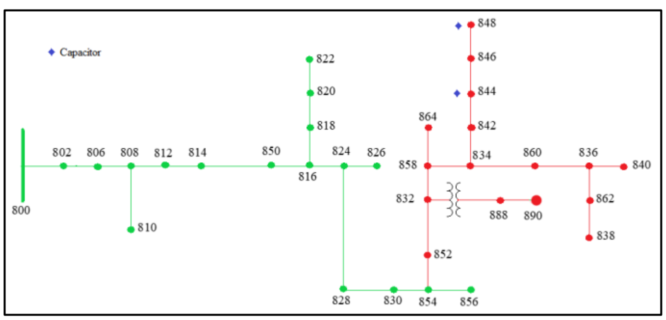

Figure 6: Regulators Disconnected and Capacitors Connected

In rural feeders, the role of the regulators is more significant as the long lines force the voltgae drop to propogate towards voltage violations if the regulators do not provide sufficient reactive power. The effect of the capacitors is local whereas the regulators have a more expanded area that it can help. We will study the impact of adding solar PV with 60% penetration (60% of peak load) on the voltage profile of the distribtion network.

A. *Impact of Solar PV on the Voltage Profile at Peak Load – 60% Penetration*

Solar PV inverters are proliferating rapidly in the distribution grid. Over the past few years, the control and capability of the solar PV inverters have evolved from just providing real power at unity power factor (UPF) to being able to modulate the real and reactive power together to operate in various modes of operation. The inverters operating in UPF and volt-VAR control (VVC) mode are considered and observations are discussed below.

1) Unity PF Mode:

Solar PV inverters operating in UPF mode do not provide any reactive power support and operate to only supply the real power generated by the solar panels. Usually, in a well-regulated system, with the addition of UPF solar PV in the grid, the voltages are expected to increase as the net demand is reduced and the regulating devices are injecting the reactive power into the grid. There are voltage violations with the solar PV inverter operating in unity power factor mode without capacitors or regulators: there are low-voltage violations at the end of the feeder while the feeder section closer to the substation experience over-voltages, however, these over-voltages are just over 1.05 pu. If the regulators and capacitors are switched on along with the inverters in UPF, most of the feeder experiences significant over-voltages as seen in brown color in Figure 7.

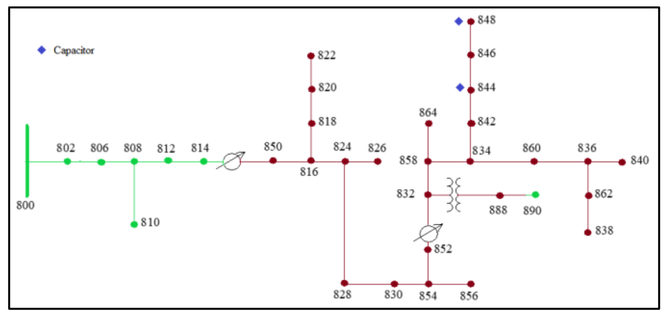

Figure 7: The feeder experiences over-voltage with PV penetration in UPF

2) Volt-VAR Control Mode:

The volt-VAR control (VVC) mode in the smart inverter enables absorption or injection of reactive power in the grid based on the voltage set-point and the voltage at the inverter node. The VVC is based on the droop control shown in Figure 2. In the present study the inverters operate in VVC mode to provide the functionality of voltage regulation reducing the requirement of the conventional voltage regulating devices. In presence of the capacitors and the regulators operating, there are voltage violations observed with the capacitors and voltage regulators switched on the network. At peak load conditions, the regulator tap positions are observed to have reduced and the capacitors need not be connected to have all the voltages within acceptable range with the VVC as shown in Figure 8.

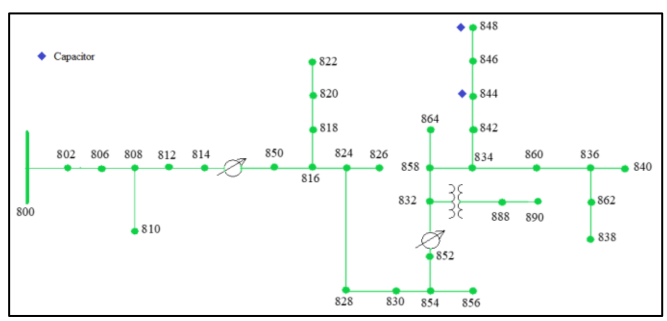

Figure 8: The feeder voltage can be maintained within limits with minimum reactive support from the regulators and capacitors

The control or operation of the various smart inverters in VVC mode along with the regulators, capacitors must be coordinated in order to minimize the operations of the conventional regulating devices as the continued operation may lead to lifetime reduction and can eventually affect the reliability of these devices. To coordinate the various voltage regulating devices along with the smart inverters, a weighted optimization problem is formulated that solves for the amount of reactive power support required from each regulating device with the constraints of the distribution system operating constraints, and the device rating limitations.

B. *Weighted Optimization for the combinations of Voltage Regulating Devices*

A weighted optimization formulation for minimizing the VAR operational cost is used to identify the best suited combination of the voltage regulating devices.

A simplified formulation of optimization is shown in Table 1 where, t is time instant. It is formulated for 24 hours. $w_1 - w_5$ are weighing factors for each part in objective function. $f_i^1(Q_{cap}), f_i^2(Q_{dvar}), f_i^3(Q_{inv})$ are cost function for i^{th} var device i.e. capacitor, d-var and inverter respectively. $g(Tap_t)$ are total number of tap operations for i^{th} tap device (OLTC and voltage regulators). P_t^{loss} represents system losses at time t. The formulation is executed for a 24-hour load profile.

Table 1: Simplified formulation of optimization

Minimize $\sum_t \begin{Bmatrix} w_1 . \sum f_i^1(Q_{cap}) + w_2 . \sum f_i^2(Q_{dvar}) + w_3 . \sum f_i^3(Q_{inv}) \\ +w_4 . \sum g(Tap_t) + w_5 . P_t^{loss} \end{Bmatrix}$
$V_{low} \leq V_{t,n} \leq V_{high} \ \forall\, t,n$
$I_{l,t} \leq \ I_{max} \ \forall\, t,l$
$Tap_{low} \leq Tap_{t,T} \leq Tap_{high} \ \forall\, t,T$
$pf_{min} \leq pf_{DG} \leq 1$
$f\big(V, V_{set}^{DG}, Tap, P_L, Q_L, P_{DER}, Q_{cap}, Q_{dvar}, Q_{inv}\big) = 0$

The optimization problem requires to linearize the distribution power flow as a constraint. Researchers have provided a basic understanding of the linear distribution power flow that is extended to a 3-phase unbalanced radial networks. The linear power flow and the optimization is written in MATLAB. The formulation is currently tested on IEEE 13-node system without capacitors or regulators and is working as expected. However, for the current project, the optimization is being extended to include regulators and capacitors in the optimization framework as shown in Table 1 in the simplified formulation.

III. CONCLUSINOS AND FUTURE WORK

The project team has performed the sensitivity analysis of understanding the role of the various voltage regulating devices in the rural distribution feeders and has concluded that regulators play a more critical role as the voltage drop spreads with lesser nodes in the rural feeders. With the proliferation of the DERs, if the solar PV inverters operate in UPF mode, there will be regulators and capacitor switching throughout the day to maintain the voltage within acceptable voltage range. This can be limited by operating the PV inverters in volt-VAR control mode. The team has developed a linear-distribution system power flow algorithm that can handle 3-phase unbalanced distribution feeders. This linear power flow method exploits the radial nature of distribution systems.

The future work in this project is:

1. Extend the sensitivity analysis to utility scale solar and identify the optimal placement of the utility scale solar for voltage regulation.
2. Integrate the voltage regulators and capacitors in the optimization formulation and incorporate the optimal placement problem along with the coordination optimization.
3. Extend the analysis to a large rural distribution feeder on the Alliant Energy's system.

REFERRENCES

[1] Voltage Ratings for Electric Power Systems and Equipment (60Hz), ANSI Std. No. C84.1-2006, New York.

[2] IEEE 1547 Standard, "IEEE Standard for Interconnection and Interoperability of Distributed Energy Resources with Associated Electric Power Systems Interfaces"

[3] GridLAB-D software manual for modeling and analysis of distribution systems

[4] Distribution System Analysis Subcommittee Report, "Radial Distribution Test Feeders"

[5] William Kirsting, "Distribution System Modelling and Analysis", Text Book.

A Tool for Mining AMI Data to Model Customer Loads for Small Utilities

Nichelle'Le Carrington
Electrical and Computer Engineering
Iowa State University
nkcarrin@iastate.edu

Zhaoyu Wang
Electrical and Computer Engineering
Iowa State University
wzy@iastate.edu

Anne Kimber
Electrical and Computer Engineering
Iowa State University
akimber@iastate.edu

***Abstract*—This project describes the development of a Smart Meter Analysis Resource Tool to facilitate small utilities in the processing of Advance Metering Infrastructure (AMI) data with limited staff resources. The proposed tool is based on MatLab-Simulink-Guide toolboxes and provides a complete set of user graphical interfaces to properly model and study customer loads using AMI data for small utilities. The propose simulator allows to model and observe customer contribution and the main determinants that affect load consumption, customer segmentation, typical load profiles, and time-varying probabilistic distributions of load consumption for various higher-level applications such as usage-specific tariff structures, conservation and consumer specific demand response programs and cos/benefit analysis of renewable energy integration programs..**

I. Introduction

Public power utilities upgrade their systems to incorporate new metering and billing technology with updated data collection methods and data processing capability. The abundant Advanced Metering Infrastructure (AMI)-based data collected by public power utilities contains valuable information of customers' consumption patterns. With the use of stochastic and probabilistic modeling techniques to help extract the customer's consumption patterns small municipal utilities can improve their understanding of their customer load behavior. By understanding the customer load behavior through these data driven methods, utilities will be able to find useful information that will help with characterization of customers and validate the existing classification traits for revenue sectors (commercial, residential, etc.). Utilizing the information from AMI data, utilities can understand how customer demand varies over selected time periods. This understanding enables utilities to make planning decisions about demand response programs, rate designs, renewable energy project locations, and distribution system infrastructure planning.

The demand curve in distribution systems fluctuates constantly with time and needs immediate response to changes in the load[1]. Majority of the small utilities have few if any staff members who are engineers or statistician that can help extract information from AMI data. The current practice of utilities is to review the monthly energy consumption based on billing for stratification criteria which makes it difficult to define the daily behavior of customers[2]. The benefit of to small municipal utilities that have AMI and those who do not is that from exploring actual data an understanding of real customer load behavior from historical data can be obtained.

This paper presents the development of a research-grade Excel-based software tool that small public utilities can uses to extract useful information from AMI-based data. This software tool is intended to help small utilities process the AMI-based data with limited staff resources and save on data processing expenses. The tool is capable of importing, processing, analyzing and exporting large volumes of AMI data recorded at intervals of 15-minutes and hourly rates. Currently there is no commercial-grade or research grade tool available to complete such tasks for small utilities.

The rest of the paper is structured as follows: Section II is the literature review of concepts and Section III is a general description of the proposed tool and its design. A demonstration of the functionality of the proposed tool is presented in Section IV. The conclusions of the present and future work of the tool is provided in Section V.

II. Literature Review

Data partitioning methods have been widely used in the energy literature [3–8]. Many of these compare different methods for producing the profiles, working in terms of how accurately the profiles capture variations in electricity demand across customers. Some papers apply demand profiles derived from clustered data in practical problems: Balachandra and Chandru [9] used nine representative load curves obtained through clustering in a system planning exercise for Karnataka in India. Albert and Rajagopal correlated consumers' consumption profile with demographics and appliance usages [10]. However, they did not attempt to identify relevant characteristics for clustering consumers. Instead, they started with a predefined set of characteristics and determined whether those can be predicted from consumer's consumption profile. This approach is rather similar with [1] where the authors used the publically available dataset to predict household demographics from consumption profiles. Regarding consumer behavior analysis, [11] presented a psychographic consumer segmentation based on how consumers feel, think, and act. However, their segmentation is based solely on survey data about consumers' behavior and attitude toward electricity and energy conservation, and did not involve processing of any consumption data. The study in [12] proposed procedures to develop probabilistic load models observed from a distribution-level feeder of a residential community. The paper does not use AMI data and only models the uncertainty of aggregated feeder-level loads.

A Matlab-Simulink-GUIDE tool focusing on the simulation of residential load at the appliance-level was proposed in [13] but did not consider the load of multiple houses or different customer classes. References [1, 2, 14–16] explore different techniques of clustering AMI data for distribution systems specifically residential for stratification. The benefit of leveraging AMI data for analysis, demand forecasting and state estimation is presented in [17–19].

The above literature has certain limitations. Firstly, the existing papers use simulated data and/or publically available AMI data of specific customers. Therefore, their data may not be sufficient enough to capture load behaviors of different customer classes, and is not representative to small municipal utilities. Our dataset is provided by AMU and Atlantic, which are typical small municipal utilities with different customer categories. Furthermore, the existing research focuses more on analyzing residential customers. The load behaviors of other classes of customers are not fully studied. In addition, to the best of our knowledge, no similar software tool has been reported in literature.

A. Data Mining

Data mining is defined as the process that integrates a data management plan to extract, process and obtain useful information from a given data set [2, 20]. The aim of the data management plan is to properly store, process and clean data that can be used in creating understandable models that allow discover patterns and trends in the behavior of loads [2]. The data management plan used for this tool is comprised of six steps[2, 20]:

a) **Storing Data-** dedicated file location used to to store the raw data files, processed data files and supporting information files in an organized manner.

b) **Preprocessing Data-** uses data mining techniques that aid in converting raw data files into an understandable processed global table for analysis in tool.

c) **Analyzing Data-** involves systematically applying statistical and logical strategies to describe, summarize, illustrate and evaluate these summary data organized by the rate code (customer class), by feeder, or time options (hour, day, week).

d) **Preserving Data** data is preserved within the tool by storing summary data a global table and calling from the global table to perform the each analysis independently from one another.

e) **Export Data-** processed data is exportable from the tool as selected tables and pictures of graphs. The tables are saved as Excel files and can be imported into Word, NotePad, WordPad, or Excel. The pictures are .png files that can be imported into Word. The pictures of the graphs can be used for reports or descriptive data for the loads.

f) **Reuse Data-** special feature of the tool is that the processed exported data files from previous analysis can be re-imported into the tool for further analysis. This is a convenient feature that allows for faster processing within the tool.

The complete data management plan used with in the tool is illustrated in the diagram of Figure 1.

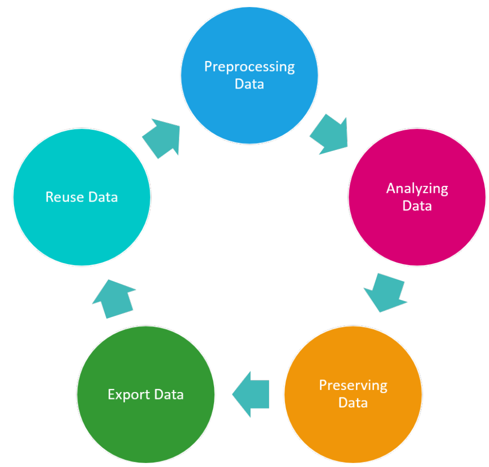

Fig. 1: Data Management Cycle for AMI Data Mining Tool.

B. Clustering Analysis

Cluster analysis is a data partitioning technique that allocates data into smaller groups based on some criteria of homogeneity [2, 14]. The K-means clustering algorithm is used over hierarchical clustering, expectation maximization(EM)

III. AMI Data Mining Tool

The technical architecture of the tool has four stages that incorporate the data management plan for data mining. The four stages are Data Import, Data Preprocessing, Data Analysis and Data Export. These four stages follow the data management plan to process and deliver uniform data files to the user. The flow chart of the architecture of the tool is a visual representation of how the data is formatted and accessed by the tool within the individual processes as a flowchart. This architecture will be presented in the stage descriptions below.

A. Stage 1: Data Import

The architecture of the Data Import stage in the flowchart of Figure 2 allows two methods of importation of AMI data within the tool. The first option is to bring in individual “raw” text and/or Excel files to be merged together into one table. Raw data refers to individual files of AMI consumption, feeder, account information, and heating/cooling/temperature data that have not been merged together. The second option is to import “processed data” that has been cleaned and formatted by the tool from a previous analysis. Processed data refers to a combined file of individual AMI consumption, feeder, account information, and heating/cooling/temperature data.

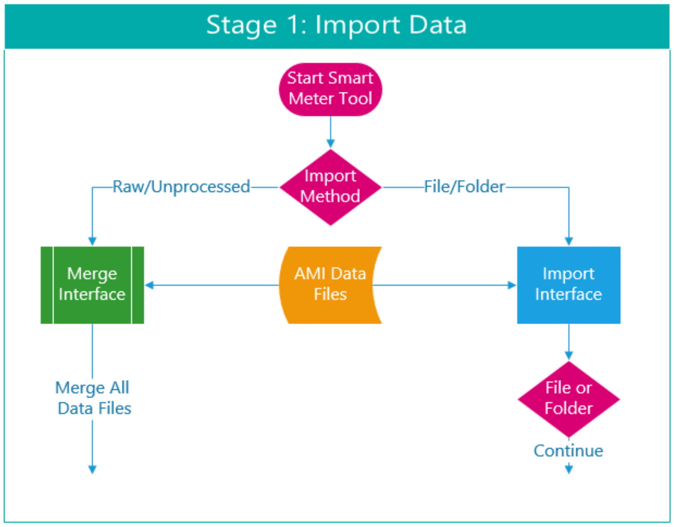

Fig. 2: Flowchart of Stage 1's options for importing data into the tool.

In Figure 2, data files are imported as either raw or previously processed data files exported from the tool. The raw data is processed using subroutines to format the data into a combined uniform information table which is then saved in a datastore internally within the tool. The combined data from the Stage 1 will be stored in a datastore within the tool as a tall array.

B. Stage 2: Data Preprocessing

The flowchart of Stage 2: Data Preprocessing in Figure 3 is the heart of the tool's intended purpose. This step helps create the data into a global variable that can be called from any analysis process in the tool and allows the results of each analyses to be independent from the datastore, saved independently, and available for further use within and outside of the tool.

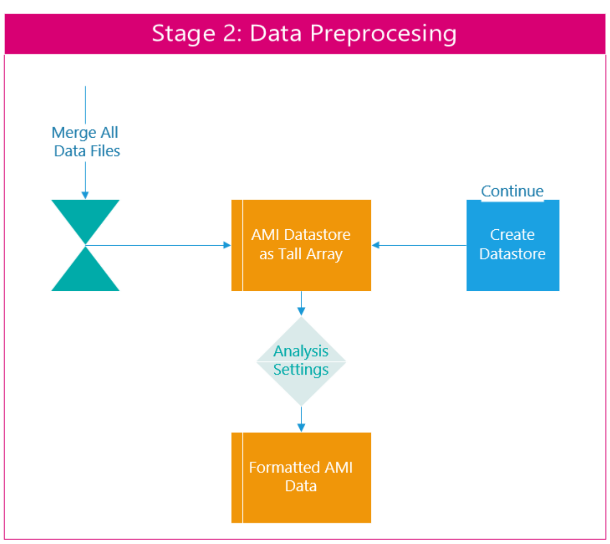

Fig. 3: Flowchart of Stage 2's process for formatting and filtering data fro analysis within the tool.

The global variable is created by filtering the data using the analysis settings. Filtering by combinations of date, feeder, customer class, hourly intervals or weekly information aid in mining data related to the defined settings. The condensed data is saved and stored for use in analysis features in the tool.

C. Stage 3: Data Analysis

In Stage 3: Data Analysis the condensed, processed data from stage 3 can be evaluated with 5 independent analyses: customer classification, customer contribution, load profile, load duration and customer statistics. The customer classification GUI has subroutine that groups customers by rate code using the unsupervised learning technique K-Means to group the customers in categories of similar consumption for the time period as in [2]. the Analysis menu is used to access the analysis procedures this stage and other interfaces except Stage 1. from the analysis menu on the Analysis Menu. The main screen serves as a centralized hub to access and review the results from each analysis process. Each analysis subroutine calls upon the datastore generated from Stage 2 to evaluate the supporting algorithm for a subroutine.

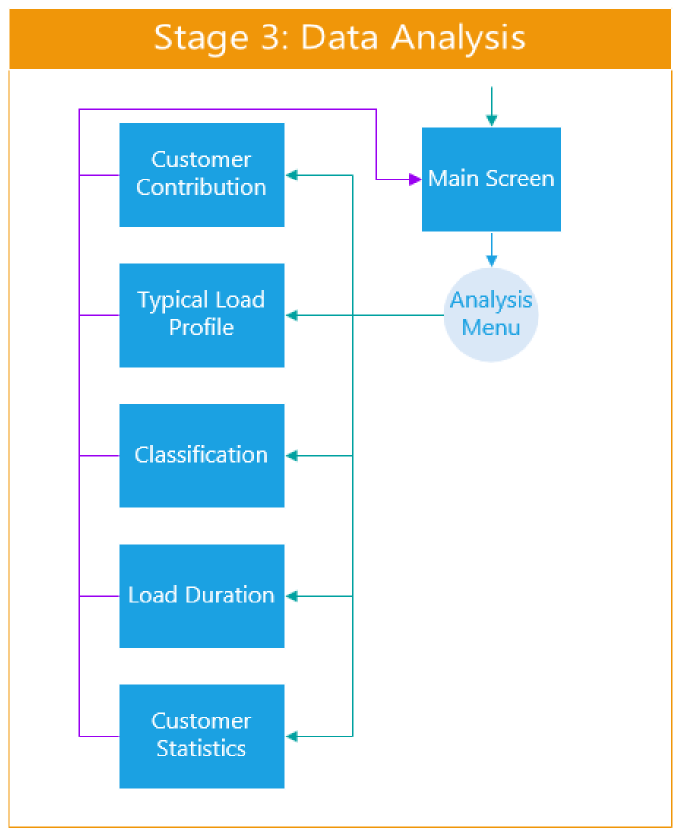

Fig. 4: Flowchart of Stage 3's options for analyzing the data within the tool.

The Customer Contribution GUI has a subroutine that displays and calculate the total contributions of a rate code within a given period at either the hour or 15-minute interval. Load Profile GUI has a subroutine that graphs the variation in the electrical load versus time. The Load Duration GUI has a subroutine that sorts and graphs the load in descending order of magnitude as a load duration curve.

D. Stage 4: Data Export

In Stage 4: Data Export the user is able to exported processed data and the graphs from analyses as tables and figures through the Export menu as shown in Figure 5.

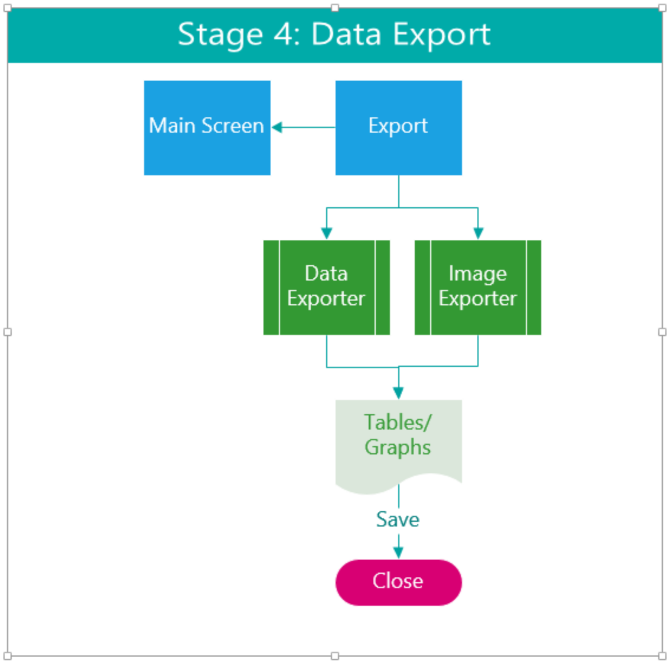

Fig. 5: Flowchart of the within the tool options for importing data.

The Data Exporter GUI allows the user to save the tables from the tool as a .csv, .xlsx, or .txt extension file to their computer. The Data Exporter GUI allows the user to save the figures from each analysis as a Portable Network Graphic (.png) file.

IV. Conclusion

During the development of this tool AMU and ISU did extensive review and error-checking of AMI data sets, comparing these with SCADA data summaries and AMU monthly reports. Some data sets had long sequences of repeated data that did not match realistic customer behavior. This was particularly true for early years when AMI meters had recently been deployed. Use of a simple tool, like the one developed in this project, would enable utilities to scan data and find odd outliers that could impact billing data or incorrectly indicate outages that did not in fact occur because of AMI meter communication errors.

Utilities planning to deploy AMI meters will want to have a plan executed with billing and meter data management contractors to retrieve and analyze the data. This plan would ensure that the data will be available, formatted, and with multipliers applied, for straightforward exploration by the utility.

By exploring the AMI data utilities can gain insights into their customer load behavior and the main determinants that affect the load consumption. Customer groupings based on load characteristics, and time-varying probabilistic distributions of load consumption can enable various higher-level applications such as usage-specific tariff structures, consumer-specific demand response programs, cost/benefit analysis of renewable energy integration programs and conservation voltage reduction.

Recommendation for future work: In this project a simple analysis of customer groupings was done using a k-means algorithm. In this method, the user selects a certain number of groupings based on the number of rate categories (maximum of 7), into which the program assigns customers. Residential customers, for example, would not be matched with the industrial customer grouping. The purpose of this test is to show if certain individual customers should be in a different rate category. It would be possible, using MATLAB, to build in machine learning into this algorithm to refine the process of grouping customers. This would be a useful addition to the tool especially to test rate designs and new customer categories.

Acknowledgement

Iowa State University is grateful to the American Public Power Association for the DEED grant that supported this work. We are also grateful for the test data, advice and support from our DEED project utility partner, Algona Municipal Utilities, and we are grateful to PCS Consulting, Denison, Iowa for their role in helping us work with Algona's AMI data.

References

[1] A. Mutanen, M. Ruska, S. Repo, and P. Jarventausta, "Customer classification and load profiling method for distribution systems," *IEEE Transactions on Power Delivery*, vol. 26, no. 3, pp. 1755–1763, 2011.

[2] J. E. Parra, F. L. Quilumba, and H. N. Arcos, "Customers' demand clustering analysis—a case study using smart meter data," in *2016 IEEE PES Transmission & Distribution Conference and Exposition-Latin America (PES T&D-LA)*. IEEE, 2016, pp. 1–7.

[3] S. Lin, F. Li, E. Tian, Y. Fu, and D. Li, "Clustering load profiles for demand response applications," *IEEE Transactions on Smart Grid*, 2017.

[4] J. Kwac, J. Flora, and R. Rajagopal, "Household energy consumption segmentation using hourly data," *IEEE Transactions on Smart Grid*, vol. 5, no. 1, pp. 420–430, 2014.

[5] Y. R. Gahrooei, A. Khodabakhshian, and R.-A. Hooshmand, "A new pseudo load profile determination approach in low voltage distribution networks," *IEEE Transactions on Power Systems*, vol. 33, no. 1, pp. 463–472, 2018.

[6] P. Balachandra and V. Chandru, "Modelling electricity demand with representative load curves," *Energy*, vol. 24, no. 3, pp. 219–230, 1999.

[7] D. Gerbec, S. Gasperic, I. Smon, and F. Gubina, "Consumers' load profile determination based on different classification methods," in *2003 IEEE Power Engineering Society General Meeting (IEEE Cat. No. 03CH37491)*, vol. 2. IEEE, 2003, pp. 990–995.
[8] M. Beccali, M. Cellura, V. L. Brano, and A. Marvuglia, "Forecasting daily urban electric load profiles using artificial neural networks," *Energy conversion and management*, vol. 45, no. 18-19, pp. 2879–2900, 2004.
[9] G. Chicco, R. Napoli, and F. Piglione, "Comparisons among clustering techniques for electricity customer classification," *IEEE Transactions on Power Systems*, vol. 21, no. 2, pp. 933–940, 2006.
[10] C. Marton, A. Elkamel, and T. A. Duever, "An order-specific clustering algorithm for the determination of representative demand curves," *Computers & Chemical Engineering*, vol. 32, no. 6, pp. 1365–1372, 2008.
[11] P. Balachandra and V. Chandru, "Supply demand matching in resource constrained electricity systems," *Energy Conversion and Management*, vol. 44, no. 3, pp. 411–437, 2003.
[12] A. Albert and R. Rajagopal, "Smart meter driven segmentation: What your consumption says about you," *IEEE Transactions on power systems*, vol. 28, no. 4, pp. 4019–4030, 2013.
[13] E. Pouresmaeil, J. M. Gonzalez, C. Canizares, and K. Bhattacharya, "Development of a smart residential load simulator for energy management in smart grids," *IEEE Transactions on Power Systems*, pp. 1–8, 2013.
[14] R. Green, I. Staffell, and N. Vasilakos, "Divide and conquer? k-means clustering of demand data allows rapid and accurate simulations of the british electricity system," *IEEE Transactions on Engineering Management*, vol. 61, no. 2, pp. 251–260, 2014.
[15] R. Li, F. Li, and N. D. Smith, "Multi-resolution load profile clustering for smart metering data," *IEEE Transactions on Power Systems*, vol. 31, no. 6, pp. 4473–4482, 2016.
[16] S. Haben, C. Singleton, and P. Grindrod, "Analysis and clustering of residential customers energy behavioral demand using smart meter data," *IEEE transactions on smart grid*, vol. 7, no. 1, pp. 136–144, 2016.
[17] J. Peppanen, M. J. Reno, M. Thakkar, S. Grijalva, and R. G. Harley, "Leveraging ami data for distribution system model calibration and situational awareness," *IEEE transactions on smart grid*, vol. 6, no. 4, pp. 2050–2059, 2015.
[18] B. Hayes, J. Gruber, and M. Prodanovic, "Short-term load forecasting at the local level using smart meter data," in *2015 IEEE Eindhoven PowerTech*. IEEE, 2015, pp. 1–6.
[19] V. Mtembo, G. A. Taylor, and A. Ekwue, "A novel econometric model for peak demand forecasting," in *2014 49th International Universities Power Engineering Conference (UPEC)*. IEEE, 2014, pp. 1–6.
[20] J. Han, J. Pei, and M. Kamber, *Data mining: concepts and techniques*. Elsevier, 2011.

Improving DFIG Wind Turbine Inertial Fast Frequency Response

EPRC final report: May 2019

Functional assessment of DFIG and PMSG-based wind turbines for grid support applications

Nicholas David, Zhaoyu Wang

I Project summary

The objectives of this project were to improve the understanding of wind turbine ancillary service capabilities and to advance the art of power electronic wind turbine control. It was performed in conjunction with the Power Systems Engineering Research Center (PSERC). The PSERC project has been completed and the final report published. Our work on DFIG control for frequency response has been submitted to journals for review and has been improved upon over several iterations. Reviewer and editor comments highlighted need for deeper investigation of the mechanisms behind our proposed DFIG controller, and to articulate the impact that generator and control parameters have on dictating frequency response performance. This EPRC report summarizes the latest and overall project findings.

Capabilities and impact of DFIG wind turbine frequency response are not well understood nor fully utilized. Bulk power system inertia has been dropping over time and is impacting transient stability [8, 10, 11]. In the Electric Reliability Corporation of Texas (ERCOT) interconnection they are anticipating need to add sources of inertia, including gas generators, solely to augment the inertial capabilty being achieved from wind turbines [6]. The reasons for lackings of DFIG fast frequency response are not well understood. There is a current need and search for enhanced understanding and creative solutions surrounding power-electronic connected generation [3–5, 7]. The work of this project aims to bring light to these issues.

We modeled self-powered DFIG wind turbine systems to estimate their capability for inertial frequency response. A novel control solution and alternative connection strategy were then developed and found to capitalize on the natural capabilities. We derived the DFIG frequency response with conventional and proposed controls, using linearized transfer functions with DFIG-powered “loose grid” assumptions. This is important because the closed-loop-system poles and zeros indicate whether the DFIG plus control system is able to provide inherent stability to support its own load. Our findings are that common droop-type controls have only a semi-stable effect on the fast frequency response and are insufficient for 100 % wind powered systems, consistent with observation in practice. The methods proposed in this project achieves a DFIG frequency response that is 10x faster and stronger than the droop-type method in common use today, evidenced by merits of frequency nadir and its time of occurrence. Participation of the DFIG in frequency regulation is increased. It could have impact to reduce dependence on auxiliary sources of inertia and raise opportunity for 100 % wind power generation.

II Improvement to wind turbine control for fast frequency response

a) Problems with the current state of art

Practice in the U.S. is moving to use of a roughly 5 % frequency-droop characteristic where possible, and advanced methods for response capability beyond this are encouraged [1, 2]. Figure 1(a) illustrates the trend of declining inertial frequency response (here within the Eastern Interconnection) with increased penetration of renewables. Figure 1(b) shows how droop control is currently used to help increase generator output during load-change induced transients. In this project we prove that the effect from droop control is insufficient for 100 % DFIG powered system. While droop control does provide a relatively slow response that acts to arrest transient and offset steady-state deviation, our work shows that it does not perform well during the first moments of transient onset, evident by a high rate of change of frequency and deep frequency nadir. The

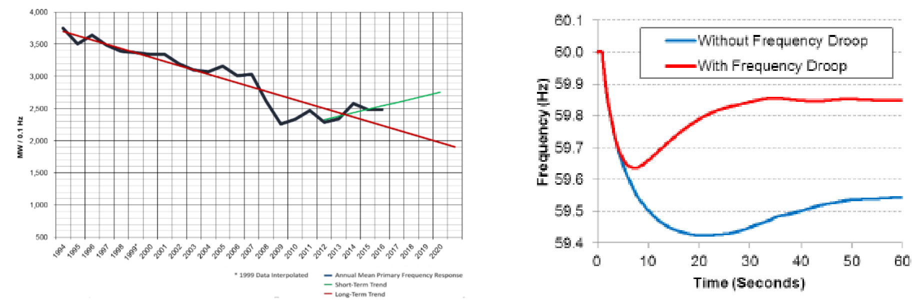

(a) (b)

Figure 1: (a) Inertia in the Eastern Interconnect in decline, a trend with increased renewables penetration [11]. (b) DFIG response in WECC to loss of generation at Palo Verde; simulated measurable frequency response event that imposes approximately 10 % DFIG demand increase [9].

controller proposed in this project can stabilize the fast frequency response, shorten the time to frequency nadir, raise its value, and reduce the settled-frequency error.

Power electronic-based wind turbines offer flexibility and advanced control, but their impact on frequency response stability during load change can vary widely according to the control methods being used. Generator controllers are usually designed with "stiff-grid" assumptions (constant frequency) but this implies that the DFIG is only following the system and not driving it.

We approached the problem differently and began by modeling the DFIG as a self-powered system. This means that we can assume the electrical frequency and rotor speed are linked, so $d\omega_e \approx d\omega_r$. The swing equation links the electromechanical dynamics with the control dynamics, and is approximately

$$\frac{2J}{P}\frac{d\omega_e}{dt} = \frac{3Pv_{qs}^e L_m}{4L_s\omega_e} i_{qr}^{\prime e*} + T_m - D\left(1-S\right)\omega_e. \tag{1}$$

This means that the way in which current command $i_{qr}^{\prime e*}$ is formed is critical to the frequency response; it normally originates from outer-loop torque control.

We found that with a grid-following converter, there is sufficient capability for good frequency regulation, but that the action of the torque controller is counter-productive to stabilizing frequency in the first moments of transient. We also found that the addition of frequency-droop control is also insufficient in quickly regulating frequency of a fully DFIG-powered load. With droop control, the frequency response from torque control is offset by the response from the frequency control, by a factor that equals the frequency-droop gain. The effect is that droop control counteracts the magnitude of the destabilizing effect from torque control, but it does not alter the speed of response. In fact, we found that the linearized fast frequency response transfer function has the same characteristic with both methods,

$$\frac{\Delta\omega_e(s)}{\Delta T_e(s)} = \frac{-3P^2 v_{qs}^e L_M K_T}{8JL_s\omega_e} \frac{\left(s+\frac{1}{\tau_T}\right)}{s\left(s+\frac{D(1-S)P}{2J}\right)}. \tag{2}$$

The fast frequency response is only semi-stable; one pole is located on the origin. The second pole is in the left half plane and its placement varies with the torque control design. The design of K_T impacts how quickly the frequency accelerates.

A flaw of droop control is that the frequency response is not usually explicitly designed. Rather, the droop gain K_f is usually assigned an arbitrary value often for a rated-power response to a 5 % frequency change (3 Hz in a 60 Hz system). Additionally, the droop control methodology assumes the electromagnetic torque is well-controlled and tracks the reference, so the frequency-droop then alters the reference value. In that way, when one considers a longer effective period of linearization, so that the torque is assumed to

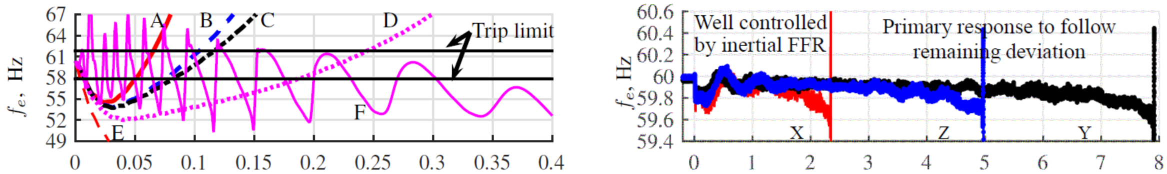

(a) (b)

Figure 2: (a) DFIG islanding frequency response over time (s) with 10 % load increase for varied torque control alone (A–D) and with addition of frequency-droop (F). (b) DFIG islanding frequency response using our proposed controller, shown here sustaining local after islanding with overload of (X) 40 % at subsynchronous speed (Z) 40 % at supersynchronous speed and (Y) 15 % at supersynchronous speed.

follow the command value, $T_e \approx T_e^*$, then the linearized response to a frequency change is

$$\frac{\Delta\omega_e(s)}{\Delta\omega_e^*(s)} = \frac{-3P^2 v_{qs}^e L_M K_T K_f}{8L_s\omega_e J} \frac{\left(s+\frac{1}{\tau_T}\right)}{s\left(s+\frac{DP}{2J}\left(1-S\right)\right)}. \tag{3}$$

This is the impulse response of the frequency controller, and it shows that the system still has one pole on the origin, meaning the frequency response is only semi-stable. Although droop control removes the long-term effect from K_T, it is still not well-suited to application in low-inertia DFIG-powered systems. This hypothesis and the results of our work are consistent with recent observation of fast frequency response stability problems in areas with high wind penetration and imposed frequency-droop control; they experience deeper frequency nadir and oscillations too, but do benefit from higher arrested frequency yet still with steady-state error. These transfer functions explain why problems exist.

Figure 2(a) illustrates the problem of DFIG instability by showing the simulated islanding response of a DFIG with a 10 % load increase. Designs A–D have progressively slower speed of torque-only response, and F is with a 5 % frequency droop added; all are unstable. To achieve a satisfactory frequency response using torque control alone, K_T must make the response so slow that it is ineffective at normally tracking the reference torque command; response time in the realm of 15 seconds – not shown. From this, we conclude that with conventional wind turbine controllers, their inertia is not well applied to frequency response. It is only because of the inertial contribution of other generators in the power system that it is possible for these types of controllers to work today. When moving to a 100 % wind powered system it is necessary to use advanced controllers tailored for self-support response capability.

b) Novel control to correct and design the frequency response

We derived a load-responsive frequency controller based on the DFIG-powered system dynamic equations. The idea of the proposed design is to augment the torque response with a brief frequency response. The existing torque-responsive current command is added to a proposed frequency-responsive component that can be made faster than the torque response, thus providing stable and specified fast frequency response. To prevent control windup and interference with slow grid dynamics, including primary frequency response from other slower units, the frequency controller bandwidth is limited using a high-pass washout filter. The current command in (1) is therefore $i_{qr}^{\prime e*} = i_{qr,\mathrm{T}}^{\prime e*} + \left(\frac{\tau_6 s}{1+\tau_6 s}\right) i_{qr,\mathrm{F}}^{\prime e*}$.

The proposed frequency control law is

$$i_{qr,\,\mathrm{F}}^{\prime e*}(\omega_e) = (\omega_e^* - \omega_e)\, K_\mathrm{F}\left(1+\frac{1}{\tau_\mathrm{F} s}\right) + \frac{r_s i_{ds}^e}{\omega_e L_M} - \frac{v_{ds}^e}{\omega_e L_M} - \frac{v_{qs}^e L_s}{r_s L_M}. \tag{4}$$

It is the result of designing the frequency impulse response to be a linear time invariant (LTI) system that uses proportional plus integral control to alter the response. It is derived using only the DFIG dynamic equations. The resulting impulse response is described by the LTI system transfer function

$$\frac{\Delta\omega_e(s)}{\Delta\omega_e^*(s)} = \frac{K_F\left(\tau_F s + 1\right)}{\left(\frac{L_s\lambda_{ds}^e}{r_s L_M} + K_F\right)\left(\tau_F s + K_F\right)} \tag{5}$$

The frequency response can be specified by virtue of the LTI system design. Assuming the frequency response is faster than the torque response so that the frequency tracks the commanded value, one can derive the linearized frequency response to apparent load-torque change, similar to (2). The transfer function is

$$\frac{\Delta\omega_e(s)}{\Delta T_e(s)} = \frac{\frac{-\alpha K_T}{\omega_e}\left(s+\frac{1}{\tau_T}\right)\left(s+\frac{1}{\tau_6}\right)}{\frac{2J}{P}s^3+\left(\frac{2J}{P\tau_6}+\gamma+\frac{\alpha v_{qs}^e L_s}{\omega_e^2 r_s L_M}\right)s^2+\left(\frac{\gamma}{\tau_6}-\frac{\alpha K_F}{\omega_e}\right)s-\frac{\alpha K_F}{\omega_e\tau_F}}. \tag{6}$$

Observe in (5) and (6) that the responses are made completely stable; the high-pass filter isolates their actions from each other. There are more poles than zeros and the variables allow for coordinated design of the zero and pole placements. The new controller gives ability to manipulate the pole location that contains J as a parameter. This means the controller design prescribes how physical inertia is used in the response. Inertial reserve can be used quicker or more slowly, and with more or less intensity depending on relative design choices. We find that with this method, the duration of off-nominal load support is limited only by the inertial capacity of the turbine. As a result, comparing (2) and (3) with (5) and (6) reveals that only the latter control has effect on stabilizing the response. Figure 2(b) illustrates the improvement. The proposed controller adapts to load-change with a stable fast frequency response and with ability to sustain regulation for a longer duration than when compared to the existing art. Our proposed controller reduces the time to nadir and also raises the nadir significantly along with the settled frequency, and for larger overload conditions too.

c) Improvement to DFIG reactive power capability for voltage support

We hypothesized that additional reactive power capability could be had from the DFIGs by configuring them with grid-connected rotor windings, so the power electronics reside on the stator-side of the machine; the so-called “rotor-tied configuration” (RTC). This configuration is shown in existing literature to have improved efficiency, thus presumably more current available for reactive power. We studied the new configuration and derived equations to estimate the reactive power capability. We found that some DFIGs offer increased generation capability, on the order of twice as much. Others we studied showed improvement at only a portion of the operating speed range, near synchronous or at high and low wind speeds. Benefit was found to arise from improved efficiency, increased use of available nameplate current ratings, and reduced reactive power loss in the generator. Test results are shown in Figure 3(a), where significant increase in available reactive power generation is observed at the machine grid-side terminal (GST). More current is available at the converter-side terminal (CST) for reactive power generation.

III Conclusions

Opportunities exist to increase DFIG reactive power generation and improve the utility of wind turbine physical inertia. Theoretical limitations of wind turbine generator reactive power capability shows that using the RTC of DFIG can increase the amount of available reactive power generation. Linearized transfer functions were derived to describe the impact that DFIG controllers have on frequency stability. They show that controls in popular use today do not have good impact on fast frequency response and are not well-suited for use in fully wind-powered systems. However, we find that the proposed controller can improve and make

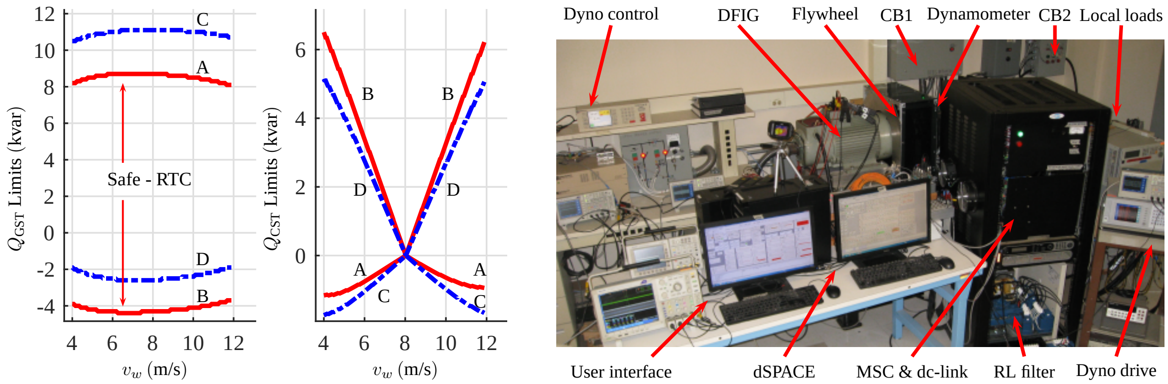

(a) (b)

Figure 3: (a) DFIG reactive power capability improved in the RTC. (b) DFIG laboratory test stand.

sufficient their inertial contribution to response. Experiments with the DFIG test stand developed in this project and pictured in Figure 3(b) gave ability to explore hypotheses and validate the proposed solutions. It will continue to be used in future grid-integration studies. Methods proposed in this project can afford added capability and improve transient response while making more fulfilled use of existing generator resources.

a) Project publications

Extensions of this work to improve the utility of PMSG wind turbines is planned to complete the student's PhD thesis. The following publications contain details of the project work:

1. N. David and Z. Wang, "Physical rotor inertia of DFIG wind turbines for short-term frequency regulation in low-inertia grids," 2017 IEEE Power & Energy Society General Meeting, Chicago, IL, 2017, pp. 1-5.
2. N. David, T. Prevost, F. Xavier, Z. Wang, "Model-based control addition to prescribe DFIG wind turbine fast frequency response," accepted to *Wind Energy*, Wiley, 2019.
3. N. David and Z. Wang, "Rotor-tied configuration of DFIG wind turbines for improving reactive power support capability," 2018 IEEE Power & Energy Society General Meeting, Portland, OR, 2018.
4. N. David and Z. Wang, "Functional assessment of DFIG and PMSG-based wind turbines for grid support applications," *final report*, Power Systems Engineering Research Center (PSERC), September 2018.

References

[1] NERC reliability standard BAL-001-TRE-1 Primary Frequency Response in the ERCOT Region.

[2] NERC reliability standard BAL-003-1.1 Frequency response and frequency bias setting, Nov 2015.

[3] North American Electric Reliability Corporation. *Reliability Guideline BPS-Connected inverter-based resource performance*. Technical report, North American Electric Reliability Corporation, September 2018.

[4] North American Electric Reliability Corporation. State of Reliability 2018. Technical report, June 2018.

[5] ERCOT. Future ancillary services - preparing to maintain reliability on a changing grid, July 2017.

[6] ERCOT. *Inertia: Basic concepts and impacts on the ERCOT grid*. Electric Reliability Council of Texas, April 2018.

[7] F. Milano, F. Dörfler, G. Hug, D.J. Hill, and G. Verbič. Foundations and challenges of low-inertia systems. In *20th Power Systems Computation Conference*, pages 1–25, June 2018.

[8] N.W. Miller, M. Shao, S. Pajic, and R. D'Aquila. *Western wind and solar integration study phase 3 - frequency response and transient stability*. National Renewable Energy Laboratory, Dec 2014.

[9] N.W. Miller, M. Shao, and S. Venkataraman. California iso (CAISO) frequency response study. Technical report, GE Energy, Nov 2011.

[10] North American Electric Reliability Corporation. *Frequency response standard background document*, Nov 2012.

[11] North American Electric Reliability Corporation. *State of Reliability 2017*, June 2017.

Optimizing Size of Lithium-Ion Battery Combined with PV Generation

Jinqiang Liu
Department of Electrical and Computer Engineering
Iowa State University
Ames, Iowa 50011-1046
Email: jinqiang@iastate.edu

Zhaoyu Wang
Department of Electrical and Computer Engineering
Iowa State University
Ames, Iowa 50011-1046
Email: wzy@iastate.edu

Chao Hu
Departments of Mechanical Engineering and Electrical and Computer Engineering
Iowa State University
Ames, Iowa 50011-2030
Email: chaohu@iastate.edu

***Abstract*—Lithium-ion batteries have been popular partners of photovoltaic (PV) arrays for more efficient utilization of solar energy. Although the lithium-ion battery price shows a continuously decreasing trend, it is still a challenge to deploy a cost-effective lithium-ion battery energy storage system (BESS) without financial incentives, especially for attaining higher profits. In order to maximize the profit of a lithium-ion BESS combined with a PV array, we proposed a two-stage stochastic optimization model that simultaneously determined the optimal size, charging and discharging schedules of the lithium-ion BESS. We considered that the PV-BESS could earn multi-source benefits by participating in the energy market, shaving the peak load demand, and alleviating power deviations from the forecast. Additionally, the capacity degradation of the lithium-ion battery was incorporated to estimate its lifetime and total revenue over its lifespan. The objective of our model is to maximize the BESS profit, i.e., total revenue minus cost. The BESS profit was formulated as a nonlinear function of the planning stage variable (battery size) and the operation stage variables (charging and discharging schedules). The optimization results suggested a trade-off between daily revenue and battery lifetime through optimizations of battery size and charging and discharging schedules.**

I. Introduction

Lithium-ion battery energy storage system (BESS) has become a popular partner combined with photovoltaic (PV) generation at multi-level power grids during recent years [1]–[5]. Because of the stochastic and intermittent nature of solar energy, large-scale PV penetration adds significant challenge to the supply-demand energy balance, voltage and frequency regulations of power systems, which stimulates the development of energy storage systems (ESS). As one of the most advanced storage technology, lithium-ion BESS possesses many attractive characteristics, such as high efficiency (>90%), high power density (177-676 Wh/L), fast response (in milliseconds), and low self-discharge rate (5%/month) [5]–[7]. With such excellent performance, lithium-ion BESS is thereby an ideal complement of PV generation though carrying out the electric energy time-shift and smooth the stochastic fluctuations of PV generation.

There is some research for grid applications of unspecified storage technologies stressing on planning the storage capacity [8]–[10], where the fixed or infinite lifetime is assumed for the general storage system. The same phenomenon occurs in the research for grid applications of BESS on the optimal scheduling and control to maximize day-ahead income [11]–[14]. Since these research neglect the BESS cost and capacity degradation, the optimization of schedules is simply to determine the optimal times to charge and discharge the BESS based on the price and PV generation profile. However, the capacity degradation is inevitable for grid-connected lithium-ion BESS, including calendar and cycle aging effects [15]. Some research incorporates the battery cycle aging during operation optimization, which maximize the daily profit by coordinating the daily revenue and the capacity degradation cost [16], [17]. Although these research considers the battery capacity degradation in short-term operation time-scale, the long-term cost and benefit over the battery life span is not studied.

Interesting for researchers and important for investors is to maximize the profitability of the lithium-ion BESS over its lifespan through a trade-off between increasing the daily profit and extending the battery lifetime. Atia and Yamada present an optimal sizing model for renewable energy and battery system in residential microgrids [18]. The model emphasizes on maximizing the annual overall profit of selling renewable electricity to the grid and thereby fails to identify the cost and benefit of the battery. Aldik et al. establish an optimization model for sizing the BESS to maximize the investor's long-term profit in energy and ancillary markets [19]. However, the battery capacity degradation is simply formulated as a linear function of throughput charge in above research, which neglects the significant impact of depth of cycles for on capacity degradation of lithium-ion batteries.

In this context, there is still a research gap of optimally sizing the BESS combined with PV generation for maximal lifetime profit considering multi-benefits and more accurate battery aging model. This paper aims at filling this gap. Integrating BESS with PV generation offer several benefits: (i) alleviating the deviation of the actual PV generation profile from the predicted one to avoid high balance charge [11], [20]–[22]; (ii) implementing energy arbitrage when there is a significant difference between the valley and peak electricity prices [12], [13], [23]; and (iii) reducing the demand charge when industrial or commercial load is involved [11], [16].

Although a BESS is also capable of participating in frequency regulation market [17], it may cause fast degradation and additional power deviation from the PV forecasts, which is unfavorable for the considered PV-BESS. Since the BESS size and operating schedules are coupled in modeling the revenue and capacity degradation, they will be optimized simultaneously in our model. The contributions of this paper are twofold: we utilize the calendar aging model and cycle aging model dependent on the depth of cycle and throughput charge to formulate the capacity degradation; we incorporate daily revenue decrease along with the capacity degradation in our model.

II. Model formulation

A. Electricity bill model

We suppose that the PV and battery are relatively small for the wholesale market and do not influence the electricity price, i.e., the price-takers. For simplicity, the day-ahead bidding is purely based on the PV generation and load forecast. The lithium-ion BESS carries out price arbitrage at real-time energy market. The electric bill of the electricity consumer with PV generation, BESS and load can be calculated as

$$\begin{aligned} B_d = \sum_{i\in\mathcal{I}} \rho_i \Bigg[& \sum_{j\in\mathcal{J}} c_{ij}^d P_{ij}^d + c_{ij}^r \left(P_{ij}^r + P_{ij}^b - P_{ij}^d\right) \\ & - c^b \left|P_{ij}^r + P_{ij}^b - P_{ij}^d\right| + c^p \min_{j\in\mathcal{J}} \left(P_{ij}^r + P_{ij}^b\right) \Bigg] \end{aligned} \tag{1}$$

The first term of the electricity bill is the day-ahead energy charge. The second term is the real-time energy charge. The third term is the balance penalty for the difference between the hourly scheduled energy and the real-time energy. The fourth (last) term is the demand charge proportional to the daily peak load. In this equation, $\mathcal{I}$ and $\mathcal{J}$ respectively denote the sets of scenarios and hours per day; ρ_i represents the probability of each scenario; c_{ij}^d, c_{ij}^r, c^b, and c^p represent the day-ahead price, real-time price, balance charge price, and demand charge price, respectively; P_{ij}^d, P_{ij}^r, and P_{ij}^b the hourly day-ahead power, real-time output power of PV minus load, and real-time output power of the battery.

B. Revenue of lithium-ion battery

In this study, the daily operating revenue of a lithium-ion battery is formulated as the reduction of electricity bill.

$$\begin{aligned} R_d = \Delta B_d = \sum_{i\in\mathcal{I}} \rho_i \Bigg[& \sum_{j\in\mathcal{J}} c_{ij}^r P_{ij}^b - c^b \left(\left|P_{ij}^r + P_{ij}^b - P_{ij}^d\right| \right. \\ & \left. - \left|P_{ij}^r - P_{ij}^d\right|\right) + c^p \left(\min_{j\in\mathcal{J}} \left(P_{ij}^r + P_{ij}^b\right) - \min_{j\in\mathcal{J}} P_{ij}^r\right) \Bigg] \end{aligned} \tag{2}$$

The total benefit of the battery is simply the sum of the daily revenues over the battery's lifetime. Therefore, for calculating the total revenue, we should estimate the following two terms: (i) the lifetime of the battery and (ii) its daily revenue.

1) Lifetime model: Different grid-connected applications may have largely different definitions of a battery's end of life [15]. In this PV-battery application, the lifetime of a battery is defined as the number of operating days from the beginning of life to when the battery capacity has degraded to 10% of the initial value. The lifetime prediction of a battery relies on the use of an aging model. In this study, we use the following aging model:

$$C = 1 - \alpha\left(T, V\right)\sqrt{t} - \left(\beta_0\left(V\right) + \beta_1 \Delta DoD\right)\sqrt{Q} \tag{3}$$

The above aging model takes into account both calender and cycle capacity degradation [15], [24]. The calender degradation is proportional to the square root of time $\sqrt{t}$, and the coefficient is dependent on the ambient temperature, T, and the average voltage in a charge/discharge cycle, V. The cycle degradation is proportional to the square root of the throughout charge, $\sqrt{Q}$, where the coefficient is a linear function of the depth of cycle, ΔDoD.

Based on the above aging model, setting the ambient temperature as 25 °C and average voltage in a cycle as the voltage at 50% state of charger (SoC), the lifetime of a battery can be calculated as

$$n_{life} = \frac{0.9^2}{\left(\alpha + \sqrt{\sum_{i\in I}\sum_{l\in L_i} 2\rho_i \Delta DoD_{il} (\beta_0 + \beta_1 \Delta DoD_{il})^2}\right)^2} \tag{4}$$

Cycle counting in grid applications is often difficult and may become computationally intractable when embedded into an optimization model [23], [25]. Hence, we propose a conservative approximation of the battery lifetime by assuming that all throughcharge during a day follows the maximal depth of cycle. The estimation of lifetime can then be rewritten as

$$n_{life} = \frac{0.9^2}{\left(\alpha + \sqrt{\sum_{i\in I}\sum_{j\in J} \rho_i (\beta_0 + \beta_1 \Delta DoD_{\max,i})^2 \left|P_{ij}^b\right| / C_0}\right)^2} \tag{5}$$

where C_0 is the battery sized defined as the initial energy capacity, and $DoD_{\max,i}$ is the maximal depth of cycle on the ith scenario day.

2) Revenue on an equivalent day: An equivalent day considers the expectation of all possible scenarios in a typical day of operation. As the capacity of a battery decreases due to calendar and cycle degradation, the benefit of the battery also decreases. Therefore, the revenue of the battery decays with aging. The actual capacity of the battery in the tth equivalent day takes the following form

$$C_t = C_0 \left(1 - \sqrt{\frac{t}{n_{life}}}\right) \tag{6}$$

Assuming the same SoC profile for every equivalent day, the charge and discharge power of the battery on a specific day are both proportional to its available capacity on that day. We then claim that daily revenue is also proportional to the available capacity. First, according to (2), this claim is strictly held for energy arbitrage and balance charge reduction components. In terms of demand charge reduction component, when charge and discharge power decrease along with the capacity, the time point of load peak keeps unchanged but the reduction of load peak shrinks with a ratio the same as charge power and capacity, so the above claim is strictly held. However, when charge and discharge power increase along with the capacity, the growth rate of reduction of load peak is less than or equal to the increase rate of charge power and capacity, depending on the net load consumption profile. Since the battery charge and discharge power are supposed to decrease with the capacity degradation in our study, so the total revenue is indeed proportional to the charge and discharge power, and the available capacity. It then follows that the daily revenue of the battery in the tth equivalent day can be expressed as the following:

$$R_d\left(C_t\right) = R_d\left(1 - \sqrt{\frac{t}{n_{life}}}\right) \tag{7}$$

By adding up the daily revenues of the battery over its lifetime, we then obtain the total revenue, expressed as

$$R_{total} = \sum_{k=1}^{n_{life}} \left(1 - \sqrt{\frac{k}{n_{life}}}\right) R_d\left(C_0\right) \approx \frac{n_{life}}{3} R_d\left(C_0\right) \tag{8}$$

C. Optimization model

1) Objective function: The aim of our study is to maximize the net profit of the battery by varying its size C_0 and operating schedule $\mathbf{P^b}$. Therefore, the objective of our optimiztion problem is to maximize the net profit function, i.e., total revenue minus initial investment, that takes the following form:

$$\max_{\mathbf{P^b}, C_0} R_{total} - c^B C_0 \tag{9}$$

where c^B indicate the price per kWh of lithium-ion BESS, encompassing the costs of the battery pack, power electronics converters, and energy management system.

We formulate this optimization problem in a way that makes it possible to achieve an optimal balance between battery performance exploitation and lifetime extension. For a battery with a fixed size, it is desirable to find an appropriate depth of discharge in a cycle that yields a good balance between maximizing daily revenue and minimizing battery degradation. When the battery size (i.e., initial capacity) is included in the optimization problem as a planning state variable, it brings about the trade-off between increasing the battery size to enable a shallower depth of discharge (thus a longer lifetime) and shrinking the battery size to reduce the initial investment cost.

2) Constraints: This optimization model considers several operating constraints of the battery, including the energy level constraints, power limitations, and continuity requirement.

The energy level of the battery should fall into the range from zeros to its available capacity.

$$0 \leq E_{i0}^b - \sum_{k=1}^{j} P_{ik}^b \leq C_0, \text{ for } (i,j) \in (\mathcal{I}, \mathcal{J}) \tag{10}$$

where E_{i0}^b indicates the initial energy level of the battery.

Too large output power will increase the stress or investment of power electronics converters and accelerate the degradation of battery. So the charge/discharge power is limited to be less than or equal to the power that can charge/discharge the fully discharged/charged battery in one hour at its beginning of life.

$$-C_0 \leq P_{ij}^b \leq -C_0, \text{ for } (i,j) \in (\mathcal{I}, \mathcal{J}) \tag{11}$$

For operating continuity and fair evaluation of the revenue of the battery, the energy level at the end of one day is required to be the same as its initial value at the start of the next day.

$$E_{i0}^b = E_{i0}^b + \sum_{j \in \mathcal{J}} P_{ij}^b, \text{ for } i \in \mathcal{I} \tag{12}$$

In addition, some practical limitations should be taken into account for avoiding meaningless results. Specifically, we set the size of the battery to be greater than zero and its lifetime to be less than 7,300 days (20 years).

$$C_0 > 0 \tag{13}$$

$$n_{life} < 7,300 \tag{14}$$

III. Case Study

We consider a lithium-ion BESS combined with 500 kW PV generation and local load demand. The load and PV generation are simply modeled as the foretasted and actual output power without considering the transmission and distribution networks. In the rest of this section, we further formulate the optimization problem solve it using an existing nonlinear optimization algorithm.

A. Data description

We use real-world data to represent PV generation and load consumption. Additionally, energy market price data is incorporated for the calculation of daily revenue. The demand charge and balance charge prices are set based on literature [11], [26]. Table I provides a complete list of datasets used in this study. The persistence method is used to forecast the load profile [27]. The load prediction for one specific day (e.g., day A) is the real load data on the same day last week (e.g., day A−7).

For the cost data, we consider the incremental cost of installing lithium-ion BESS combined with PV system compared to the standalone PV system. The co-locating BESS and PV system produces cost saving by sharing hardware, land acquisition etc. The unit cost is set as $\$312.5/kWh$ according to the results in [28].

TABLE I
SUMMARY OF REAL-WORLD DATASETS USED IN THE STUDY

Name of dataset	Time period	Time interval	Source
Actual PV power series	01/08/2006-12/31/2006	5 min	NREL
Day-ahead forecasted PV power series	01/08/2006-12/31/2006	1 hour	
Actual load profile	01/08/2004-12/31/2004	1 hour	OpenEI
Day-ahead forecasted load profile	01/08/2014-12/31/2004	1 hour	Persistence
Day-ahead and real-time LMP	01/05/2017-12/28/2017	1 hour	PJM

TABLE II
PROBABILITIES OF SCENARIOS

Scenarios	S1	S2	S3	S4	S5	S6
Probability	0.0726	0.2039	0.2598	0.1758	0.1536	0.1341

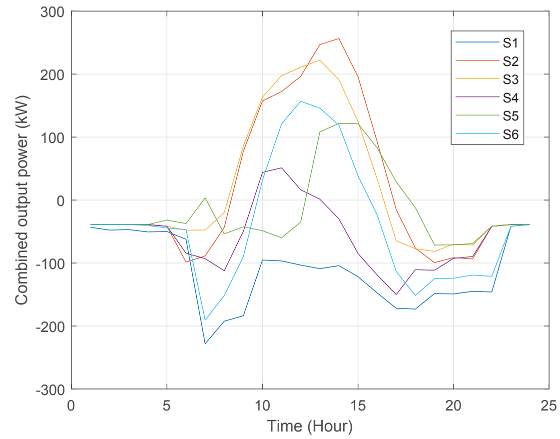

Fig. 1. Combined output power curves (PV minus load) of the six scenarios

B. Scenarios

Scenarios are utilized to represent the uncertainty of PV generation, load, and electricity price. We use the K-means method to divide the one-year sample into six distinct scenarios. The probability of each scenario is estimated as its proportion among the population and the probabilities of the six scenarios are listed in Table II. The combined output power curves (PV minus load), and real-time and day-ahead locational marginal pricing (LMP) curves of the scenarios are shown in Fig. 1−3, respectively. From the curves in Fig. 1, we can see that for sometime during the day the PV generation is larger than the load consumption, while for other times the PV generation cannot cover the load consumption. From Figs. 2 and 3, two different scenarios may have very different electricity price profiles and a day-ahead LMP curve is generally smoother than a real-time LMP.

With the introduction of the scenarios and their probabilties, an average scenario (i.e., during an equivalent day) can be established by doing a weighted-sum of all six scenarios with the weights being their probabilities [16], [25]. The daily revenue and battery degradation mentioned earlier are all calculated based on the average scenario during an equivalent day.

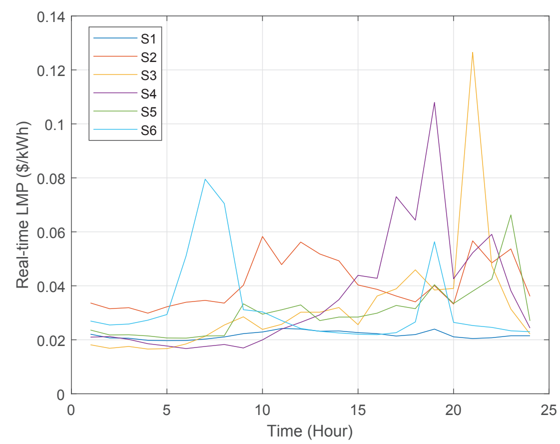

Fig. 2. Real-time LMP curves of the six scenarios

C. Optimization results

We use the MATLAB optimization toolbox (@fmincon) to solve the nonlinear optimization problem in search for a local optimal solution. The optimal size of the battery is found to be 123.5 kWh, and the corresponding lifetime is 20 years. The battery's profit over its life-span is $32,541, while its investment is $38,603. The maximal ΔDoD_{max} is shown in Table III for all six scenarios.

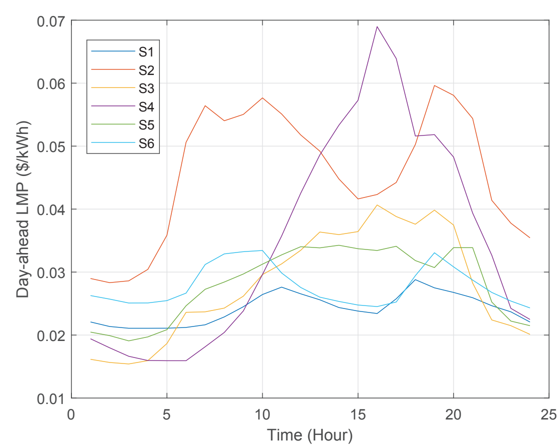

Fig. 3. Day-ahead LMP curves of the six scenarios

TABLE III
OPTIMAL MAXIMAL DEPTHS OF DISCHARGE FOR ALL SIX SCENARIOS

Scenarios	S1	S2	S3	S4	S5	S6
ΔDoD_{max}	0.67	0.50	0.67	0.73	0.63	0.76

The optimal schedule of the battery finds the trade-off between gaining more revenue and prolonging battery lifetime. Take the sixth scenario S6 as an example. The

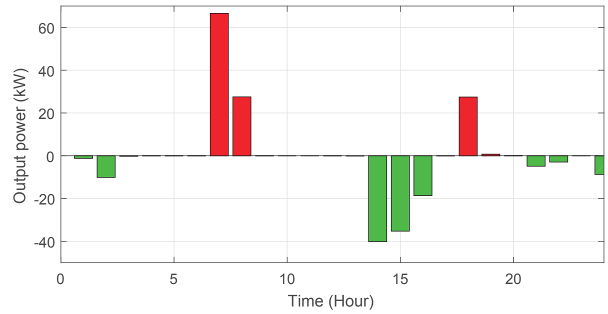

Fig. 4. Optimal output power of battery in S6

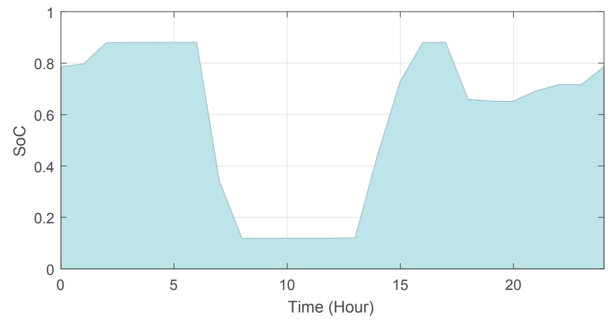

Fig. 5. Optimal SoC curve of battery in S6

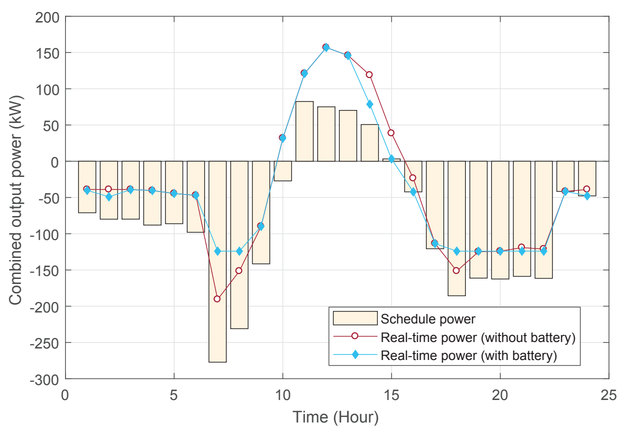

Fig. 6. Combined output power in S6

charge/discharge power schedule is shown in Fig. 4. Based on the initial energy level and charge/discharge power schedule, we obtain the SoC curve of the battery, shown in Fig. 5. We can see the energy level of the battery is always within the physical range [0, 1].

The scheduled and real-time output power curves are shown in Fig. 6. The real-time LMP curve in S6 is presented in Fig. 7. From these figures, we can see that the battery tries to level the load peak and reduce the demand charge at hours 7, 8, and 18−22. While at the non-peak time points, such as hours 14-16, the battery tends to alleviate the deviation of real-time combined output power from the scheduled value and to reduce the balance charge. Also, the battery significantly

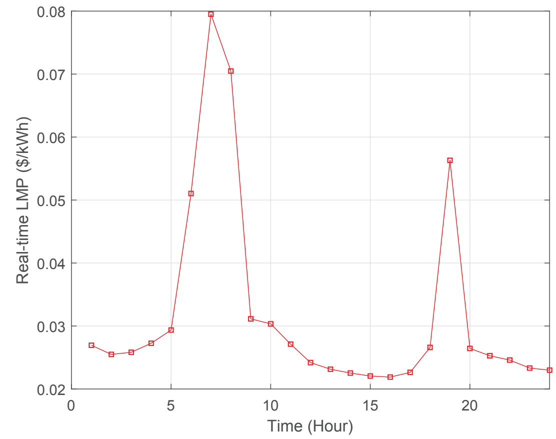

Fig. 7. Real-time LMP in S6

store electricity at a low price level (e.g., at hour 15) and sell it at a high price rate (e.g., at hour 7), which is essentially implementing energy arbitrage.

Sometimes, there are natural conflicts among multi services: energy arbitrage, peak shaving, and power deviation reduction, such as at hours 7, 8, and 18−22. Our optimization model manages to deal with these conflicts and yield the compromise among them by coordinating the dynamic revenue and degradation cost for each service.

From the aforementioned analysis, we can see that the obtained optimal solution makes great sense and offers us a cost effective BESS planning and operation options. Even though the solution by Matlab toolbox may be a local minimum due to the nonconvex optimization model, we still provide researchers and investors an effective and innovative methodology to determine the optimal size of lithium-ion battery paired with PV generation.

IV. Conclusions and Future Work

By taking into account the battery capacity degradation and corresponding revenue decrease, we develop a battery size optimization model to maximize long-term profit. Our proposed model is capable of finding a trade-off between gaining more daily revenue and prolonging battery lifetime. The case study based on real-world data shows that our model could provide the investors a cost-effective battery planning and operation scheme with a decent return on investment. In the future work, we plan to involve new established five-minute real-time energy market into the optimization model.

References

[1] N. Kakimoto and R. Asano, "Linear operation of photovoltaic array with directly connected lithium-ion batteries," *IEEE Transactions on Sustainable Energy*, vol. 8, no. 4, pp. 1647–1657, 2017.

[2] B. Liu, L. Wang, D. Song, M. Su, J. Yang, D. He, Z. Chen, and S. Song, "Input current ripple and grid current harmonics restraint approach for single-phase inverter under battery input condition in residential photovoltaic/battery systems," *IEEE Transactions on Sustainable Energy*, vol. 9, no. 4, pp. 1957–1968, 2018.

[3] A. Nadkarni, A. Maktal, G. G. Karady, and K. Alteneder, "Value analysis of 2 kw/4.4 hour energy storage in residential pv systems in arizona," in *2013 IEEE Power & Energy Society General Meeting*. IEEE, 2013, pp. 1–5.

[4] J. Song, V. Krishnamurthy, A. Kwasinski, and R. Sharma, "Development of a markov-chain-based energy storage model for power supply availability assessment of photovoltaic generation plants," *IEEE Transactions on Sustainable Energy*, vol. 4, no. 2, pp. 491–500, 2013.

[5] H. Hesse, M. Schimpe, D. Kucevic, and A. Jossen, "Lithium-ion battery storage for the grida review of stationary battery storage system design tailored for applications in modern power grids," *Energies*, vol. 10, no. 12, p. 2107, 2017.

[6] T. Kousksou, P. Bruel, A. Jamil, T. El Rhafiki, and Y. Zeraouli, "Energy storage: Applications and challenges," *Solar Energy Materials and Solar Cells*, vol. 120, pp. 59–80, 2014.

[7] G. Graditi, M. Ippolito, E. Telaretti, and G. Zizzo, "Technical and economical assessment of distributed electrochemical storages for load shifting applications: An italian case study," *Renewable and Sustainable Energy Reviews*, vol. 57, pp. 515–523, 2016.

[8] P. Harsha and M. Dahleh, "Optimal management and sizing of energy storage under dynamic pricing for the efficient integration of renewable energy," *IEEE Transactions on Power Systems*, vol. 30, no. 3, pp. 1164–1181, 2015.

[9] Y.-Y. Hong and M.-Y. Wu, "Markov model-based energy storage system planning in power systems," *IEEE Systems Journal*, 2019.

[10] E. Nasrolahpour, S. J. Kazempour, H. Zareipour, and W. D. Rosehart, "Strategic sizing of energy storage facilities in electricity markets," *IEEE Transactions on Sustainable Energy*, vol. 7, no. 4, pp. 1462–1472, 2016.

[11] Z. Wang, A. Negash, and D. S. Kirschen, "Optimal scheduling of energy storage under forecast uncertainties," *IET Generation, Transmission & Distribution*, vol. 11, no. 17, pp. 4220–4226, 2017.

[12] B. Cheng and W. B. Powell, "Co-optimizing battery storage for the frequency regulation and energy arbitrage using multi-scale dynamic programming," *IEEE Transactions on Smart Grid*, vol. 9, no. 3, pp. 1997–2005, 2018.

[13] D. Krishnamurthy, C. Uckun, Z. Zhou, P. R. Thimmapuram, and A. Botterud, "Energy storage arbitrage under day-ahead and real-time price uncertainty," *IEEE Transactions on Power Systems*, vol. 33, no. 1, pp. 84–93, 2018.

[14] H. Mohsenian-Rad, "Optimal bidding, scheduling, and deployment of battery systems in california day-ahead energy market," *IEEE Transactions on Power Systems*, vol. 31, no. 1, pp. 442–453, 2016.

[15] J. Schmalstieg, S. Käbitz, M. Ecker, and D. U. Sauer, "A holistic aging model for li (nimnco) o2 based 18650 lithium-ion batteries," *Journal of Power Sources*, vol. 257, pp. 325–334, 2014.

[16] Y. Shi, B. Xu, D. Wang, and B. Zhang, "Using battery storage for peak shaving and frequency regulation: Joint optimization for superlinear gains," *IEEE Transactions on Power Systems*, vol. 33, no. 3, pp. 2882–2894, 2018.

[17] B. Xu, Y. Shi, D. S. Kirschen, and B. Zhang, "Optimal battery participation in frequency regulation markets," *IEEE Transactions on Power Systems*, vol. 33, no. 6, pp. 6715–6725, 2018.

[18] R. Atia and N. Yamada, "Sizing and analysis of renewable energy and battery systems in residential microgrids," *IEEE Transactions on Smart Grid*, vol. 7, no. 3, pp. 1204–1213, 2016.

[19] A. Aldik, A. T. Al-Awami, F. Alismail *et al.*, "Fuzzy optimization-based sizing of a battery energy storage system for participating in ancillary services markets," in *2018 IEEE Industry Applications Society Annual Meeting (IAS)*. IEEE, 2018, pp. 1–7.

[20] A. Attarha, N. Amjady, and S. Dehghan, "Affinely adjustable robust bidding strategy for a solar plant paired with a battery storage," *IEEE Transactions on Smart Grid*, 2018.

[21] A. Cervone, G. Carbone, E. Santini, and S. Teodori, "Optimization of the battery size for pv systems under regulatory rules using a markov-chains approach," *Renewable Energy*, vol. 85, pp. 657–665, 2016.

[22] A. González-Garrido, A. Saez-De-Ibarra, A. Milo, H. Gaztañaga, and P. Eguia, "Sensitivity analysis of the storage system sizing for solar plants in energy and reserve markets," in *2018 15th International Conference on the European Energy Market (EEM)*. IEEE, 2018, pp. 1–5.

[23] G. He, Q. Chen, C. Kang, and Q. Xia, "Optimal operating strategy and revenue estimates for the arbitrage of a vanadium redox flow battery considering dynamic efficiencies and capacity loss," *IET Generation, Transmission & Distribution*, vol. 10, no. 5, pp. 1278–1285, 2016.

[24] A. Barré, B. Deguilhem, S. Grolleau, M. Gérard, F. Suard, and D. Riu, "A review on lithium-ion battery ageing mechanisms and estimations for automotive applications," *Journal of Power Sources*, vol. 241, pp. 680–689, 2013.

[25] G. He, Q. Chen, C. Kang, P. Pinson, and Q. Xia, "Optimal bidding strategy of battery storage in power markets considering performance-based regulation and battery cycle life," *IEEE Transactions on Smart Grid*, vol. 7, no. 5, pp. 2359–2367, 2016.

[26] J. McLaren, "A survey of u.s. demand charges."

[27] Y. Chu, H. T. Pedro, A. Kaur, J. Kleissl, and C. F. Coimbra, "Net load forecasts for solar-integrated operational grid feeders," *Solar Energy*, vol. 158, pp. 236–246, 2017.

[28] R. Fu, T. W. Remo, and R. M. Margolis, "2018 us utility-scale photovoltaics-plus-energy storage system costs benchmark," National Renewable Energy Lab.(NREL), Golden, CO (United States), Tech. Rep., 2018.

Co-Optimized Expansion Planning to Enhance Resilience of the Electrical System in Puerto Rico

Cody J. Newlun[1], Armando L. Figueroa[2], James D. McCalley[1]
[1]Department of Electrical & Computer Engineering, Iowa State University, Ames, Iowa 50011, USA
[2]Policy Studies Department, MISO, Eagan, Minnesota 55121, USA
cnewlun@iastate.edu, afigueroa-acevedo@misoenergy.org, jdm@iastate.edu

***Abstract*—In September of 2017, the island of Puerto Rico (PR) was devastated by a category 4 hurricane, Hurricane Maria. The island experienced complete blackout and full restoration of the electrical system took nearly 11 months to complete. Therefore, it is of high-interest to re-develop the infrastructure at the generation, transmission, and distribution (GTD) levels to create a hurricane-resilient infrastructure. This report details the methodologies behind developing a more resilient electric infrastructure using a co-optimized expansion planning (CEP) software tool. First, a model of the PR electric power system was developed to perform long-term CEP studies. The CEP tool developed seeks the minimum total cost of the PR system in a 20-year planning horizon while exploring various levels of expansion investment options. The CEP also models the system under extreme events (i.e. hurricanes) to allow for data-driven resilience enhancement decisions. Second, the report details infrastructure visions that contain resiliency investment options while the amount of distributed generation (DG) and centralized resource investments vary. Lastly, key findings from these visions are reported and the performance of the CEP model is discussed**

***Index Terms*—resiliency, expansion planning, hurricane events, distributed generation, optimization**

I. Introduction

The electric infrastructure on the island of PR is in dire need of transformation in order to withstand powerful hurricanes and avoid the devastation that the island experienced from Maria [1]. This report is intended to provide possible solutions to transform the electric infrastructure of PR to be more resilient, economic, and practical. Resilience is a widely used topic that can take on different meaning and can be confused with the term reliability. A report written by Pacific Northwest National Laboratory details the issue between defining resilience and reliability. They define resilience as the ability to withstand grid stress event without suffering operational compromise or to adapt to the strain so as to minimize compromise via graceful degradation [2].The presidential policy Directive 21 defines the term resilience as the ability to prepare for and adapt to changing conditions and withstand and recover rapidly from disruptions [3],[4]. These definitions are used throughout this study to form an understanding of the models overall performance and ability to formulate an infrastructure with the integrity to withstand extreme natural disasters.

The island of Puerto Rico is a commonwealth of the United States that lies in the Caribbean Sea as a part of the Greater Antilles. As seen in Figure 1, PR is susceptible to extreme hurricane events [5]. With an ever-changing climate and uncertainty of the frequency of strong hurricanes, such as Maria, it is crucial to study these hurricanes and use their data to help make investment decision. Thus, the CEP model developed for PR seeks to improve the resilience of system in order develop a more robust infrastructure that can withstand multiple hurricanes events.

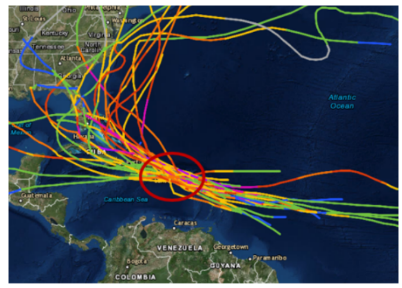

Fig. 1: Historical paths of hurricanes through PR (red circle)

A. Electric System of Puerto Rico

To meet the islands energy needs and due to no reserves of conventional fuels, the island relies heavily on imported fossil fuels. Figure 2 below details the fuel types used for centralized existing generation units.

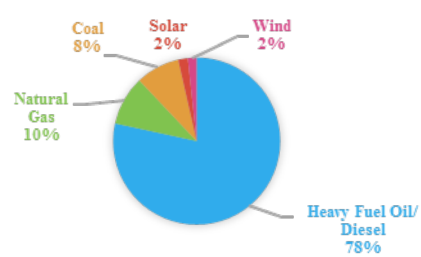

Fig. 2: Fuel types of existing generation sources in PR [6]

Figure 3 displays the existing generation and transmission infrastructure. The islands electric infrastructure is owned and operated by the Puerto Rico Electric Power Authority (PREPA). PREPA has an installed centralized generation capacity of 5,839 MW. The AES coal plant and EcoEléctrica Cogeneration plant are privately owned and contribute 454 MW and 507 MW respectively. The transmission network consists of 2,478 miles of lines at the 230 kV, 115 kV, and 38 kV voltage levels [7]–[9]. The database used in this study contains approximately 102 transmission buses with 75 of those buses being load buses. The transmission network contains approximately 135 lines at the 230 kV and 115 kV. The distribution system is modeled as well containing 225 distribution buses and 225 distribution segments. A schematic of this distribution feeder system is displayed in Figure 11.

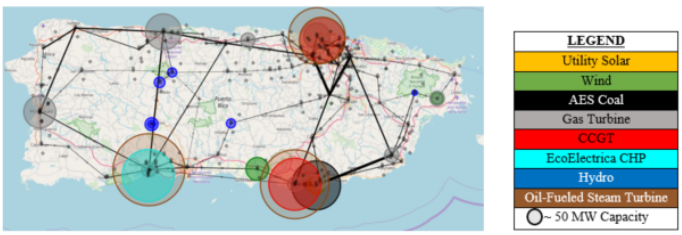

Fig. 3: Existing electrical infrastructure on the island of PR

The island of PR is roughly 110 miles long and 35 miles wide with a wide range of terrain types. Figure 4 displays the terrain types on the island [10]. Figure 5 provides the location of the load centers at the transmission level. A major issue the island faces with the current network topology is dependence of the majority of the load centers located in the north relying on the majority of the generating sources in the south.

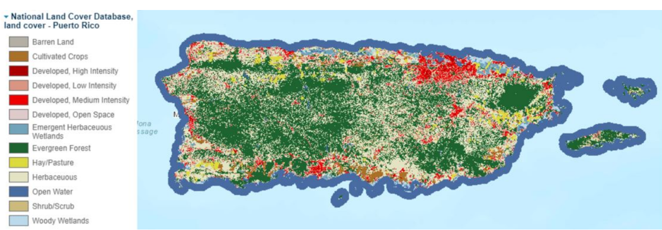

Fig. 4: Terrain types in PR

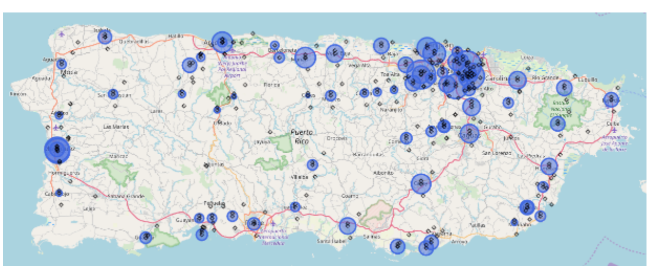

Fig. 5: Load centers on the island of PR

Due to the mountainous terrain in the center of the island that separate the load centers from the generators, the current infrastructure is deemed vulnerable during a natural disaster such as a hurricane. This is yet another motive to evaluate the penetration of DG into the system.

B. Co-Optimized Expansion Planning (CEP)

For the purposes of this report, a highly vetted co-optimized expansion planning (CEP) model is being used to conduct a 20- year simulation on the infrastructure of PR. The overall function of this model is to form a mixed integer linear program (MILP) that seeks to minimize the overall costs of the system while following several constraints that are specified by the user.

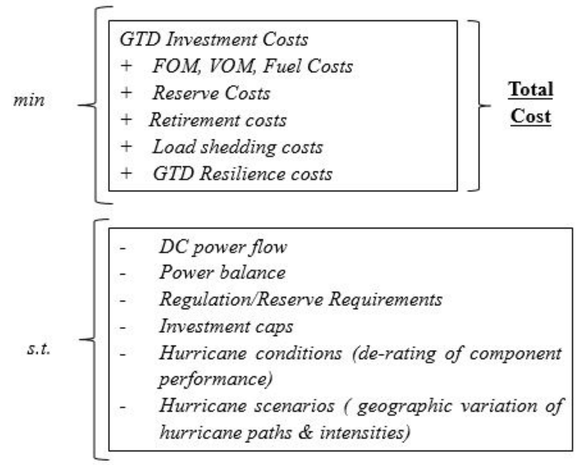

Fig. 6: High-level view of the CEP model developed for the PR system

The model used in this study was adapted from previous work completed for larger systems in the continental United States [11]. Figure 6 provides a high-level view of the model developed to increase resiliency of the PR system. The conventional CEP models simulate the operational and investment decisions over *N* years based on several assumptions such as fuel prices, investment costs, load growth, and wind/solar performance. The model developed for PR utilizes the functionality of the conventional CEP with the addition of providing the system the ability to enhance the resiliency.

II. Database Development

Hourly load profiles were developed utilizing publicly available data from PREPA [7]. Overall, the island of PR does not see much seasonal variation in load due to a steady climate. Figure 7 displays the yearly 8760 hourly load profile for the PR system being modeled. This figure represents the systems load profile for 2014.

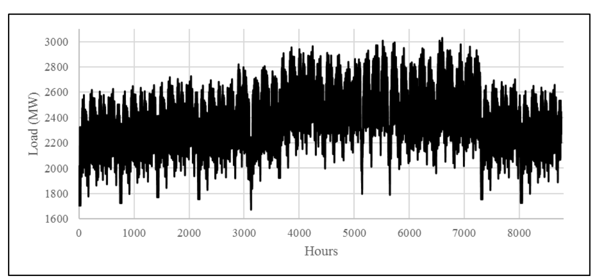

Fig. 7: Annual load profile of the PR system

This load data was used to develop load blocks to construct characteristic operating conditions for both hurricane years and non-hurricane. The system contains 75 load buses where the load is allocated based off a power flow snapshot of the system from 2014 data. Due to the decreasing population in PR, no annual load growth was taken into account for the CEP simulations in this study. Several sources were used to evaluate the operating conditions of the new and existing generation technologies in the PR. Projected fuel prices for the islands thermal unit fleet are displayed in Figure 8 [12].

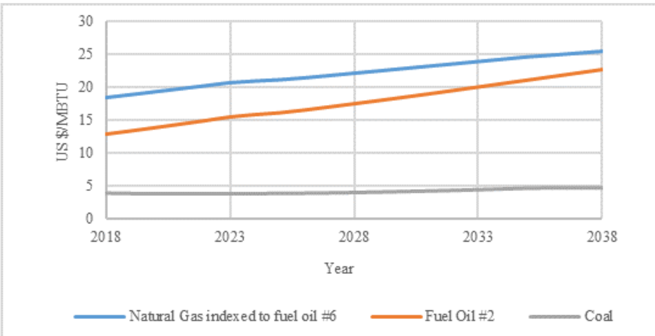

Fig. 8: Projected fuel prices in PR though 2038

A. Investment Costs

Line terrain multipliers are also considered due to the diverse terrain types in Puerto Rico, as seen in Figure 4. In order to capture the effect of the terrain type on the investment decisions four terrain types and their respective multipliers are considered: urban, farmland, mountainous, and suburban. Table 1 provides the assigned cost multipliers used for the PR model [13].

TABLE 1: Line Terrain Cost Multipliers

Line Terrain	Cost Multiplier
Urban	1.59
Farmland	1
Forested/ Mountain	2.25
Suburban	1.27

Expansion costs of each line was calculated based off line distances and costs were developed on a $ /MW-mile basis from previous studies [11]. To accurately allow the model to make generation investments at the most appropriate year, the change in capital expense (CAPEX) of each candidate technology was taken into account. Figure 9 provides the maturation of candidate generation technologies' CAPEX as provided by NRELs Annual Technology Baseline [14].

B. Wind / Solar Profiles

In order to accurately model the performance of solar and wind technologies, capacity factors were developed using NRELs PVWATTS calculator [15], NRELs System Advisor Model [16] and NOAAs National Data Buoy Center [17]. This allowed for solar and wind profiles to be constructed for every hour within a year and for every bus location. The wind profiles were modeled to be at a hub-height of 100m and to have the power output of a Vestas V100 (2MW). Offshore

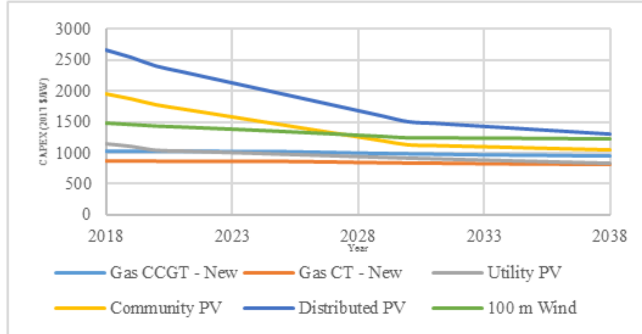

Fig. 9: CAPEX of candidate generation technologies through 2038

wind turbines were not considered in this study due to their vulnerability to hurricanes.

Fig. 10: Solar irradiance map of PR (W/m^2)

Solar profiles were calculated for large-scale ground mounted plant and for rooftop installation. Figure 10 displays the solar irradiance on the island of PR [18]. For each transmission bus, an hourly solar profile was calculated for round mounted PV and for every distribution bus, hourly profiles were developed for rooftop PV technologies. These candidate solar technologies are considered to be fixed-axis. Single and dual-axis tracking PV technologies were not considered due to their lack of structural integrity during natural disasters.

III. Methodologies

A. Baseline CEP Modeling Features

The distribution system is modeled as a 3-segment feeder that is placed at the load buses of the PR system. This is an important aspect for PR due to the high interest in distributed energy resources (DER). This modeling feature has been adapted from the previous work of P. Liu and S. Sharma and their work with the Bonneville Power Administration system [19]. Figure 11 details the 3-segment feeder that is placed at all 75 specified load buses in the PR system. The load allocation is detailed in Figure 11 and is approximately 1/2, 1/3, and 1/6 of the load level at the transmission bus respectively.

Regulation and reserve constraints are included in the model in order to meet certain operating levels on the island. All generators are subject to maintaining a minimum stable level as specified by the 2017 Siemens Integrated Resource Plan (IRP) [12]. Ramping up and ramping down parameters are also calculated by the model and the corresponding cost is

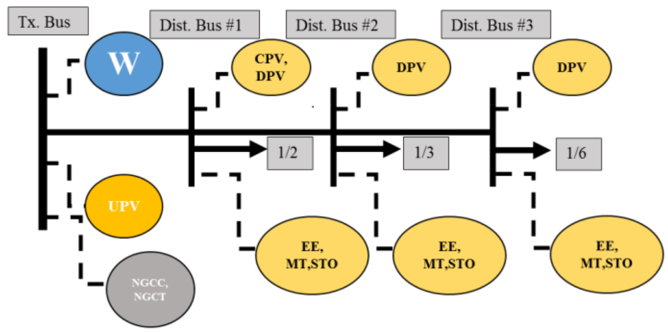

Fig. 11: 3-segment distribution feeder placed at load buses

included in the objective function. Each eligible generator is also subject to providing a contingency reserve (CR). For this study the ramping parameters, are set at 10% of the systems demand in the particular load block. The contingency reserve is assumed to be 5% of the systems demand in the particular load block. Note, in order to meet the peak demand, these constraints are not deployed during the peak load block. These constraints are also not deployed during hurricane years due to the de-rating of the systems performance.

A system wide planning reserve margin (PRM) of 40% was chosen to be implemented. This high PRM is common when modeling isolated systems such as in PR due to the lack of interconnection with other systems. In order to calculate the PRM, capacity credits for generation technology were assigned. Table 2 details the assigned capacity credits for each generating resource.

TABLE 2: Capacity credits for generation technology

Technology	Capacity Credit
PC	1.00
NGCC	1.00
CT	1.00
Wind	0.15
Oil	1.00
Utility PV	0.40
Comm. Rooftop PV	0.40
Dist. Rooftop PV	0.40
Microturbine (MT)	1.00
Energy efficiency (EE)	1.00
Dist. Storage	0.94

Fig. 12: planning regions utilized by PREPA [7]

Another modeling feature considers planning reserve margins within the planning regions of PREPA, as seen in Figure 12. For this study a regional PRM of 30% is used. The motivation for this feature is to allow the model to build resources geographically close to the load and identify what resilience investments need to be made across the island.

Each generator in the system has a specific minimum operating level as specified by PREPA [7]. It is important to note that the minimum stable level is enforced only in years where hurricanes are not effecting the system. These reserve requirements play a vital role in the investment decision-making process especially when the system is exposed to hurricane conditions. A complete model formulation with the reserve requirements can be found in the Appendix. Figure 11 also displays the candidate technologies available for investment throughout the simulations. Table 3 provides these candidate technologies along with their respective maximum investable capacity at each bus and the maximum annual investable capacity for the entire system. These investment caps were put into place to provide a realistic build-out plan and to help model the availability of funding, resources and labor.

TABLE 3: Generation candidates' investment caps

Investment Candidates	Candidate Capacity (MW per bus)	Maximum Annual Invested Capacity (MW)
NGCC	500	500
NGCT	500	500
Utility PV	100	1000
Comm. Rooftop PV	50	500
Dist. Rooftop PV	20	500
Wind	100	1000
Micro-Turbine (MT)	1.00	50
Dist. Storage	1.00	50
EE	0.5	2% of Peak

Under normal operating conditions, DC power flow analysis is used to calculate the power flow of transmission lines and distribution segments. This is appropriate so that the system performs within its physical limitations. During hurricane conditions, however, DC power flow is not used due to the resilience line candidates that are available for investment opportunities. Thus, for hurricane years the transportation model is used for all resilience candidate circuits [20]. Line losses are also modeled using a linear loss approach as detailed in source [21]. Transmission lines and distribution segments are modeled with an efficiency of 97% and 95% respectively.

Lastly, in order for the net present value (NPV) to be modeled correctly for each year a discount factor of 5.7% is used. End-effects are also taken into account by assuming a 20-year horizon.

B. Hurricane Modeling

Due to the severe devastation to the PR electrical system caused by Hurricane Maria, it is of great interest to incorporate hurricane conditions into the model to influence investment decisions towards a more resilient system. The major contribution of this work is to incorporate a hurricanes influence on the electrical system and then evaluate its effect and use that information to make an investment decision [22]–[24]. Within the CEP formulation, each year is denoted as either a year with a hurricane occurrence or a year without a hurricane occurrence. These years both are made up of load blocks that are characteristic to that years operating condition. For a hurricane year, five hurricane periods (HP) have been developed with each HP being divided into hurricane blocks (HB). Table 4 and Table 4 and Table 5 provides a breakdown of each HP and HB that make up a hurricane year respectively. The HPs are constructed in increasing order of amount of time they span because of a hurricane event occurring. For instance, HP #1 has a duration of 24 hours and represents the day that the hurricane event occurs. HP #2 through #5 signify sections of time after the hurricane to assist with modeling recovery efforts of the systems components. The HBs are simply used to develop proper load profiles that correspond to the time of day in each hurricane period. It is also assumed that every hurricane year is an investment year.

TABLE 4: Breakdown of hurricane periods

Hurricane Period	Time within year	Corresponding Event
1	0-23	Hurricane occurring
2	24-192	Week after hurricane
3	193-912	Month after hurricane
4	913-4512	5 months after hurricane
5	4513-8760	Remaining 6 months

TABLE 5: Breakdown of hurricane blocks

Hurricane Block	Time of Day
1	11pm-6am
2	7am-1pm
3	2pm-6pm
4	7pm-10pm

Non-hurricane years, on the other hand, are modeled to represent normal operating conditions for the system. There was nine load blocks developed to capture the normal operating conditions. The blocks correspond to the two seasons in PR (rainy and dry) and the time of day. Table 6 details the breakdown of each load block for a non-hurricane year.

Note, that load block 9 is denoted as a peak block and consists of the top 40 hours extracted from block 7, which was where the system experienced the annual peak load. Non-hurricane years also have the option to be investment years.

TABLE 6: Breakdown of non-hurricane blocks

Hurricane Block	Season	Time of Day	# of hours
1	Rainy	11pm-6am	1712
2	Rainy	7am-1pm	1498
3	Rainy	2pm-6pm	1498
4	Rainy	7pm-10pm	1070
5	Dry	11pm-6am	1208
6	Dry	7am-1pm	1057
7	Dry	2pm-6pm	755
8	Dry	7pm-10pm	604
9	Peak	-	40

For the entire planning horizon, the CEP formulation is built up of three types of years: hurricane, non-hurricane investment years, and non-hurricane operational years. For each hurricane year, a series of six unique hurricane scenarios are modeled. The hurricane scenarios are explained later in this report.

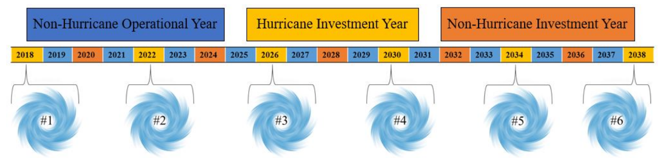

Fig. 13: Planning horizon used for PR CEP simulations

In an effort to develop a more resilient system that is able to withstand and bounce back after a natural disaster, three levels of resiliency have been developed for transmission lines, distribution segments, solar candidates, and wind candidates. For conceptual purposes, these levels are defined as standard resilience, semi-resilience, and full-resilience. These levels are defined to have an increasing amount of resilience to significant hurricane events as well as an increasing cost multiplier. In this study the cost multiplier for the standard, semi, and full resilient levels are denoted to be 1, 1.5, and 2 respectively. For transmission lines, fragility curves, which provide the failure probabilities as a function of wind speeds, have been heavily researched and accepted as a valid method to identify line failures [22], [25]. Figure 14 displays the fragility curves that were used in this study for analyzing wind speeds influence on overhead transmission lines and distribution segments.

To distinguish the performance of higher resilient levels from the accepted standard level, the fragility curves of the semi and full resilient levels were shifted to the right by 20 mph and 40 mph respectively. Therefore, the higher resilient levels are able to sustain a higher wind speed. Performance of the different resilient levels also has a temporal component to it. In Table 7, the performance status of technology for each resilient level with respect to the hurricane periods within the hurricane year.

TABLE 7: Performance status of each resilience level

Hurricane Period	Standard	Semi	Full
1	***De-Rated***	***De-Rated***	***De-Rated***
2	***De-Rated***	***De-Rated***	Normal
3	***De-Rated***	***De-Rated***	Normal
4	***De-Rated***	Normal	Normal
5	Normal	Normal	Normal

If the technology has the performance status of de-rated, that technology will perform as it would under the hurricane conditions. For example, a standard line or resource will be de-rated in hurricane periods 1-4, which represents the hurricane event and the following five months. If the technology has a normal performance, that technology will be able to operate as it would in a non-hurricane year. These different levels of resilience are generalized levels and represent different classes of grid hardening techniques and practices. Several references are available to further define these resilience levels for solar, wind, transmission, and distribution technologies [26]–[29], however for the purposes of this study these resilience levels will remain categorized simply by their performance under hurricane conditions.

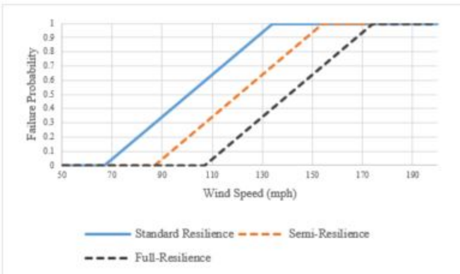

Fig. 14: Fragility curves of transmission lines/ distribution segments and their resilient levels

With the defined generalized levels of resilience for transmission lines and distribution segments, it is necessary to develop a method to quantify the performance of these circuits during hurricane conditions so that the model can make an informed resilience investment decision. In order to accomplish this a spatial-temporal analysis of a hurricane event must be utilized. The island was split up into seven meteorological regions as seen in Figure 15. Each region was assigned a 24-hour wind profile that corresponds to a hurricane event. In Figure 14, the regions and the hurricane path correspond to Hurricane Maria [30]. For this study, a time-series of wind data from a wind sensor that survived Hurricane Maria was collected from NOAAs database [17]. Wind profiles were extrapolated from that data based on the regions location to the path of Maria.

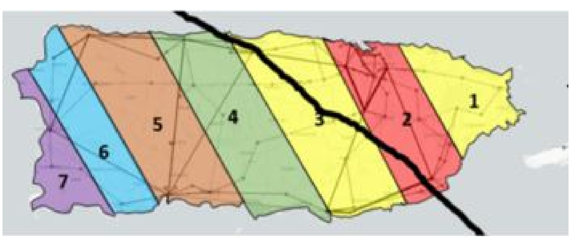

Fig. 15: Meteorological regions for hurricane modeling in PR

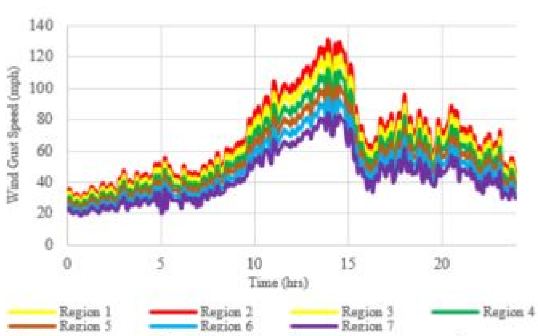

Fig. 16: 24-hour wind profile for each region corresponding to Hurricane Maria

Using the wind speeds in Figure 16 and the fragility curves in Figure 14 failure probabilities of circuits as a function of time were developed for each resiliency level. Li et al. developed a method utilizing a Monte Carlo Simulation (MCS) to determine the damage a natural disaster can impose on a system [25]. A similar approach was performed in this study to develop a set of failure probabilities for each line in the system for each resiliency level during the event of a hurricane. The MCS algorithm was developed in Matlab and was used for calculations external to the optimizer. This MCS algorithm is used to determine the failure probability of transmission lines and distribution segments for all resiliency levels. These failure probabilities are then used in the optimizer to identify critical lines eligible for resiliency upgrades.

A method to quantify the resilience of the circuit elements in the system was developed using the MCS and the concept of the fragility curves for the different resilience levels. To allow the model to differentiate between the resilient levels for wind and solar technology candidates, a series of hurricane path bus multipliers (HPBMs) were developed. Therefore for each solar or wind technology candidate there will be an assigned HPBM based on its geographic location and resiliency level (Table 8).

TABLE 8: HPBM's by region and resiliency levels

Hurricane Period	Standard	Semi	Full
1	0.1	0.15	0.2
2	0.05	0.075	0.1
3	0.1	0.15	0.2
4	0.25	0.375	0.5
5	0.45	0.675	0.9
6	0.65	0.975	1.00
7	0.85	1.00	1.00

These HPBMs displayed in Table 8 are corresponding to the meteorological regions in Figure 14. These figures were used to de-rate the performance of the generators during hurricane conditions by multiplying the HPBM by the capacity factor of the generator to develop a hurricane specific capacity factor. To distinguish between the resiliency levels multipliers of 1, 1.5, and 2 were used respectively to signify that the higher resilience levels perform better in hurricane conditions. Thus with the HPBM the solar and wind technologies are being modeled as though they are affected by a hurricane, the model will choose what technologies, and where to invest in them based off their performance. It is important to note that the HPBM was not allowed to exceed a value of one.

So far, all of the methodologies have been based off the hurricane path from Hurricane Maria. The CEP model formulation is designed to model multiple hurricane years within the planning period. PR is prone to experiencing hurricanes in all parts of the island so it is necessary to model hurricane scenarios that vary geographically and based off historical hurricane paths (Figure 17).

Due to lack of historical wind data, the data developed from Hurricane Maria was used for all other hurricane scenarios. Since Hurricane Maria was such a devastating natural disaster, it was seen that each scenario was modeled the worst case

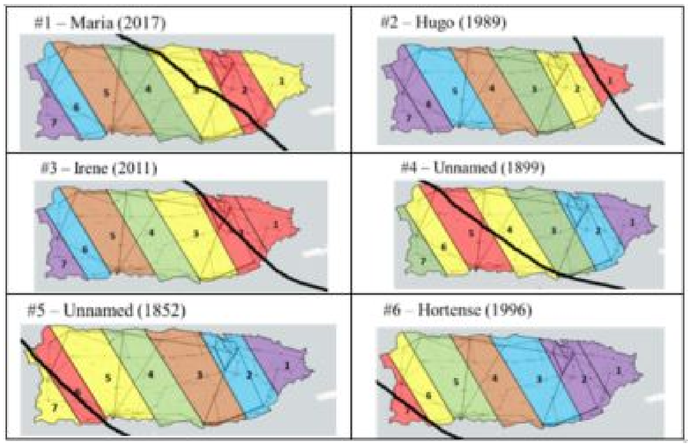

Fig. 17: Hurricane scenarios developed for PR with historical hurricane paths [5]

scenario. Thus, the variation in data between the scenarios was in the geographic location of the hurricane paths. As a result, for each scenario, the wind intensities varied causing failure probabilities and HPBMs to be characteristic to each hurricane scenario.

C. Resilience Modeling

With resilience measurements, such as the line failure probabilities and the HPBMs, already being calculated exterior from the CEP model, it is necessary to integrate them into the formulation so that correct investment portfolio can be produced. To model the resiliency line candidates, binary variables,$B_{l,r,h}$, were introduced. The following constraints (Eqs. 1 and 2) were constructed to de-rate the transmission lines and distribution segments thermal limits TL_l utilizing the failure probabilities ($Fail_{l,h,p_h}$) constructed from the MCS. It is important to note these constraints are deployed in hurricane years h for all resilience levels, r, and hurricane blocks p_h.

$$PF_{l,h,p_h} \leq (1 - Fail_{l,h,p_h}) * TL_l * B_{l,r,h} \quad \forall l, r, h \tag{1}$$

$$PF_{l,h,p_h} \geq -(1 - Fail_{l,h,p_h}) * TL_l * B_{l,r,h} \quad \forall l, r, h \tag{2}$$

To ensure that only one resilience level of each line and segment is invested in, the following constraint is enforced in equation 3.

$$\sum_r B_{l,r,h} \leq 1 \quad \forall l, r, h \tag{3}$$

With each hurricane year, invested resiliency level ($RL_{l,h}$) is tracked for the next hurricane year to allow for resilience upgrades. The model does not allow for backwards resiliency investments (i.e. a line cannot be upgraded to full resiliency in one year (h') and standard resiliency in the next year(h)). This made possible by equations 4 and 5.

$$RL_{l,h} = \sum_r RCM_{l,r} * B_{l,r,h} \ \forall l, h \tag{4}$$

$$RL_{l,h} \geq RL_{l,h'} \text{ where } ord(h) = ord(h') + 1 \ \forall l, h, h' \tag{5}$$

The resiliency level in the last hurricane year of each line that was chosen to be upgraded in resiliency is then included in the objective function with the corresponding resiliency cost multiplier $RCM_{l,r}$. This cost multiplier is applied to the line expansion cost for building the line to its existing capacity. This cost represents the cost to enhance the resilience on the circuit.

In an effort to reduce computational time, select circuits were chosen to be resilient upgrade candidates. The process for choosing this was to rank the circuits based off their standard resiliency level failure probabilities. From that ranking, the top 50% of transmission lines and top 33% of distribution segments were chosen. Thus for every hurricane scenario, a unique set of circuits (approximately 147 circuit elements) are eligible for resiliency upgrades.

To model the performance of resilient generating sources Equation 6 is used along with the HPBM applied to the capacity factors (CF_{g,h,p'_h}) and capacities ($C_{g,h}$ of the technologies (g) in the select hurricane periods (p'_h) that the unit is de-rated. The dispatched power for each generator is denoted as $Pgen$.

$$Pgen_{g,h,p'_h} \leq C_{g,h} * CF_{g,h,p'_h} * HPBM_{b,r,h} \forall g, r, h, p'_h \tag{6}$$

During the hurricane years, the system will seek to service the load in the most economical way while the system is inhibited by the imposed hurricane conditions. A value of lost load (VOLL) of $31,897/ MW-hr was chosen for this study [33]. Under normal operating conditions the system does not see any load shed thus under the hurricane conditions the model will seek to minimize any load shed due to its high cost. Therefore, the model will seek to find the optimal mix of generation, transmission, and distribution technologies that mitigate load not being served based off the hurricane conditions, the technologies performance, and the overall investment costs.

IV. Infrastructure Visions

Due to the exploratory nature of the CEP software, three infrastructure visions were developed that contain unique sets of resilience and expansion investment options. For each vision, the amount of investments made in centralized and decentralized resources vary. For the purposes of this study, centralized resources are defined to only be built at the transmission level and include NGCC, NGCT, Utility PV, and 100m-Wind. Decentralized resources or DG are designed to be built at the distribution buses closer to the load. These candidate resources include community PV, rooftop PV, energy storage, and micro-turbines. Table 9 provides the breakdown of the resource investment constraints made for each vision. Visions 1 through 4 (V1-V4) vary in the amount of centralized and decentralized resources that can be invested in. In vision 5 (V5), the model is allowed to freely invest in transmission or distribution level resources and a regional PRM is in place.

With these visions formulated, it is of interest to see how each one performs under hurricane conditions. These visions

TABLE 9: Investment matrix (% of invested capacity)

Investment Feature	V1	V2	V3	V4	V5
Natural Gas CC / CT	30	25	10	5	-
Utility PV	35	25	20	5	-
Commercial PV	0	15	30	40	-
Rooftop PV	0	10	30	45	-
100m Wind	35	25	10	5	-

are designed to perform differently with respect to overall investment cost and amount of load shed during the hurricane conditions. Studying these infrastructure visions will provide insight on how the model 1.) Designs a resilient infrastructure and 2.) values DG investments over shedding load during hurricane events.

V. Results

Table 10 provides a breakdown of what technologies were invested for each infrastructure vision. There was a cap put on the total amount of invested resource capacity of 5.00 GW for the entire planning horizon. Retirements were made based off if a generating unit is not dispatched within a year inside of the planning horizon. To ensure that no units were retired that may mitigate load shed during hurricane years, the summation of the dispatched energy in the hurricane years of all generators was determined. If a unit did not dispatch it was eligible for retirement. Retirement costs were calculated into the model using figures from source [31].

TABLE 10: Summary of resource capacity investments

Invested Capacity (MW)	V1	V2	V3	V4	V5
NGCC	1356	1215	486	243	1096
Wind	1582	1215	486	243	-
Utility PV	-	1215	972	243	-
Comm. Rooftop	-	729	1457	1940	2084
Dist. Rooftop PV	-	486	1457	2182	1610
Microturbine (MT)	-	-	-	-	71
Dist. Storage	-	141	141	149	140
Total Fossil Retirements	3709	3985	3477	3147	3890

Table 11 provides a breakdown of the resilience investments made in each vision. The resilience upgrades in the lines are broken down into transmission and distribution segments. Resilient investments in wind and solar technologies are also displayed as the amount of megawatts the model invested in for each resilience level. The model was able to identify what components in the system needed resilience upgrades and it was able to identify to what level these components needed in order for the system to become hurricane resilient.

Table 12 provides a breakdown of the costs associated with each vision. It is important to note that operational costs include costs associated with FOM, VOM, fuel consumption, line loss considerations, and regulation/reserve costs. A take-away from these results is the correlation between increased investment costs, due to the increased DG penetration, and the decrease in load shed costs between V1-V4. In Figure 18, the load shedding cost versus the total cost (without the load shed cost) is displayed.

TABLE 11: Resilience Investments

	V1	V2	V3	V4	V5
LINES (tx. lines / dist. segments)					
Standard-Resilience	1/0	1/1	1/1	5/1	3/0
Semi-Resilience	18/35	15/43	14/43	22/44	21/41
Full-Resilience	11/31	12/31	41/31	34/30	28/33
GENERATION (MW)					
Standard-Resilience	1946	2578	2087	2691	2079
Semi-Resilience	845	839	1844	1501	1121
Full-Resilience	373	228	442	416	494

TABLE 12: Summary of costs for each vision

COST ($B)	V1	V2	V3	V4	V5
LINES					
Resilience	9.28	9.40	9.60	9.68	9.67
Expansion	7.91E-4	5.86E-3	0	4.73E-3	0
Generation	2.87	5.56	8.64	9.53	9.50
Operational	39.62	39.14	41.96	42.27	40.91
Retirements	0.809	0.835	0.763	0.706	0.828
TOTAL (w/out load shed costs)	52.58	54.94	60.96	62.19	60.91
Load Shedding Costs	784.43	692.69	637.09	649.11	598.34

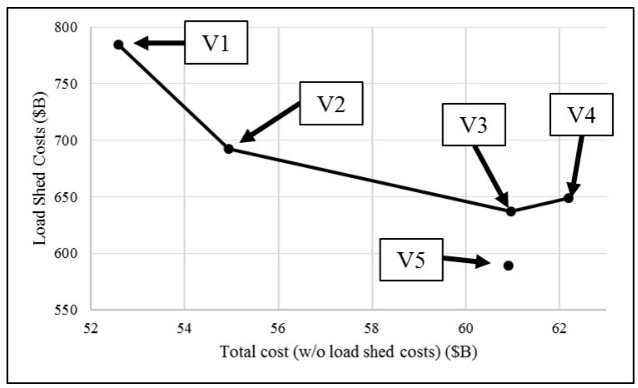

Fig. 18: Plot of load shed costs versus total costs for visions 1 through 5 (V1-V5)

Vision 3 resulted in the lowest load shed costs compared to vision 1,2, and 4. This may mean that there is a saturation point in DG penetration that increase the system's resiliency. Vision 5 contained the least amount of load shed and may shed light on the importance of imposing the regional PRM constraints. Overall, based on the performance of these visions there is a value to adding DG to the system to increase the resiliency in the event of a catastrophic hurricane.

VI. Conclusion

A CEP model was constructed to identify key investments at the generation, transmission, and distribution levels of the PR system to increase the resilience of the system in a cost effective manner. Multiple modeling scenarios were developed and tested to determine the overall cost of building a hurricane resilient infrastructure while evaluating the penetration of DG. Hurricane conditions were effectively implemented to produce an environment for the model to seek an economic but resilient infrastructure. As a result, it was found that with increased investment cost the resiliency of the islands system would increase as reflected by the mitigation of load shedding.

With a changing climate and uncertain weather forecasts, various electric infrastructure systems similar to the PR system are prone to extreme events that can be devastating to society. Therefore this expansion planning tool has the potential to be used on several electric systems around the world in an effort to increase resilience. With proper validation of this CEP model, this tool could be used extensively to help solve the engineering problem of quantifying the value of resilience and the benefits of various GTD investments.

VII. Acknowledgement

The authors would like to acknowledge Dr. Efrain ONeill-Carrillo and Gustavo A. Cuello Polo from the University of Puerto Rico-Mayagüez for their contributions of system data for this study.

References

[1] R. J. Pasch, A. B. Penny, and R. Berg, *National Hurricane Center Tropical Cyclone Report Hurricane Maria*. National Hurricane Center, 2018.

[2] J. D. Taft, "Electric Grid Resilience and Reliability for Grid Architecture," no. June, 2017.

[3] A. Smith, "Presidential Policy Directive 21 Implementation," *Department of Homeland Security*, no. February, 2015. [Online]. Available: https://www.dhs.gov/sites/default/files/publications/ISC-PPD-21-Implementation-White-Paper-2015-508.pdf.

[4] W. Bush, "Critical Infrastructure Resilience Final Report And Recommendations," pp. 1–43, 2009. DOI: 10.1080/14662043.2014.894284. [Online]. Available: https://www.dhs.gov/sites/default/files/publications/niac-critical-infrastructure-resilience-final-report-09-08-09-508.pdf.

[5] NOAA, *Hurricanes*. Available: https: [Online], 2017.

[6] U. E. I. Administration, *Puerto Rico Territory Energy Profile*. Available: https: [Online], 2018.

[7] PREPA, "Prepa electric system," *https://aeepr.com/es-pr/qui%C3%A9nes-somos/sistema-electrico. Accessed*, 2014.

[8] ——, (2015). Sistema de transmisin de la aee, PREPA, [Online]. Available: http://energia.pr.gov/datos/transmision/.

[9] ——, (2015). Plantas generadoras de energa en puerto rico, [Online]. Available: http://energia.pr.gov/datos/plantas/$\#$1442369540309-10157bcc-cd6b.

[10] C. C. H. Homer, L. Yang, B. Wylie, and M. Coan, "Developmentof a 2001 national landcover database for the united states," *Photogrammetric Engineering and Remote Sensing*, vol. 70, no. 7, pp. 829–840, 2004.

[11] F.-A. A. Luis. (2017). Opportunities and benefits for increasing transmission capacity between the us eastern and western interconnections. D. G. T. and, Ed., [Online]. Available: https://lib.dr.iastate.edu/etd/16128.

[12] S. PTI, *Integrated Resource Plan Volume 1: Supply Portfolio and Futures*. Available: https//www.aeepr.com/Documentos: [Online], 2015.

[13] Black and Veatch, *2014 TEPPC Transmission Capital Cost Calculator*. Available: https: [Online], 2014.

[14] NREL, *Annual Technology Baseline*. NREL, 2017.

[15] ——, *PVWATTS Calculator*. Available: https.pvwatts.nrel.gov/pvwatts.php: [Online], 2018.

[16] ——, (2018). System advisor model (sam), [Online]. Available: https://sam.nrel.gov/.

[17] NOAA, *Natioal Data Buoy Center*. Available: https: [Online], 2018.

[18] I. R.A.A.C.-R.J.A.O.-C. Efrain, "Final report of the study "achievable renewable energy targets for puerto rico's renewable energy portfolio standard"," Mayaguez, PR, 2009. [Online]. Available: www.uprm.edu/aret.

[19] M. J.M.P.L.P.H.B. X. Q., "Cooptimization and anticipative planning mehtods for bulk transmission and resource planning under long-run uncertainties, final project report, submitted to the bonneville power administration," September 28, 2018.

[20] R. R.M.A.G.A. H. S., "Test systems and mathematical model for transmission network expansion planning," *IEEE Proceedings - Generation, Transmission, and Distribution*, vol. 149, pp. 27–36, 1 2002.

[21] H. Zhang, V. Vittal, G. T. Heydt, and J. Quintero, "A mixed-integer linear programming approach for multi-stage security-constrained transmission expansion planning," *IEEE Transactions on Power Systems*, vol. 27, no. 2, pp. 1125–1133, 2012, ISSN: 08858950. DOI: 10.1109/TPWRS.2011.2178000.

[22] M. Panteli and P. Mancarella, "Modeling and evaluating the resilience of critical electric power infrastructure to extreme weather events," *IEEE Systems Journal*, vol. 11, no. 3, pp. 1733–1742, 2017.

[23] ——, "Influence of extreme weather and climate change on the resilience of power systems: Impacts and possible mitigation strategies," *Electric Power Systems Research*, vol. 127, pp. 259–270, 2015.

[24] B. J. Pierre, B. Arguello, A. Staid, and R. T. Guttromson, "Investment optimization to improve power system resilience," in *PMAPS 2018, Boise, Idaho*, 2018.

[25] B. Li, R. Roche, and A. Miraouri, *A temproal-spatial natural disaster model for power system resilience improvement using DG and line hardening*. IEEE Manchester PowerTech, 2017, pp. 1–6.

[26] N. Abi-Samra, *Power Grid Resiliency for Adverse Conditions*. Nowrood, MA: Artech House, 2017.

[27] S. Mohagheghi and P. Javanbakht, "Power grid and natural disasters: A framework for vulnerability assessment," in *2015 Seventh Annual IEEE Green Technologies Conference*, 2015.

[28] C. Burgess and J. Goodman, *Solar Under Storm*. Rocky Mountain Institute, Boulder, CO, 2018.

[29] FEMA.

[30] A. R. Cross. (2018). Hurricane maria (2017): Preliminary peak wind gust (mph), [Online]. Available: https://maps.redcross.org/website/DROMaps/Images/Current/ARA_Hurricane_Maria_Wind_Maps_v13.pdf..

[31] G. D. Meija, "Energy generation expansion planning model-considering emissions constraints."

Iowa Army National Guard (IAARNG) Energy and Water Master Plan

Summary Report

Benjamin Robertson, Song-Charng Kong, Iowa State University

Objective

The objective of this report is to create an Energy and Water Master Plan (EWMP) for the Iowa Army National Guard (IAARNG). The EWMP is to be used as a roadmap for IAARNG in meeting energy and water goals and mandates by evaluating IAARNG's current water and energy status and providing action plans to reach these goals and mandates.

Organization and Methodology

Iowa State University researchers are tasked to produce the EWMP, with the project duration from September 2018 to August 2020. The report will be organized into five sections that answer three questions related to the current state of IAARNG's energy and water systems. Where are we? Where do we want to go? How do we get there? In doing this IAARNG is best able to organize their current energy and water information and systematically reach the goals and mandates expected of them.

Introduction

The first section provides important background information that influences energy and water usage. This information includes mandates, regulations, executive orders, and goals set for IAARNG energy and water use. IAARNG's physical setting is discussed in the introduction because it plays a crucial role on resources available. For instance, water is an abundant resource in Iowa, which may not be the case in other states, and so water reduction goals carry less weight in Iowa as they would in a state like California. Finally, the Introduction provides discussion on building type classification and determining the average buildings, in terms of energy consumption, within these classifications. Finding the "average" building for each building type is crucial for identifying possible areas of improvement. In order to calculate the average building for a building type, the energy intensities for each type of building were averaged, and the building with an energy intensity nearest to this value was selected. This average can then be used to calculate the standard deviation of energy intensities, which highlights buildings with both high and low energy intensities. By doing this, high energy intensity buildings can be better updated to model low energy intensity buildings.

Mission and Vision

The second section provides the Army National Guard Mission in Sustainability, the Army National Guard Vision for Sustainability, and the Army National Guard Energy and Water Program.

Energy and Water Profiles

The third section gives an overview of IAARNG water and energy supply, distribution, and consumption and answers the question: Where are we? It also contains a review of recent audits as well as data measurement and management techniques employed by IAARNG. A goal of 2.5% annual reduction in energy consumption intensity, with a 25% total reduction by fiscal year 2025 set for IAARNG is displayed using a graph. This graph shows IAARNG energy intensity from 2015 through current data, as well as yearly marks through 2025. This section then further breaks down energy consumption into electricity, natural gas, and renewables. In each of these sections graphs of annual consumption and consumption intensity from 2015 to the most recent year, as well as a graph of the most recent year's monthly consumption of the select source. The consumption and consumption intensities of each building type are analyzed here. The goal of this analysis is to identify buildings in each type with high consumption patterns in an effort to reduce base consumption. Similar strategies are followed with analyzing the water systems, however IAARNG is currently in the process of installing smart water meters, and so they do not have water data available to produce consumption graphs. At the end of each section the resiliency and overall condition of each resource is discussed. This section is crucial when moving forward because it highlights vulnerabilities and areas for improvement.

Goals

The fourth section first contains a strength, weakness, opportunities, and threats analysis (SWOT analysis) to identify internal and external attributes that either help or impede progress towards IAARNG goals. Next, a trend analysis will outline the direction installation energy and water systems are heading based on current and projected trends. Following this analysis a list of endpoint goals for the energy and water systems will be presented in the scenario testing sub-section, and an introduction to the actions plans that reach these goals will be presented in the sub-section implementing the vision. The overall goals can be classified into four types of goals: conservation, security, communication, and education. Conservation goals are goals that lead to the reduction of energy and water use through conservation and efficiency efforts. Security goals are goals that lead to the protection of energy and water resources, systems, and function. They also assist in mitigating risk to all missions. Communication goals are goals that lead to an increase in awareness and knowledge of sustainability, energy, and water policies, as well as goals that improve communication channels. Finally, education goals are ones that improve individual soldiers' knowledge of conservation and sustainability.

Action Plans

The final section presents clear plans for reaching each goal outlined in the previous section, and answers the question: How do we get there? Each plan includes a benefit-cost analysis or life-cycle cost analysis in accordance with the Office of Management and Budget Circular A-94 and the current Army Cost Benefit Analysis Guide. The plans will also include potential avenues for funding as well as a section aimed towards presenting the plan in legislature or a legal setting.

ASSESSING AND MITIGATING THE IMPACT OF GEOMAGNETIC DISTURBANCE ON TRANSMISSION SYSTEM RELIABILITY

Rishi Sharma, James D. McCalley

1. ABSTRACT

GICs induced in the transmission network due to geomagnetic disturbance (GMD) events may lead to large-scale power outages and power system equipment damage. As per the FERC order 830, the two key developmental needs regarding defense against GMD events are; accurate modeling of GICs and determination of a credible 1-in-100 year GMD benchmark scenario. In this work, we have developed a modeling approach that unifies the 3-D earth conductivity representation and the transmission network representation; this enables accurate computation of the GICs directly using the B-field data. We also estimate the 1-in-100 year return level of GICs for the transmission network of Iowa, based on extreme value analysis (EVA) of historic GICs calculated using historic (1979-2018) B-field data.

2. INTRODUCTION

Coronal mass ejection (CME) occurring on the surface of the sun during a solar flare leads to geomagnetic disturbance (GMD) on the surface of Earth [1]. The change in the geomagnetic field during a GMD event, induces a voltage on the transmission lines which causes geomagnetically induced currents (GIC) to flow in the power system. These quasi-dc GICs leads to generation of transformer harmonics, variation in reactive power flows and temperature rise in transformers and reactors.

In this report, in section 3, we have proposed a unique unified Earth conductivity and transmission network modeling approach. The model parameters are estimated using the observed GIC and B-field time series, and then to verify accuracy of the model we compare the computed and measured GIC. Next in section 4 we determine the 1-in-100 year return level of GICs by means of EVA. The EVA is performed by fitting the historical GIC distribution on a family of distribution models, including power law, lognormal, and generalized extreme value. The distribution parameter estimation is done by maximizing the log-likelihood function with respect to the extreme historical GIC observations. The 95% confidence interval (CI) of the estimated parameters and the GICs are determined for the 1-in-100 year return level.

3. UNIFIED EARTH CONDUCTIVITY AND TRANSMISSION NETWORK MODELING

In order to compute the geomagnetically induced currents (GIC) using the B-field, the Earth conductivity model and the transmission network model is needed as indicated in Figure 1.

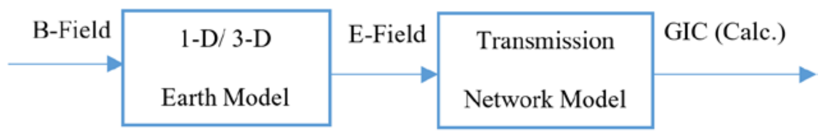

Figure 1: Computing GIC using model parameters and B-field

But due to unavailability of either synthetic the 3-D Earth models or the accurate transmission network models, is becomes important to find alternative ways of determining model parameters. An alternate way of computing the model is to fit model parameters based on the GIC and B-Field observations [2]. To avoid the interdependency between earth and transmission models in determining each of them we introduce a unified modeling approach as indicated in, figure 2, to compute GIC directly using the B-field values.

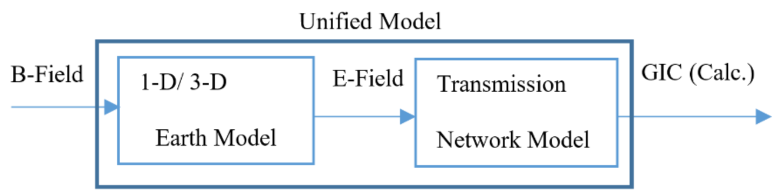

Figure2: Unified model to compute GIC using B-field values.

The unified model can be mathematically be expressed as indicated in (1). In a system with n buses and m transmission lines, the GIC matrix can be written in terms of unified model parameters $a_{n,m}$ and magnetic field B as (1).

$$\begin{bmatrix} GIC^1 \\ GIC^2 \\ \vdots \\ GIC^n \end{bmatrix}_\omega = \begin{bmatrix} \sum_{i=1}^{m} a_{1,(2i-1)} & \sum_{i=1}^{m} a_{1,2i} \\ \vdots & \vdots \\ \sum_{i=1}^{m} a_{n,(2i-i)} & \sum_{i=1}^{m} a_{n,2i} \end{bmatrix} \begin{bmatrix} B_x \\ B_y \end{bmatrix}_\omega \quad (1)$$

3.1. Unified model parameter determination and verification:

The parameters $P^{s1} = \sum_{i=1}^{m} a_{s,(2i-1)}$ and $P^{s2} = \sum_{i=1}^{m} a_{s,(2i-1)}$ are estimated based on the minimization of the least squared error between the measured and calculated GIC as indicated in (2).

$$\min\{\sum\left(GIC^{s}_{meas.}(\omega) - [P^{1s}(\omega).B_x(\omega) + P^{2s}(\omega).B_y(\omega)]\right)^2\} \quad (2)$$

The 1 Hz sampling rate B-field and GIC data, spanning 8 days for Dec 2015 GMD event, was obtained from the permanent B-field and GIC monitors located at the Oak Grove substation in Iowa. The transmission network data for Iowa was provided by MidAmerican Energy Company (MEC). This data includes the resistance values of all network components, substation locations and transformer vector groups. The 3-D earth conductivity transfer functions were provided by Paul Bedrosian of the U.S.Geological.Survey (USGS).

Using equation (2), and a 1 day B-field and GIC time series, the parameters P^{s1} and P^{s2} were estimated. Using (1), the estimated model parameters and B-field measurements (spanning 8 days), the GIC was computed. In Figure 3 (a), the calculated and measured GIC is plotted for a span of 4 hours. In Figure 3 (b), the GIC calculated using separated 3-D earth conductivity model (provided by USGS) and transmission network model (Provided by MEC) is plotted along with the measured GIC data. In Figure 3 the visual comparison of (a) and (b) shows that in (a) the computed GIC traces the measured GIC more accurately. Analytically, the net error in Figure 3 a) and b) is 0.3322 amps and 0.8880 amps, respectively. Over the span of all 8 days, the error is 0.1631 amps and 0.2650 amps. Hence, it can be said that the unified model parameter estimated using the observed GIC and B-field is relatively more accurate than that obtained using the 3-D earth conductivity and transmission network parameter.

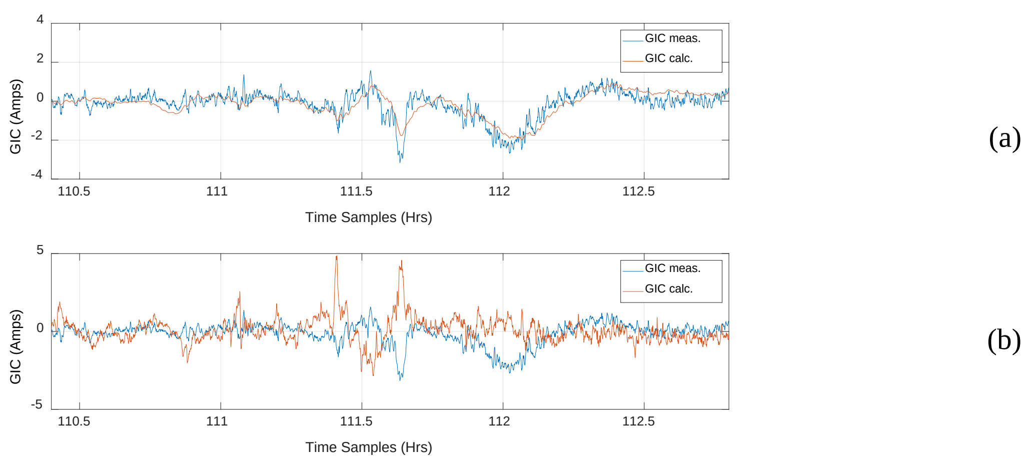

Figure 3: Comparison between measured and computed GIC: a) using the estimated unified model parameters. b) using USGS 3-D earth conductivity model and MEC transmission network model.

4. EXTREME VALUE ANALYSIS (EVA) OF HISTORICAL GIC

EVA is a method by means of which one can describe the behavior of a stochastic process whose outcome has extreme deviation from its median [3]. In the literature, EVA has been used extensively to determine the 1-in-100 year B-field [4] [5] and E-field [6] [7]. In fact, the NERC E-field Benchmark has been determined by performing EVA of the E-fields obtained using the historic B-fields and the 1-D earth conductivity model of Quebec[8].

In order to determine the impact of 1-in-100 year GMD events on the power system, it is critical to determine the 1-in-100 year GIC. In the literature, these have been determined using the NERC benchmark, as indicated in Figure 4 (a). But as the NERC benchmark uses regional 1-D earth conductivity models and spatial averaging of the E-fields, there could be considerable error in predicting the 1-in-100 year GIC, as indicated in FERC order 830. One alternative is to use the 1-in-100 year E-field maps as determined in [9], using the 3-D earth conductivity. This method is indicated in Figure 4 (b). The problem with using these E-field maps is that they are determined for a particular electromagnetic frequency, secondly, to use them one has to assume that the 1-in-100 year extreme magnitudes will occur simultaneously at all locations on the map, and thirdly there is no suggestion on the direction of the 1-in-100 year E-field. To avoid the problems associated with procedures described in Figure 4 (a) and (b), we introduce a procedure described in Figure 4 (c), in which we determine the 1-in-100 year GIC by performing the EVA on the historical GICs, calculated using historical B-field data and transmission network model.

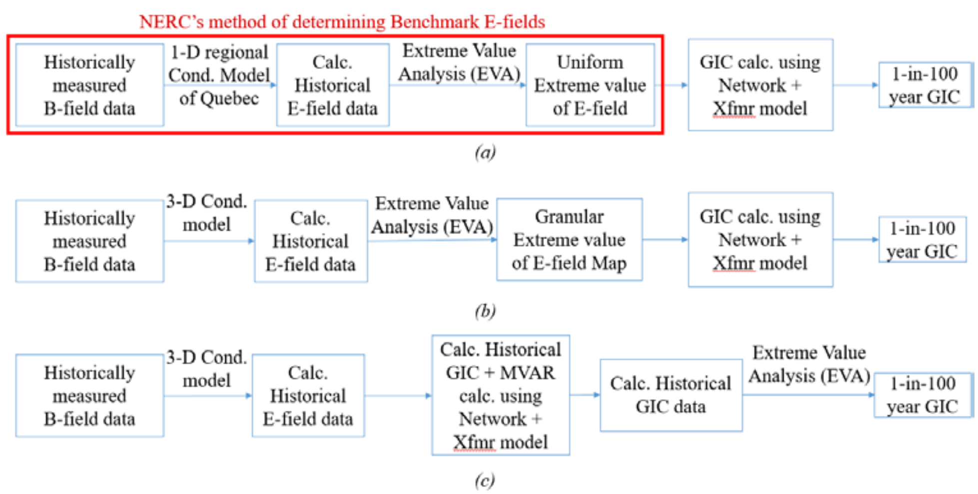

Figure 4: Comparison of different approaches to determine the 1-in-100 GIC flows.

4.1. Statistical modeling of extreme GICs

The historical 1-min sample B-field data between 1979-2018 (spanning 40 years) was obtained from the superMAG database[1] [10] [11]. As indicated in Figure 4 (c), the historical GICs are calculated using the historic B-field, the 3-D earth conductivity transfer functions and transmission network model. The 1-in-100 year GIC is determined by performing the EVA on the 40 years of calculated GIC data. In the EVA,

[1] For the ground magnetometer we gratefully acknowledge the SuperMAG collaborators; Intermagnet; USGS, Jeffrey J. Love.

the probability distribution of the extreme GICs is fitted on certain family of distributions to determine the 1-in-100 year GIC. The family of distributions considered in this study are, generalized extreme value (GEV) [3], power law [12] and lognormal distribution [13]. The probability distribution functions (CDF) of these three distributions are indicated in (3) as $f(x \mid \theta)$, where x is a value in sample space and θ is the parameter set.

$$
\begin{aligned}
f_{GEV}(x \mid \mu, \sigma, \xi) &= \frac{1}{\sigma}\left[\left[1+\xi\left(\frac{x-\mu}{\sigma}\right)\right]^{-1/\xi}\right]^{\xi+1} \exp\left\{-\left[1+\xi\left(\frac{x-\mu}{\sigma}\right)\right]^{-1/\xi}\right\} \\
f_{\log normal}(x \mid \mu, \sigma) &= \frac{1}{x\sigma\sqrt{2\pi}} \exp\left[-\frac{(\ln x-\mu)^2}{2\sigma^2}\right] \\
f_{powerlaw}(x \mid k, \alpha) &= \frac{\alpha-1}{k+x_{\min}}\left(\frac{k+x}{k+x_{\min}}\right)^{-\alpha}
\end{aligned} \tag{3}
$$

$$
l(\theta) = \sum_{i=1}^{n} \log f(x_i; \theta) \tag{4}
$$

θ is estimated by maximizing the log-likelihood function $l(\theta)$ as indicated in (4), by means of an optimization algorithm. In (4) x_i are the observed data points, i.e. the GIC data for a particular substations. The observed data used for GEV fitting is the one year block maximum GICs, and for the lognormal and power law fitting it is all the GIC data above a set threshold (=1.68 in our case).

Based on the parameters obtained by maximizing the log-likelihood $l(\theta)$, we plot the annual exceedance rate ($365*(1-CDF)$) in Figure 5 (a) for the Power law and Lognormal distribution along with the GIC data greater than the threshold GIC (=1.68 amps). In Figure 5 (b) a similar plot is drawn for GEV and the one year block maximum GIC data. In both figures, the black dotted line at 0.01 represents the annual exceedance rate, i.e. the 1-in-100 year return level.

Though by using the estimated parameters and the CDF, the 1-in-100 year return value can be determined. But as these parameters are an 'estimate' and not the true value, we predict a 95% confidence interval (CI) of the estimated parameters based on the central limit theorem. And based on CI of parameters, the CI of the 1-in-100 year return level of GIC can also be estimated. Figure 6 shows the profile log likelihood plot with respect to the 1-in-100 year return level and the black dashed line is the $0.5 \times c_{1,0.05}$ below the maximum log-likelihood. $c_{1,0.05}$ is the 95% quantile of the χ_1^2 distribution, and the point where this line meets the curve is the CI of the 1-in-100 year GIC. The CI for power law from Figure 6 is [21.9, 67.5] amps, similarly for the lognormal case the CI was found to be [34.67, 53.15] amps and for GEV it was [23.61, 102.4] amps. In the future, based on the Kolmogorov–Smirnov (KS) goodness of fit test, we can identify the best distribution fit for the GIC data, and thus identify the most reliable 1-in-100 year CI.

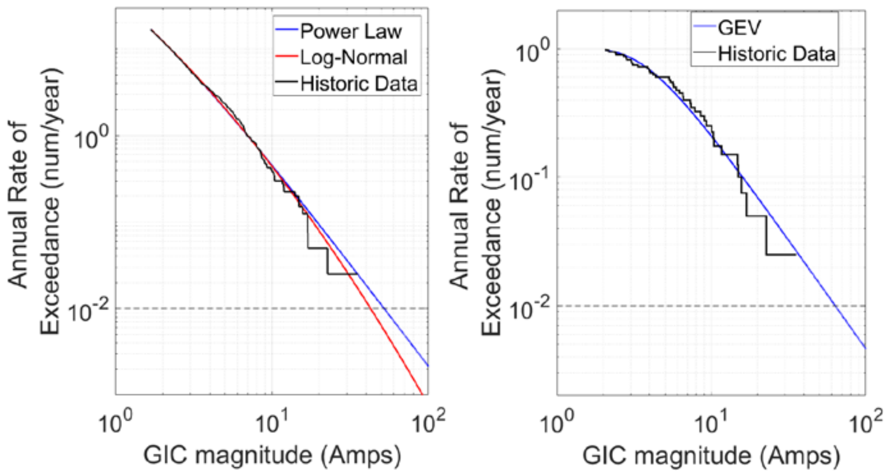

(a) (b)

Figure 5: Annual Exceedance Rate vs GIC magnitude plot for: (a) Lognormal and Power law fit on the historic GIC (>1.68 Amps) (b) Generalized Extreme Value fit on the annual maximum GIC data.

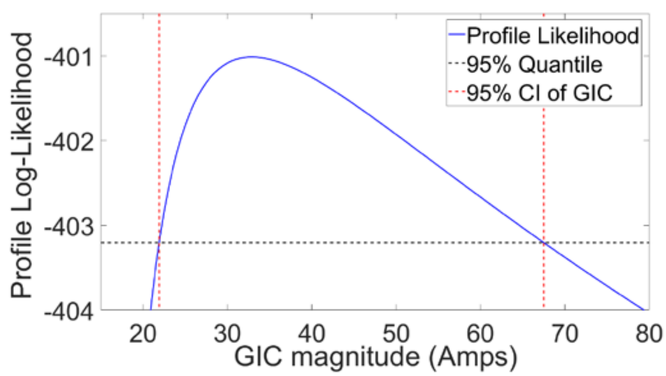

Figure 6: Profile log likelihood for Power Law distribution.

5. CONCLUSION

It can be said that the unified model parameter estimated using the observed GIC and B-field is relatively more accurate than that obtained using the 3-D earth conductivity and transmission network parameter. But the estimation technique estimates very low value of model parameters P^{s1} and P^{s2} for lower time period electromagnetic waves. Hence in Figure 3, though the GIC calculated matches very closely with the GIC measurements for slow changing GIC. But this isn't true about the faster changing GIC. Hence the technique needs to be adjusted so that the lower time period parameters are estimated more accurately.

The 1-in-100 year CI for the GIC at the Oak Grove substation was determined using the EVA statistics. Based on the KS test the best fit can be determined and hence the 95% CI of GIC can be estimated. Similarly, the 1-in-100 year MVAR values and 1-in-100 year voltage drop assessment can be done to determine the system impact.

6. REFERENCES

[1] NERC, "Effects of Geomagnetic Disturbances on the Bulk Power System," no. February, p. 137pp., 2012.

[2] S. Watari, "Estimation of geomagnetically induced currents based on the measurement data of a transformer in a Japanese power network and geoelectric field observations," *Earth, Planets Sp.*, vol. 67, no. 1, 2015.

[3] C. Stuart, *An Introduction to Statistical Modelling of Extreme Values*. 2001.

[4] J. J. Love and J. L. Gannon, "Revised <I>D_{st}</I> and the epicycles of magnetic disturbance: 1958–2007," *Ann. Geophys.*, vol. 27, no. 8, pp. 3101–3131, 2009.

[5] J. Chen, S. P. Slinker, and I. Triandaf, "Bayesian prediction of geomagnetic storms: Wind data, 1996-2010," *Sp. Weather*, vol. 10, no. 4, pp. 1–11, 2012.

[6] J. J. Love, A. Pulkkinen, P. A. Bedrosian, and Et.al., "Geoelectric hazard maps for the continental United States," *Geophys. Res. Lett.*, vol. 43, no. 18, pp. 9415–9424, 2016.

[7] J. J. Love, G. M. Lucas, A. Kelbert, and P. A. Bedrosian, "Geoelectric Hazard Maps for the Mid-Atlantic United States: 100 Year Extreme Values and the 1989 Magnetic Storm," *Geophys. Res. Lett.*, vol. 45, no. 1, pp. 5–14, 2018.

[8] NERC, "Benchmark Geomagnetic Disturbance Event Description," pp. 1–26, 2014.

[9] J. J. Love, P. Coïsson, and A. Pulkkinen, "Global statistical maps of extreme-event magnetic observatory 1 min first differences in horizontal intensity," *Geophys. Res. Lett.*, vol. 43, no. 9, pp. 4126–4135, 2016.

[10] J. W. Gjerloev, "The SuperMAG data processing technique," *J. Geophys. Res.*, vol. 117, no. A09213, 2012.

[11] J. W. Gjerloev, "A Global Ground-Based Magnetometer Initiative," *EOS, 90, 230-231*, 2009.

[12] A. Clauset, C. R. Shalizi, and M. E. J. Newman, "Power-law distributions in empirical data," 2007.

[13] J. J. Love, E. J. Rigler, A. Pulkkinen, and P. Riley, "On the lognormality of historical magnetic storm intensity statistics: Implications for extreme-event probabilities," *Geophys. Res. Lett.*, vol. 42, no. 16, pp. 6544–6553, 2015.

Supplementary frequency control of VSC-MTDC for primary frequency support among asynchronous AC systems

Qian Zhang, James D. McCalley, Venkataramana Ajjarapu
Department of Electrical and Computer Engineering, Iowa State University, Ames, USA
Emails: qzhang15@istate.edu, jdm@iastate.edu, vajjarap@iastate.edu

***Abstract*—Voltage source converter based multi-terminal HVDC (VSC-MTDC) is identified to be a promising technology to facilitate the integration and utilization of large amounts of renewable energy resources in power systems across large geographic areas, and potentially multiple AC systems. One major issue caused by the increased penetration of renewable generation and the decommitment of conventional generators is the decreasing system inertia, which is expected to have adverse impact to the frequency dynamics and pose great challenges to frequency control in power systems. The proposed approach addresses this frequency control challenge by developing supplementary frequency control strategies for the VSC-MTDC to facilitate the exchange of primary frequency reserves among asynchronous AC systems, thus providing frequency support among each other. The proposed frequency control is a droop based global scheme and is shown to be superior to the popularly explored local frequency droop scheme in the literature. The benefits of reduced load shedding, reduced need of total online spinning reserves and reduced impact to the DC voltage profile are illustrated via time domain simulation on an AC-MTDC test system. The VSC-MTDC model and the proposed control are implemented in the commercial grade software PSS/E thus is suitable to study large-scale realistic systems and can be incorporated into the power system planning process at utilities and ISOs.**

***Index Terms*—VSC-MTDC, frequency support, droop control, PSS/E**

I. Introduction

In order to achieve decarbonization targets for a sustainable future, there has been a global trend to integrate large-scale renewable energy resources into the existing power grid. Under high penetration level of renewable energies, compared to building lots of redundant generation and transmission within each region, interconnection is more cost effective to reduce power system risks by sharing capacity and reserves. In the United States, a joint effort from the national labs, universities and inustry partners have performed the “Interconnection Seam Study” [1], [2] to identify the cost-effective options for upgrading the electric grid to strengthen the connections (i.e. to increase the power transfer capabilities) between three major interconnections - the Western Interconnection (WECC), the Eastern Interconnection (EI) and the Electric Reversibility Council of Texas (ERCOT), with the aim to facilitate the development and utilization of the nation’s abundant energy resources such as wind in the midwest and solar in the southwest [3]. One of the proposed topologies, so called “Macrogrid” [4], is a continental level HVDC overlay as shown in Fig. 1. Direct economic benefits resulting from such

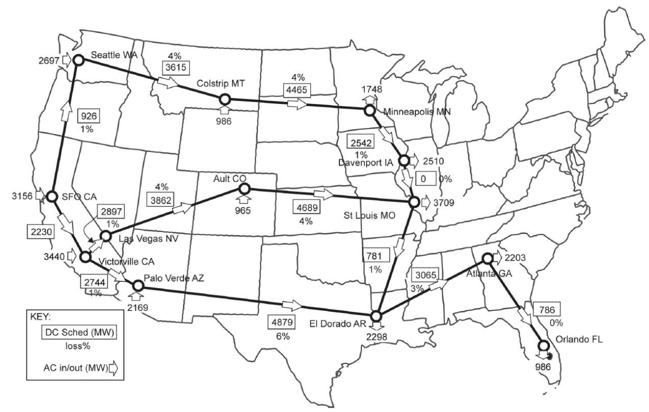

Fig. 1. HVDC macrogid network [4]

an HVDC cross-seam transmission include: 1) access of the load to richer renewable resources 2) interregional sharing of the renewable resources on a diurnal basis due to load diversity across different time zones 3) interregional sharing of the capacity to satisfy the peak load in each region thus reducing the investment in capacity in each region. Besides these economic benefits, such an infrastructure can also enhance the energy security and improve the reliability of the overall system, by taking advantage of the power control capability of the converters. In [4], the authors performed a initial feasibility study of the Macrogrid using power flow and transient stability models in the commercial grade software PSS/E, assuming all converters are line commutated converters (LCC) and all HVDC lines are point-to-point links. Results show the potential reliability benefits such as frequency response support between WECC and EI.

As compared to point-to-point HVDC links, an MTDC grid possesses advantages in that: it can significantly reduce the number of costly converter stations; it allows easy tapping of renewable integration in the middle of a DC line; it is easier to control and coordinate as a single entity to maintain generation and load balance [5]. Therefore, it is of interest to investigate the possibility of realizing HVDC cross-seam transmission with an MTDC configuration. To harvest the benefits of the MTDC, VSC is the only viable option because power reversal is realized by reversal of the current instead of alternating terminal DC voltages as in LCC, which is hard to coordinate in a multi-terminal configuration. Moreover, multiple decisive advantages such as flexible and independent active power and reactive power control capabilities of VSC would greatly contribute to the overall system reliability with proper controls.

In this work, we investigate the capability of VSC-MTDC to provide primary frequency support among asynchronous AC systems. The converters in the healthy AC system can be controlled to adjust its active power setpoint to react to the frequency variations in the AC system that needs the support, achieving the benefit of exchanging primary frequency reserves between asynchronous AC systems. This not only reduces the risk of load shedding and cascading failure in the area experiencing generation loss, but also reduces the total amount of expensive online spinning reserves needed in the whole system.

For most existing work in the literature utilizing frequency droop control, the frequency reference is set to be the nominal frequency 60Hz (1 p.u.). This makes the frequency control dependent on the DC voltage control to transfer the information of frequency deviation, causing adverse impact to the DC voltage profile while the frequency control is activated. In order to mitigate the impact and reliance on the DC voltage control, we propose to use a global frequency reference in this work which reflects the overall frequency dynamics of all asynchronous AC systems. The proposed control outperforms the existing frequency droop control with the following major benefits: reduced load shedding, reduced need of total online spinning reserves and reduced impact to the DC voltage profile. These advantages are illustrated via time domain simulation on an developed AC-MTDC test system. The VSC-MTDC model and the proposed control are implemented in the commercial grade software PSS/E thus is suitable to study large-scale realistic systems and can be incorporated into the power system planning process at utilities and ISOs.

II. Modeling of VSC-MTDC

There have been many recent efforts in the literature focusing on the development of power flow and dynamic VSC-MTDC models suitable electromechanical transient stability study [6]–[11]. These models are developed for different transient stability software such as MatDyn [7], [8], PSAT [6] and PSS/E [9]–[11]. Since PSS/E is a widely used commercial software in the United States, it has been chosen to be used in this work due to its capability to handle realistic large scale power systems.

To date there is still no standard dynamic model for VSC-MTDC in PSS/E, thus user defined models have to be used for the study. This work adopts the user defined model developed in [11]. The following sections will briefly describe the structure and the major components of the VSC-MTDC model used in this study and its integration with PSS/E. The readers are referred to [11] for more details.

A. VSC Model Structure

A conceptual illustration of the converter model is shown in Fig 2. Each converter bridges an AC bus and a DC bus. The AC side of the converter is modeled as a controllable voltage

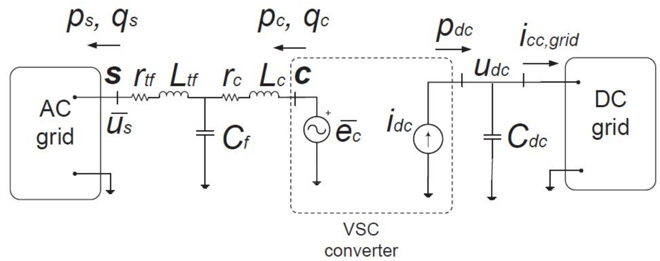

Fig. 2. VSC converter modeling [11]

source $\bar{e_c} = e_c \angle \delta_c$ coupled to the AC bus $\bar{u_s} = u_s \angle \delta_s$ through a phase reactor $z_c = r_c + j\omega L_c$, a capacitor $z_f = -j1/(\omega C_f)$ and a transformer $z_t r = r_{tr} + j\omega L_{tr}$. The DC side of the converter is modeled by a current injection i_{dc} into the DC grid. The AC side and the DC side are related by the energy conservation principle considering the converter loss which is quadratically dependent on the rms converter current on the AC side [11]. By transforming the AC quantities into the dq frame, each VSC is able to independently control the d and q axis currents [12]. The d-axis current can be used to either control active power injected into the AC bus p_s, or the DC bus voltage U_{dc}. The q-axis current can be used to either control reactive power injected into the AC bus q_s or the AC bus voltage magnitude u_s. The AC and DC side of the VSC is coupled by the power conservation principle as shown in (1), in which the power losses are a quadratic function of the magnitude of converter current i_c.

$$p_c + p_{dc} + p_{loss} = 0 \quad , \quad p_{loss} = a + bi_c + c{i_c}^2 \qquad (1)$$

B. VSC-MTDC Dynamic Model

The VSC model is a simplified model with cascaded control loops in the dq frame. The overall structure of the VSC model is shown in Fig. 3. The outer controllers control either P or u_{dc}, and Q or u_{ac} depending on the d axis and q axis control mode and generate current references in the dq axis i_{cd}^{ref}, i_{cq}^{ref} to the inner current controllers. DC voltage droop control can also be enabled to have all converters participate in the DC voltage control, in which an additional signal $\Delta P_{su_{dc}}$ is added to the P control reference P_s^{ref} for all converters. The inner current controllers are approximated by first oder transfer functions since their dynamics are much faster than the generator controllers in the AC system. The time constants τ_d, τ_q are typically selected in the range of 0.5-5ms [12]. The inner current controllers track the current orders i_{cd} and i_{cq} from the outer controllers and generate the actual currents in the dq axis after taking the current order limits into consideration. The current limits can be utilized as P-priority, Q-priority or P-Q equal priority [6], [11]. Finally, the currents are transformed back to the $\alpha\beta$ frame and used to compute the converter inner voltage $\bar{e_c}$ and the equivalent Norton current I_{SOURCE} of the VSC model used in PSS/E.

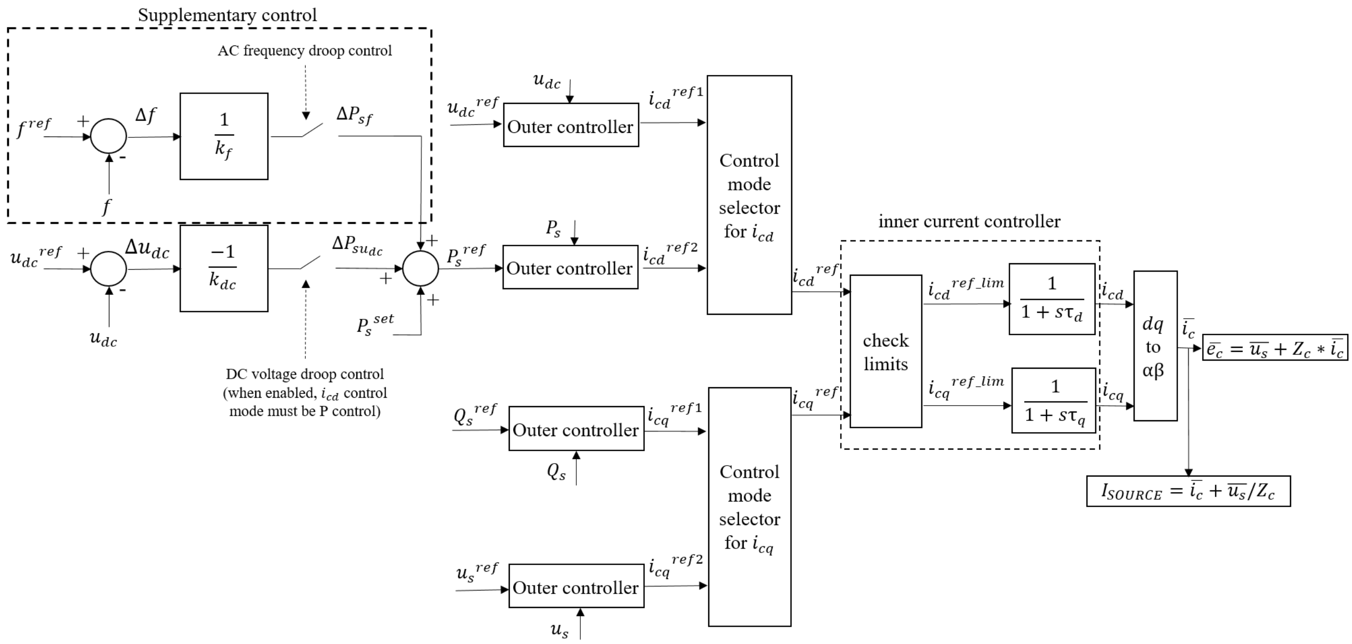

Fig. 3. VSC dynamic model with supplementary frequency control

Typically, the outer controllers are implemented as PI controllers. In this work, a variant is used for the P and Q outer controller as the following:

$$i_{cd}^{ref} = \frac{P_s^{ref}}{u_s} \tag{2}$$

$$i_{cq}^{ref} = \frac{Q_s^{ref}}{u_s} \tag{3}$$

which means that the PI controller gains for the P and Q controllers are set to zeros. This is enabled by the ideal phase locked loop assumed in this work, which aligns the converter AC voltage with the d axis.

III. VSC Frequency Control Strategy

A. Overall Control Structure

The supplementary frequency control adds an additional signal ΔP_{sf} to the set point of the active power controller P_s^{set}, as shown in the dashed box in Fig. 3. The value ΔP_{sf} is proportional to the frequency error $\Delta f = f^{ref} - f$ with a droop. Combined with the DC voltage droop control, the overall active power reference is given by:

$$P_{si}^{ref} = P_{si}^{0} - \frac{1}{k_{vi}}\Delta u_{dci} + \frac{1}{k_{fi}}\Delta f_i \tag{4}$$

for each converter i, where $k_{vi} > 0$ and $k_{fi} > 0$ are called DC voltage droop constant and AC frequency droop constant, respectively. P_{si}^0 is the initial active power set point for each converter i obtained from the steady state power flow solution. The major difference between the local frequency control in the literature and the proposed global scheme is the selection of the signal used as the frequency reference value f^{ref}, as detailed in the following sections.

B. Local Control

In the local control scheme for frequency support proposed in the literature [13]–[20], the frequency reference is set to be equal to the nominal frequency $f^{ref} = 1\ p.u.$ Since no communication is required among the converters to implement such scheme, it is herein referred as “local” control. The major drawback of the local scheme is that it degrades the DC voltage profile while the frequency control is activated due to the strong coupling between the frequency and DC voltage droop control, as will be shown later in the simulation results.

C. Proposed WAF Control

To overcome the above mentioned drawbacks, a global frequency control scheme called weighted average frequency (WAF) control is proposed to achieve frequency support among asynchronous AC systems. In the WAF control, the frequency reference value for each converter is set to a common value, which is the weighted average of frequencies measured at all converter terminals:

$$f^{ref} = \bar{f} = \sum_{i=1}^{n} \alpha_i f_i \tag{5}$$

where $\alpha_i \in [0,1]$, $\sum_{i=1}^{n} \alpha_i = 1$ are the weights of the measured frequency of the converters, n is the total number of converters in the VSC-MTDC system.

This control scheme was originally proposed in [21] for the purpose of improving the transient stability of a single AC system with embedded VSC-MTDC network. It is still effective for VSC-MTDC connecting asynchronous AC systems because frequency is a scaler quantity, which is also comparable in asynchronous AC systems. The main idea is that converters with terminal frequencies higher than the weighted average frequency tend to draw more power from the AC system, whereas those with terminal frequencies lower than the weighted average frequency tend to inject more power into the connected AC system. This effectively achieves the goal of exchanging primary reserves among asynchronous AC systems.

In [21], the authors also discuss about the procedure of weight selection for the α_i's. The principle is to achieve minimum impact to the DC voltage profile while the frequency control is activated. It is shown that when α_i's are chosen as in (6), the impact to the DC voltage will be zero theoretically. The interaction between the DC voltage droop control and the frequency droop control is thus mitigated.

$$\alpha_i = \frac{\frac{1}{k_{fi}}}{\sum_{i=1}^{n} \frac{1}{k_{fi}}} \tag{6}$$

IV. Case Study

A. Test System Development

In order to study the proposed the control strategy, an AC-MTDC test system is developed as shown in Fig. 4. Each AC system is represented by IEEE benchmark 2-area test system [22]. The effects of renewable integration and decommitment of conventional generators generally involve reducing system inertia and less spinning reserves. In order to simulate these effects, the inertia constants of all generators are reduced from 6.5s to 3.5s. The nameplate MVAs of all generators are reduced from 900MVA to 600MVA, and the maximum active power output from 765MW to 550MW. Besides, in order to properly simulate frequency response of power systems, a governor model is added to each generator using the IEEEG1 model, whose parameters are chosen based on the typical values for steam turbines proposed in [23]. The nominal DC voltage of the MTDC network is 320kV. VSC ratings are 500MVA. The DC voltage droop constant k_{dc} and frequency droop constant k_f are set to $0.1pu$ and $0.005pu$ on the converter MVA base for each VSC.

The steady state operating point of the test case is modified to emulate the realistic WECC to EI case developed in [4], by proportionally modifying the generation, load and the power transmitted between the AC systems. The procedure is briefly outlined as follows. Before interconnecting the AC systems, there is no power interchange between the two. Each AC system is serving its own load which is 1800MW in total. In [4], to capture the load diversity benefits, the load in the WECC is reduced by 14GW, which is about 7.5% of the total load in WECC to simulate a slightly off-peak condition in WECC, and the peaking generation in EI is turned off by the same amount. The excessive generation in WECC is then transfered to EI via the HVDC network. Similarly in the proposed test system, the load in the AC system 1 (A1) is

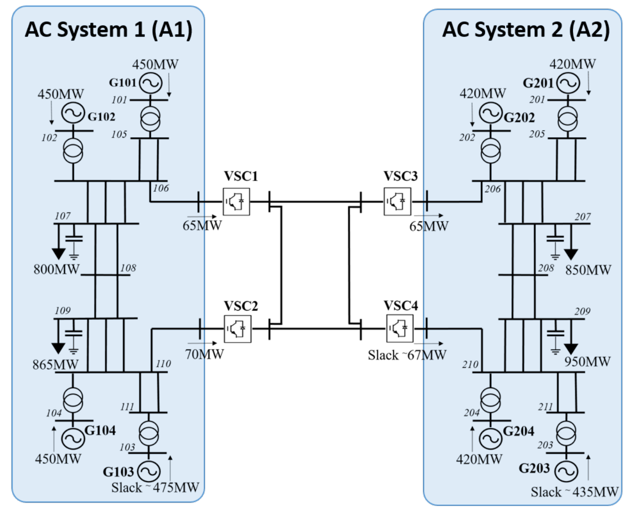

Fig. 4. Developed AC-MTDC test system

TABLE I
UFLS SETTINGS USED FOR THE STUDY

Load Shedding Block	Load Dropped (% of original)	Frequency Set-point (Hz)	Under-frequency Pickup Time (cycle)	Breaker Time (cycle)
1	5.6	59.3	14	3
2	5.6	59.2	14	3
3	5.6	59	14	3
4	5.6	58.8	14	3
5	5.6	58.6	14	3

decreased by 135MW (7.5% of total load), and the generation in the AC system 2 (A2) is decreased by the same amount to model the outage of peaking generation. The excessive generation of 135MW in the A1 is then transferred to A2 via the VSC-MTDC network. The resulting power flows are shown in Fig. 4. The loads in both areas are modeled as 100% constant current for active power and 100% constant impedance for reactive power respectively. A five block UFLS scheme is adopted from a WECC standard table [24], as shown in Table I, and is realized by the model "LDS3BL" in PSS/E.

B. Simulation Results

Time domain dynamic simulation is performed in PSS/E. The contingency used is the generator outage of Gen102 in A1. The resulting AC system frequencies along with the load shed in each AC system and the DC voltage are shown in Fig. 5 and Fig. 6 respectively. As can be seen from Fig. 5, both local frequency control and WAF control are able to increase the frequency nadir and bring the system frequency to a satisfactory settling frequency which is above 59.5Hz. However, the proposed WAF control provides more effective frequency support to A1 with a higher frequency nadir (59.18Hz) and lower load shedding amount (6%) due to the mitigation of the coupling with the DC voltage droop, and keeps the frequency performance in a safe region in A2 without causing any load shedding. On the DC side, it is obvious that the local frequency control causes severe impact

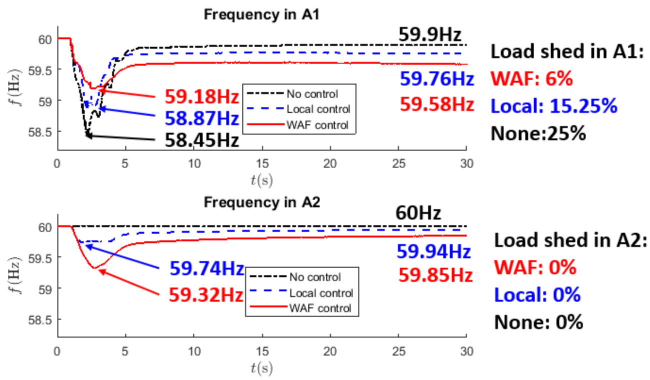

Fig. 5. AC system frequencies and load shed

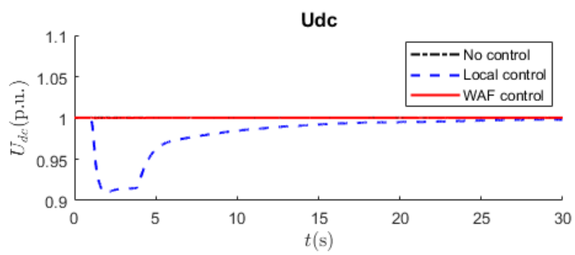

Fig. 6. DC voltage

to the DC voltage profile with a DC voltage nadir of $0.91pu$, which is quite close to the limit of $0.9pu$. On the other hand,the proposed WAF control introduces unnoticeable impact to the DC voltage profile. Therefore, the proposed WAF control is superior to the existing local frequency control in terms of both AC and DC side performances.

V. Conclusions

A global frequency control scheme based on weighted average frequencies (WAF) of all converter AC terminals is proposed to provide frequency support among asynchronous AC systems and is shown to outperform the existing local frequency control scheme in the literature. Three major benefits of the proposed WAF control are reduced load shedding, reduced need of total online spinning reserve, and reduced impact to DC voltage profile as compared to the local scheme, which are illustrated through dynamic simulation on an AC-MTDC test system. The proposed control is implemented in the commercial grade software PSS/E thus is suitable to study large scale realistic power systems and can be incorporated into the power system planning process at ISOs and utilities.

References

[1] "Interconnections seam study," https://www.nrel.gov/analysis/seams.html.

[2] J. McCalley, A. Figueroa, A. Jahanbani, H. Nosair, and A. Venkatraman, "Interconnections seam study," https://www.nrel.gov/analysis/seams.html.

[3] D. Osborn and D. Orser, "Converter selection for products of the HVDC network," in *2016 IEEE Power and Energy Society General Meeting, PESGM 2016*. IEEE Computer Society, 2016.

[4] M. A. Elizondo, N. Mohan, J. O'Brien, Q. Huang, D. Orser, W. Hess, H. Brown, W. Zhu, D. Chandrashekhara, Y. V. Makarov *et al.*, "HVDC macrogrid modeling for power-flow and transient stability studies in north american continental-level interconnections," *CSEE Journal of Power and Energy Systems*, vol. 3, no. 4, pp. 390–398, 2017.

[5] D. Van Hertem and M. Ghandhari, "Multi-terminal VSC HVDC for the European supergrid: Obstacles," *Renewable and sustainable energy reviews*, vol. 14, no. 9, pp. 3156–3163, 2010.

[6] J. Beerten, S. Cole, and R. Belmans, "Modeling of multi-terminal VSC HVDC systems with distributed DC voltage control," *IEEE Transactions on Power Systems*, vol. 29, no. 1, pp. 34–42, 2014.

[7] S. Cole, J. Beerten, and R. Belmans, "Generalized dynamic VSC MTDC model for power system stability studies," *IEEE Transactions on Power Systems*, vol. 25, no. 3, pp. 1655–1662, 2010.

[8] J. Beerten, S. Cole, and R. Belmans, "Generalized steady-state VSC MTDC model for sequential AC/DC power flow algorithms," *IEEE Transactions on Power Systems*, vol. 27, no. 2, pp. 821–829, 2012.

[9] P. J. Chainho, A. A. Van der Meer, R. Hendriks, M. Gibescu, and M. Van Der Meijden, "General modeling of multi-terminal VSC-HVDC systems for transient stability studies," in *Proc. 6th IEEE Young Researchers Symposium in Electrical Power Engineering, Delft, the Netherlands*, 2012.

[10] S. Liu, Z. Xu, W. Hua, G. Tang, and Y. Xue, "Electromechanical transient modeling of modular multilevel converter based multi-terminal HVDC systems," *IEEE Transactions on Power Systems*, vol. 29, no. 1, pp. 72–83, 2014.

[11] J. Renedo, A. García-Cerrada, L. Rouco, L. Sigrist, I. Egido, and S. S. Verdugo, "Development of a PSS/E tool for power-flow calculation and dynamic simulation of VSC-HVDC multi-terminal systems," 2017.

[12] A. Yazdani and R. Iravani, *Voltage-sourced converters in power systems: modeling, control, and applications*. John Wiley & Sons, 2010.

[13] T. M. Haileselassie and K. Uhlen, "Primary frequency control of remote grids connected by multi-terminal HVDC," in *IEEE PES General Meeting*. IEEE, 2010, pp. 1–6.

[14] T. K. Vrana, L. Zeni, and O. B. Fosso, "Active power control with undead-band voltage & frequency droop applied to a meshed DC grid test system," in *2012 IEEE International Energy Conference and Exhibition (ENERGYCON)*. IEEE, 2012, pp. 612–616.

[15] N. R. Chaudhuri, R. Majumder, and B. Chaudhuri, "System frequency support through multi-terminal DC (MTDC) grids," *IEEE Transactions on Power Systems*, vol. 28, no. 1, pp. 347–356, 2013.

[16] I. M. Sanz, B. Chaudhuri, and G. Strbac, "Frequency changes in AC systems connected to DC grids: Impact of AC vs. DC side events," in *2014 IEEE PES General Meeting— Conference & Exposition*. IEEE, 2014, pp. 1–5.

[17] L. Papangelis, X. Guillaud, and T. Van Cutsem, "Frequency support among asynchronous AC systems through VSCs emulating power plants," 2015.

[18] S. Akkari, J. Dai, M. Petit, and X. Guillaud, "Interaction between the voltage-droop and the frequency-droop control for multi-terminal HVDC systems," *IET Generation, Transmission & Distribution*, vol. 10, no. 6, pp. 1345–1352, 2016.

[19] S. G. Vennelaganti and N. R. Chaudhuri, "Selective power routing in MTDC grids for inertial and primary frequency support," *IEEE Transactions on Power Systems*, vol. 33, no. 6, pp. 7020–7030, 2018.

[20] A. E. Leon, "Short-term frequency regulation and inertia emulation using an MMC-based MTDC system," *IEEE Transactions on Power Systems*, vol. 33, no. 3, pp. 2854–2863, 2018.

[21] J. Renedo, A. García-Cerrada, and L. Rouco, "Active power control strategies for transient stability enhancement of AC/DC grids with VSC-HVDC multi-terminal systems," *IEEE Transactions on Power Systems*, vol. 31, no. 6, pp. 4595–4604, 2016.

[22] L. Lima, "IEEE PES Task Force on benchmark systems for stability controls," *SAT*, vol. 15, p. 14, 2014.

[23] "Dynamic models for steam and hydro turbines in power system studies," *IEEE transactions on power apparatus and systems*, no. 6, pp. 1904–1915, 1973, iEEE Committee Report.

[24] "WECC off-nominal frequency load shedding plan," https://www.wecc.org/Reliability/Off-Nominal%20Frequency%20Load%20Shedding%20Plan.pdf, 2011.

Impact of Power Transformer Overload Ratings on Transformer Reliability and Life

Farzad Azimzadeh Moghaddam and James D. McCalley

farzadam@iastate.edu, jdm@iastate.edu

May 2019

ABSTRACT

Power transformers are usually operated within their nameplate MVA rating, as identified by the transformer manufacturer. There are, however, conditions under which a transformer may experience loading beyond which it was originally intended, a situation that drives consideration of alternative responses of either making capital investments, employing operational constraints, or operating the unit beyond its rating. This project aims to define guidelines and criteria to support such decision-making, identifying power transformer loadings that achieve good balance among economics, reliability, and transformer life while considering the influence of increased renewable penetration in the network and the influence of geomagnetic disturbances on transformer performance. In order to address the project objectives, a system called the "Transformer Management Tool (TMT)," is under development; this system will be described. The current focus of the project is on addressing issues raised by Cedar Falls Utilities (CFU); CFU project objectives are presented. Also, a proposed procedure for processing dissolved gas analysis test results is provided.

Coordinating Conventional Voltage Control Devices with Smart Inverters in Rural Distribution Networks with DER Penetration

Alok Kumar Bharati
Venkataramana Ajjarapu
Department of Electrical and Computer Engineering
Iowa State University, Ames, IA - 50011

***Abstract*— The project focuses on rural distribution feeders and studying the impact of high penetration of distributed energy resources (DERs) on voltage performance. Voltage performance in power system is closely related to the reactive power & the losses in the system and these have direct impact on the voltage stability of the system. We have found that rural feeders have the tendency to have significantly higher voltage violations depending on the loading conditions due to the longer lines in the network. The amount of unbalance is also not easily controlled and does see some parts of the network being single phase or two-phase causing voltage imbalance in these feeders. This can result in significant load unbalance in the system. IEEE 34-node system is chosen for the setting up of tools and analytical methods as it characterizes most of the rural distribution system features like long lines, lightly loaded and unbalanced system. The sensitivity analysis of the IEEE 34 node system reveals that the voltage regulation devices should be distributed along the feeder to ensure minimum voltage violations. Due to one of the phases being heavily loaded, voltage regulation using 3-phase regulators or capacitor banks tend to cause voltage violations in the other phases while trying to regulate voltage in one phase. The solar PV is a positive impact on the voltage profile in the IEEE 34-node system.**

A. Smart Inverter for Voltage Regulation

The power distribution system has all the above-mentioned voltage regulating devices that function together in a coordinated way. Each of these voltage regulating devices have a role to play depending on the location of the device in the grid. The modern distribution system is being proliferated by more complex devices like smart inverters that have flexible real and reactive power modulation capability depending on the primary source of power that the inverter is fed from. With solar PV inverters, the ratings of the PV inverter are fixed, and the reactive power modulation capability varies with the amount of real power being supported by the smart inverter. In this project we are exploring the coordination of smart inverters along with the conventional voltage regulating devices in a rural distribution system. Figure 1 shows an example of the droop characteristics that will be used to control the node voltage of the smart inverter locations. Inverter based resources (IBR) like solar PV, battery storage and electric vehicles are integrated to the grid using inverters. The latest IEEE 1547 grid integration standard that governs the integration of various IBR to the grid requires the inverters be rated to allow 44% of the kVA rating for reactive power modulation which means they should be ~10% overrated based on the real power capacity. If the inverters are rated for 100% real power rating, then they will be required to curtail real power to provide the 44% reactive power modulating capability.

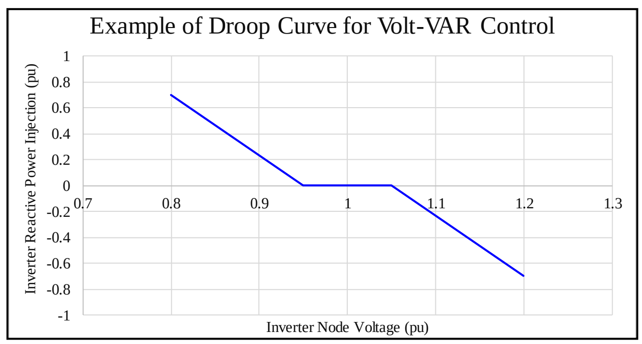

Figure 1: Volt-VAR Droop Curve Example Implemented in a Smart Inverter to Control Node voltage

The droop curve in Figure 2 shows that if the voltage goes below 0.95 pu, the inverter will inject reactive power into the grid to bring the voltage back within the 0.95 – 1 pu range and if the voltage exceeds 1.05 pu, it will absorb reactive power to maintain the voltage in the range. The ±5% voltage from 1 pu can be reduced to 0% making it strictly follow the voltage set-point. This can be done with various slopes of the voltage control to ensure the control is a stable control to maintain the voltage set-point. The smart inverter control has the potential to provide the required reactive power while supplying the real power from the DERs. We explore the utilization of the smart inverters for voltage control and reduce the usage of the conventional voltage regulating devices and explore the amount of DER penetration required to minimize the tap changes and capacitor switching in the distribution grid.

Investigation of Relevant Distribution System Representation with DG for VSM Assessment

Alok Kumar Bharati and Venkataramana Ajjarapu
Department of Electrical and Computer Engineering,
Iowa State University,
Ames, Iowa, USA – 50011.
alok@iastate.edu ; vajjarap@iasate.edu

***Abstract*— This poster emphasizes the importance of including the unbalance in the distribution networks for stability studies in power systems. The distribution system is evolving rapidly with high proliferation of distributed energy resources (DERs); these are not guaranteed to proliferate in a balanced manner and uncertainty resulting due to these DERs is well acknowledged. These uncertainties cannot be captured or visualized without representing the distribution system in detail along with the transmission system. We show the impact of proliferation of DERs in various 3-phase proportions on voltage stability margin through T&D co-simulation. Higher percentage of net-load unbalance (NLU) in distribution system aggravates the stability margin of the distribution system which can further negatively impact the overall stability margin of the system**

Keywords*— T&D Co-simulation, Voltage Stability Margin, VSM, Unbalanced Distribution System, Distributed Generation (DG), Equivalent Feeder Impedance, Net-Load Unbalance (NLU)

I. Overview

THE power system is a large complex network of various components that are geographically spread in the form of transmission and distribution sub-systems. For accurate voltage stability margin assessment in the presence of large DER penetration, there is a need to represents the distribution system with sufficient detail. Net-Load Unbalance (NLU) is determined and is used to demonstrate the relation between NLU and the voltage stability margin of the system. Relevant representation of the distribution system is important for accurate assessment of the voltage stability margin of the system. With the proliferation of DERs in the distribution system, there is no/ minimal control over how these DERs are proliferating in the three phases which can affect the NLU thereby affect the VSM of the system. We have used T&D co-simulation to demonstrate its need as the equivalent distribution feeder cannot capture the complete system details for VSM studies. DERs can be controlled to reduce the NLU and thereby improve the stability margin of the system.

We define the net-load unbalance as percentage:

$$P_{avg} = \frac{P_A+P_B+P_C}{3} \quad (1)$$

$$U_i = \frac{P_i-P_{avg}}{P_{avg}} \qquad \forall\, i = A,B,C \quad (2)$$

$$NLU = \max(\,|U_i|) \times 100\,\% \qquad \forall\, i = A,B,C \quad (3)$$

Where,

P_A, P_B, P_C — The net-loads on phases A, B, C.

NLU % — Percentage of maximum net-load unbalance.

This work is funded by Power System Engineering Research Center (PSERC) project S-70.

II. Key Results

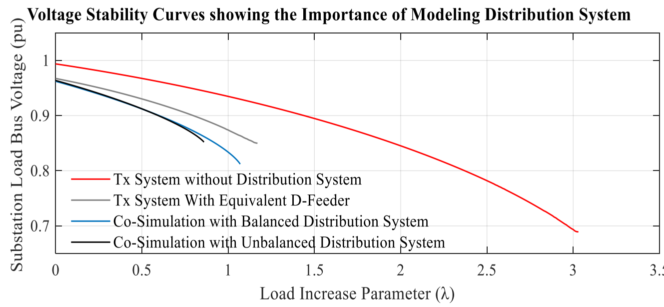

Fig. 1. Voltage Stability Curves with Various Method of Simulations: IEEE 9-Bus Transmission + IEEE 4-Node Distribution System

The study is extended to the IEEE 123-bus distribution system. The loads are modeled with ZIP profile [ZIP] = [0.4 0.3 0.3]. The total load on the 3 phases A, B, C are 45.44 MW, 29.28MW and 36.96 MW respectively. 40%, 60% and 80% DG of the total load is added in various proportions in the 3 phases.

TABLE I. Impact of DG Operating in VVC Mode versus UPF mode on Load Margin- IEEE 9 –bus T + 123-Bus D-System

Total DG Penetration	DG Distribution across 3-Ø (% A,% B,% C)	Net-Load Unbalance (%)	Load Margin/ VSM (MW)	
			DG in VVC Mode	DG in UPF Mode
40% DG (44.67 MW)	50, 10, 50.3	17.80	273.49	243.86
	40,40,40	25.53	267.69	240.61
	55, 55, 10	48.73	260.80	237.81
	10, 62, 61	88.05	241.38	231.75
60% DG (67 MW)	60, 60, 60	25.53	299.17	256.44
	72, 25, 72	41.47	290.05	258.93
	77, 77, 25	85.93	284.66	254.14
	25, 85, 85	134.85	260.10	240.98
80% DG (89.34 MW)	90, 50, 90	17.80	317.48	271.28
	80, 80, 80	25.53	316.60	268.83
	95, 95, 50	147.93	296.81	269.24
	52, 100, 100	200.00	294.25	254.48

Title: Demand Response Prediction and Setpoint Control of Heterogeneous Residential Air Conditioners

Authors: Nicholas Brown and Venkataramana Ajjarapu, Iowa State University

Residential air conditioners are a potential source of demand response. They can be dispatched to address renewable power variability by providing operating reserves. To deliver reserves, air conditioners' temperature setpoints can be temporarily adjusted without requiring large changes in thermal comfort.

A challenge in incorporating air conditioner demand response is in predicting aggregate changes in power demand across thousands of devices. Scalable, air conditioner-level predictions are supported by neural networks, which provide expected ON/OFF states. Through resampling of device-level historical cycling data, the expected states of individual air conditioners are used to create aggregate prediction intervals. The predictions implicitly capture the heterogeneity of building characteristics and thermostatic cycling, while explicitly accounting for state (ON/OFF), setpoints and ambient temperatures.

An Evaluation of Wind Energy Production in Iowa at Elevated Hub Heights

Bin Cai[1], Phuong Vo[2], Sri Sritharan[3] and Eugene S. Takle[4]

[1,2,3] *Department of Civil, Construction and Environmental Engineering, Iowa State University, Ames, Iowa 50011, USA*

[4] *Department of Geological and Atmospheric Science, Iowa State University, Ames, Iowa 50011, USA*

Iowa is a leading state when it comes to generating electricity from wind energy. According to the U.S. Department of Energy, wind power accounted for 33.7 percent of all electricity in Iowa in 2018 while the overall highest recorded capacity factor of Iowa wind farms was 39 percent, as reported by wind farm developers. Today, a majority of wind turbines in both Iowa and the nation stand only at 80 m or lower. This height limit exists due to transportation constraints associated with the steel tubular technology, which can now be overcome by using the Hexcrete tower technology that uses precast concrete. Since tall wind turbine towers have the potential to reduce the Levelized Cost of Energy (LCOE), evaluating wind energy production at elevated hub heights is of significant interest. However, this information cannot be easily established because wind data at higher hub heights are not readily available.

Due to the lack of wind resource information, simulated data developed by the National Renewable Energy Laboratory (NREL) known as Wind Integration National Dataset (WIND) Toolkit, were obtained and used to forecast the wind energy production. However, this model was established from measurements from nearby sites where topographical differences and seasonal changes have not fully been examined and evaluated for accuracy. Therefore, an evaluation of wind power production based on the WIND Toolkit at elevated hub heights may not yield reliable outcomes.

Using measured wind data from five sites in Iowa, this paper: a) evaluates the wind energy potential at 100 m through 140 m, and b) examines the accuracy in estimating wind power production using WIND Toolkit. Results show that the hourly averages of wind speed recorded from WIND Toolkit slightly underestimated the true values, suggesting that calculating the energy production using the WIND Toolkit would yield conservative results. An average of 17 percent increase in wind energy potential was observed from 80 m to 140 m for the selected turbine and the corresponding average increase was 7.7 percent when the height was increased from 80 m to 100 m. It is concluded that increasing the wind turbine tower height by at least 20 m is more advantageous to Iowa.

[1] Graduate Assistant, binc@iastate.edu
[2] Undergraduate Researcher, phvo@iastate.edu
[3] Wilkinson Chair in Engineering and Professor of Structural Engineering, sri@iastate.edu
[4] Emeritus professor of Agricultural Meteorology, gstakle@iastate.edu

A Tool for Mining AMI Data to Model Customer Loads for Small Public Power Utilities

Nichelle'Le Carrington

May 8, 2018

Abstract

This project describes the development of a Smart Meter Analysis Resource Tool to facilitate small utilities in the processing of Advance Metering Infrastructure (AMI) data with limited staff resources. The proposed tool is based on MatLab-Simulink-Guide toolboxes and provides a complete set of user graphical interfaces to properly model and study customer loads using AMI data for small utilities. The propose tool allows to model and observe customer contribution and the main determinants that affect load consumption. Customer segmentation, typical load profiles, and time-varying probabilistic distributions of load consumption will be useful for various higher-level administration applications such as usage-specific tariff structures, consumer-specific demand response programs and cost/benefit analysis of renewable energy integration programs. The tool will result in a stand alone software that allows import and process of raw AMI data files.

Title: ISU team participation in the DOE Collegiate Wind Competition

Author: Nicholas David

Abstract:

An interdisciplinary first-ever team of undergraduate students from ISU participated in the Department of Energy Collegiate Wind Competition, along with 11 other teams from across the United States. After their first successful event in 2018, they were invited back for a second round of events in 2019. Competition took place at the annual conference of the American Wind Energy Association and at the National Wind Technology Center, respectively. Experts from the National Renewable Energy Laboratory judged the teams based on a technical design challenge, a business development challenge, and a wind farm siting challenge. Students range in class from first years to seniors and are associated with the ISU Wind Energy Student Organization advised by graduate students. They applied concepts learned in class, and expanded their knowledge with experiment-based learning. They built a complete wind turbine with active pitch control and a dc-dc power electronic converter, and created applications to charge a battery and supercapacitor. Participation in this national design competition has had the impact of boosting the knowledge and abilities of ISU students and has spring-boarded their careers in wind energy.

Anomaly Detection and Mitigation for Wide-Area Control System using Machine Learning and Hardware-in-the-loop CPS Security Testbed Demonstration

Gelli Ravikumar and Manimaran Govindarasu, Iowa State University

Abstract:
In an interconnected multi-area power system, wide-area measurement based damping controllers are used to damp out inter-area oscillations, which jeopardize grid stability and constrain the power flows below to their transmission capacity. The effect of wide-area damping control (WADC) significantly depends on both power and cyber systems. At the cyber system layer, an adversary can inflict the WADC process by compromising either measurement signals, control signals or both. Stealthy and coordinated cyber-attacks may bypass the conventional cybersecurity measures to disrupt the seamless operation of WADC. It is identified to devise an attack-resilient WADC(AR-WADC) system for the detection of cyber-attack anomalies and deployment of suitable mitigation techniques.

This project proposes an anomaly detection (AD) algorithm using Machine Learning and a rule-based systematic process for mitigation. The proposed AD algorithm considers measurement (input of WADC) and control (output of WADC) signals as input to evaluate the type of activity such as normal, perturbation(small or large signal faults), attack and perturbation-and-attack. In the kind of attack activity detection, the mitigation module tunes the WADC signal and sets the control status mode such as wide-area mode or local mode. The proposed anomaly detection and mitigation (ADM) module works in line with the WADC at the control center for the attack activity detection of both measurement and control signals and eliminates the need for ADMs to the geographically distributed actuators. It demonstrates the impact of data-integrity attacks on the WADC and the efficacy of ADM algorithm for a two-area four-machine power system. Results such as attack-activity detection and mitigation with low false positive and negative rates evaluate the effectiveness of the algorithm.

Optimization of Cyber-Security Investment Strategies in a Smart Grid Using Game-Theory

Burhan Hyder
Department of Electrical and Computer Engineering
Iowa State University
Ames IA, USA
bhyder@iastate.edu

Govindarasu Manimaran
Department of Electrical and Computer Engineering
Iowa State University
Ames IA, USA
gmani@iastate.edu

***Abstract*—With the increasing penetration of cyber systems in the power grid, the large scale Cyber-Physical System (CPS), namely, the Smart Grid, is increasingly becoming more vulnerable to attacks from adversaries that intend to disrupt the serenity and the economy of a region. It has now become imperative to deploy adequate security measures all across the grid that can fend off any kind of cyber threat. Since investment in security has its own limitations as far as financial resources are concerned, the allocation of these resources optimally is important but challenging at the same time due to the uncertain behavior of attackers. This paper addresses the problem of optimizing investment strategies in the cybersecurity infrastructure of a smart grid using a game-theoretic approach. The proposed approach involves modeling of attackers and defenders separately within a game-theoretic framework. The attacker is modeled using various attacker profiles that are generally considered as possible types of adversaries in the context of CPS. Each profile has certain characteristics to bring out the aspect of uncertain behavior. The defender is modeled with various pragmatic characteristics that can be easily translated to the real-world grid scenarios for implementation. These characteristics include the standards laid down by the North American Electric Reliability Corporation (NERC) for Critical Infrastructure Protection (CIP) commonly known as the NERC-CIP standards. These models allow us to obtain the Effort and Capital Expenditure (ECE) incurred by the attacker and the defender for various possible scenarios or strategies to attack and defend the grid, respectively. These strategies along with the corresponding ECEs of the attacker and the defender form the payoff matrix for the game formulation. The game is then solved to obtain optimal strategies to be used by the defender to minimize their ECE against various attacker actions.**

***Index Terms*—CPS, Smart Grid, Cyber Security, Game Theory, Attacker model, Defender model, NERC-CIP**

I. Methodology

The flowchart in Fig. 1 shows the overall methodology used in this work.

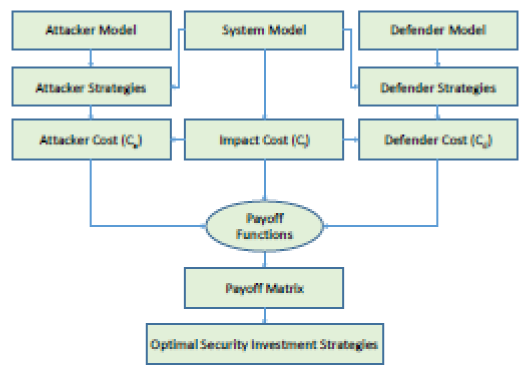

Fig. 1. Framework Flowchart

II. Key Models

A. Attacker Model

The attacker is modelled by considering various possible profiles of an attacking entity with certain characteristics for each profile. Some of the proposed profiles have been listed below:

1) Basic User
2) Insider
3) Nation State
4) Cyber Terrorist

Some of the various characteristics assigned to the attacker profiles are listed below:

1) Knowledge of the system
2) Financial Resources
3) Manpower
4) Determination

B. System Model

The system model involves modelling of cyber-physical substations in a smart grid using North American Electric Reliability Corporation's(NERC) Critical Infrastructure Protection (CIP) standards and the Electricity Subsector Cybersecurity Capability Maturity Model (ES-C2M2) proposed by the United States Computer Emergency Readiness Team (US-CERT) involving assignation of Maturity Indicator Level (MIL) to various characteristics of each substation.

C. Defender Model

The Defender Model uses the costs assigned to various actions that a defender can take when we consider a cyber-physical smart grid Using these models, strategies and costs for attacker and defender are modelled which are fed in to the game-theoretic engine which outputs the optimal investment strategies for the defender with respect to cybersecurity investment.

Community-scale residential building energy modeling in Cedar Falls, Iowa

Elham Jahani and Kristen Cetin, Iowa State University

Growing energy consumption in urban areas as well as the general migration of the U.S. population from rural to urban areas has raised the importance of energy planning for the future. To engage in such energy planning, improving the modeling abilities for predicting energy consumption at the community scale is crucial.

This research focuses on statistical sampling method, Numerical Moment Matching (NMM) method, as a technique to predict the energy consumption of a large dataset of residential buildings in Cedar Falls, Iowa. In this method, utilizing the results of an energy modeling sensitivity analysis, several key building parameters, obtained from energy audit and county assessor's data, are identified as key features in defining the energy performance of the studied buildings. These parameters are used to define a set of index buildings and associated weighting factors that statistically represent the building characteristics of the dataset. To validate the results of this study, a large data set of electricity use data from single family buildings in Cedar Falls, IA are used to obtain the electricity consumption profile of single family buildings in Cedar Falls.

Optimal bidding for lithium-ion batteries in frequency regulation markets

Authors: Jinqiang Liu (ISU). Zhaoyu Wang (ISU), Chao Hu (ISU)

Poster Abstract

The grid deployment of lithium-ion (Li-ion) batteries has grown fast during recent years. High energy density and mature packaging techniques enable MW/MWh-scale Li-ion battery storage systems. In particular, Li-ion batteries are competitive in frequency regulation markets to trace the high-frequency and energy-neutral instruction signals, such as the ISO New England (ISO-NE) ENC and PJM's RegD signals. However, Li-ion batteries may encounter fast degradation in tracing these fast-changing and high-power instruction signals. In order to maximize the daily profit of Li-ion batteries in frequency regulation markets, we developed a model to optimize the capacity bidding and 5-min economic basepoints for frequency regulation. One-year real data in the PJM 5-min real-time energy market and pay-for-performance regulation market are utilized to calculate the revenue of the Li-ion battery storage system, while cycling-induced capacity degradation is considered in estimating the battery cost. The variance of Li-ion battery state-of-charge (SOC) profile is selected as an input feature for estimating cycle degradation, and this input feature shows a fairly linear correlation (C_p=0.98) with the battery capacity degradation. Finally, the optimization model is formulated as a mix-integer quadratic programming (MIQP) problem. Simulation results show that the proposed model can obtain optimal and cost-effective real-time energy schedule and frequency regulation capacity bidding with minimum battery capacity degradation. Additionally, the computing time of our method is on average 14s on a DELL computer with Intel Xeon E3-1240 CPU, which is approximately 99.44% shorter than the computing time of a state-of-the-art method in the literature.

Data-Driven and Machine Learning Based Load Modeling

Abstract

Zixiao Ma, Zhaoyu Wang

WECC composite load model is a newly developed load model that has drawn great interest from the industry. To analyze its dynamic characteristics with both mathematical and engineering rigor, a detailed mathematical model is needed. However, there is no complete mathematical representation of the full WECC composite load model in literature till now. Therefore, this work has developed a detailed mathematical representation of WECC CMPLDWG model. Moreover, the full WECC composite load model is a high-order system which has more than 25 states. The difference among time constant parameters of the dynamic equations also makes the solution of this dynamic system a stiff problem. To this end, we have applied singular perturbation-based order-reduction method to the WECC composite load model, to significantly reduce its order and computational time. The developed mathematical model and its reduced model are verified using both Matlab and PSS/E to show their effectiveness.

Development of a Modelling Framework for Refined Residential Occupancy Schedules

Authors: D. Malekpour Koupaei (Iowa State University), F. Hashemi (Penn State University), V. Tabard-Fortecoëf (INSA Lyon), U. Passe (Iowa State University)

Poster Abstract

Occupancy schedules are a leading source of uncertainty in building energy simulations. This uncertainty often results in an undesired gap between actual performance and predictions. Past efforts to develop more proper occupancy behavioral models have often been either oversimplified and hence underestimating or more precise but simply too complicated to become common practice. This study is an effort to find a balance between complexity and accuracy among the aforementioned models for the sole purpose of energy use studies in the context of residential neighborhoods. We start with a probabilistic occupancy model based on the American Time Use Survey (ATUS) and use input from the population of study to develop representative occupancy schedules.

SIEM-based Distributed IDS for SCADA

Sathya Mohan, Ravikumar Gelli, Manimaran Govindarasu

Abstract: Modern cyber attacks are getting more sophisticated day-by-day. Critical infrastructures like power, oil, gas and water use SCADA communication to manage and control their outstations, which are spread across wide area.

In this research, we are focusing on the anomalous alerts that occur at the different areas(Clients), which are visualized at the control center(Master). The rules are formulated to determine the anomalous behavior and are defined based on the SCADA traffic that uses DNP3 protocol between SCADA Master and outstations. Different format of IDS rules are shown based on time factor threshold, packet payload and functions to recognize abnormal activity in a network. This production mode is also deployed in a power utility environment. Results in real-time testing and analysis are performed.

Title: Co-Optimized Expansion Planning to Enhance Resilience of the Electrical System in Puerto Rico

Authors: Cody J. Newlun[1], Armando L. Figueroa[2], James D. McCalley[1]

[1]Department of Electrical & Computer Engineering, Iowa State University, Ames, Iowa 50011, USA
[2]Policy Studies Department, MISO, Eagan, Minnesota 55121, USA cnewlun@iastate.edu, afigueroa-acevedo@misoenergy.org, jdm@iastate.edu

Abstract—In September of 2017, the island of Puerto Rico (PR) was devastated by a category 4 hurricane, Hurricane Maria. The island experienced complete blackout and full restoration of the electrical system took nearly 11 months to complete. Therefore, it is of high-interest to re-develop the infrastructure at the generation, transmission, and distribution (GTD) levels to create a hurricane-resilient infrastructure.

This report details the methodologies behind developing a more resilient electric infrastructure using a co-optimized expansion planning (CEP) software tool. First, a model of the PR electric power system was developed to perform long-term CEP studies. The CEP tool developed seeks the minimum total cost of the PR system in a 20-year planning horizon while exploring various levels of expansion investment options. The CEP also models the system under extreme events (i.e. hurricanes) to allow for data-driven resilience enhancement decisions. Second, the report details infrastructure visions that contain resiliency investment options while the amount of distributed generation (DG) and centralized resource investments vary. Lastly, key findings from these visions are reported and the performance of the CEP model is discussed.

Advancements in autothermal processing of biomass to produce biorenewable fuel oil

Authors: Joseph P. Polin (ISU), Lysle E. Whitmer (ISU), Ryan G. Smith (ISU), Robert C. Brown (ISU)

Poster Abstract

Electrical power generation using biorenewable resources have focused on combustion of biomass feedstocks in power plants, but this is difficult to achieve in traditional equipment due to the differences in solid fuel properties from coal. This poster focuses on thermochemical processing of biomass to produce biorenewable fuel oil which can be used to offset traditional fossil fuels in power generation equipment. Fast pyrolysis can convert biomass into bio-oil using heat to thermally deconstruct biopolymers into bio-oil products. This research addresses the process bottleneck of conventional pyrolysis systems (external heat transfer) and alternatively operates the reactor in an autothermal mode, which oxidizes pyrolysis products to provide process heating. Process intensification conditions were achieved as a result of air-blown, autothermal operation and the reactor throughput of woody and herbaceous biomass feedstocks was increased three-fold. Carbon balances of the process indicate that lesser value pyrolysis products (biochar and low molecular weight, bio-oil light ends) were consumed via oxidative reactions to provide process heating. The yield and quality of the most valuable pyrolysis product (organic-rich, bio-oil heavy ends) were not significantly affected by autothermal operation. These bio-oil heavy ends can be used as a biorenewable fuel oil or be blended with traditional petroleum-derived, bunker fuel oil. This advancement in fast pyrolysis can help to reduce capital costs and operating expenses for larger-scale systems and improve the overall process economics of biorenewable fuel oil production.

IOWA STATE UNIVERSITY
OF SCIENCE AND TECHNOLOGY

CPrE-539 Cyber Physical System Security for Smart Grid

Title: Testbed-based Grid Exercise (GridEx) using PowerCyber CPS Testbed.

Subtitle: CprE 539 CPS Security Smart Grid, Course Project, Team-3

Abstract:

The objective of the project was to mimic the biennial NERC Grid Exercise (GridEx) at lab scale. GridEx is modelled on the Department of Homeland Security's Cyber Storm Series developed to test the robustness of electric power grid to cybersecurity threats. The task was divided into three moves namely Move 0, Move 1 and Move 2 dealing with the planning of scenarios, allocation of cyber physical resources for protection of vulnerable assets, and final testing. Mock risk assessment and optimal budget allocation was also performed as part of the project. Contingency analysis of the IEEE 39 Bus New England test system modelled within the ISU Power Cyber Testbed was performed by each team and optimal locations were chosen for PMU placement. Software based rules within Security Onion framework were developed for protecting the system from external attacks. This included writing rules in Firewall, Intrusion Prevention System and Intrusion Detection System. The final ISU GridEx program included students in three different teams called blue teams, responsible for protecting the power system from attacks from the red team. The Red team attacked the blue teams in predefined moves to test the defense put up by their respective networks. Blue teams were expected to defend their system and keep a log of incoming attacks from the voltage, frequency and current profiles along with the monitoring of packets in Wireshark. The model, methodology, attack vectors and mitigation strategies were tested during the entire exercise. This poster provides an overview on the activities undertaken in this project, highlighting the step by step analysis undertaken and the process flows. The poster also brings to knowledge, the benefits and learning outcomes.

Instructor

Prof. Manimaran Govindarasu

Co-Instructor

Dr. Gelli Ravikumar

Team Members

Mortada Saeed, Masters Student
Jeyanth Rajan Babu, Masters Student
Mohammad Aqueel, Masters Student
Anam Kalair, Doctorate Student

Real Time Synchrophasor Measurements Based Voltage Stability Monitoring and Control

Amarsagar Reddy Ramapuram Matavalam & Venkataramana Ajjarapu

With the increasing need for economic operation of the power grid, the system is being operated closer to their limits and so there is a need to address the increasing risk of voltage instability in the power grid. In this work, we have proposed methods that can monitor and mitigate the both short-term (in this case FIDVR) and long-term voltage instability by utilizing the Phasor Measurement Units and utilizing smart thermostats for control.

In the first part of our work [1], we look at the FIDVR phenomenon where the voltage recovery is delayed due to the stalling of 1-phase motors. Existing methods have utilized the voltage to quantify and mitigate FIDVR by load shedding. However, these methods do not utilize the composite load model dynamics. Thus, they are susceptible to oscillations in the voltage waveform occurring due to system dynamics and the control schemes is heuristic based. We have overcome these drawbacks by monitoring the admittance at the substation PMU. The sudden rise in susceptance indicates to the PMU that an FIDVR event has taken place at the substation and the rise in the susceptance provides the PMU with a reasonable estimate of the proportion of the load that is stalled. This information can be used to estimate the time to recovery and to determine the proportion of the air conditioners to disconnect for recovering within a set amount of time. To verify that this method indeed works as expected, multiple simulations in PSSE on the IEEE 162 Bus system are done with the results showing the expected behavior. To test the real-time nature of the method, the FIDVR phenomenon is simulated in a real-time test-bed and is shown to be able to determine the control amount in an online manner.

In the second part of our work [2], we look at the long term voltage stability phenomenon. Existing online methods utilize the Thevenin index for large systems but the theory is only valid for the simple two-bus system. This lack of theoretical basis is the reason why the existing local index methods cannot be validated at the control center leading to a cyber-security concern. To improve the understanding of the Thevenin index, we have derived an analytical relation between the local index and the system Jacobain, and thus we provided a mathematical justification for the use of the local index as an indicator for global stability. Exploiting this relation, we define a sensitivity based index and have verified that this index at the control center can validate the local Thevenin index on large systems (up to MATPOWER 3120 Systems). This sensitivity base index can be modified to account for various what-if scenarios (reactive limit reached, line outage, etc.) in an intuitive and computationally efficient manner. This enables the operator to assess the true state of the system with the ability by considering the generator reactive limits which is not possible using present Thevenin indices.

[1] Amarsagar Reddy R.M. and V. Ajjarapu, "PMU based Monitoring and Mitigation of Delayed Voltage Recovery using Admittances," Accepted for publication in IEEE Transactions on Power Systems.

[2] Amarsagar Reddy R.M. and V. Ajjarapu, "Sensitivity Based Thevenin Index With Systematic Inclusion of Reactive Power Limits," in IEEE Transactions on Power Systems, vol. 33, no. 1, pp. 932-942, Jan. 2018.

Iowa Army National Guard (IAARNG) Energy and Water Master Plan

Authors: Benjamin Robertson, Song-Charng Kong, Iowa State University

Abstract

The Iowa Army National Guard (IAARNG) intends to produce an Energy and Water Master Plan (EWMP) every five years. Iowa State University researchers are tasked to produce this mater plan, with the work started September 2018. The results presented here are focused on the methodology to produce this master plan. A three-step process is employed that breaks the report into the following sections: Profiles, Goals, and Action Plans. First, Profiles are the current state of the energy and water systems and provide graphical representations of IAARNG's yearly water consumption and consumption intensities of each system. They also provide an assessment of the resiliency and the overall condition of these systems. Second, Goals lists all the current mandates, laws, executive orders, and goals that apply to IAARNG's energy and water systems and that are focused on in this report. Finally, the methodology for producing action plans is discussed. In particular, the development of cost-analysis and business models for each plan, as well as discussion for acquiring funding for each plan.

Data-driven Identification and Prediction of Power System Dynamics Using Linear Operators

Pranav Sharma, Bowen Huang, Umesh Vaidya, Venkatramana Ajjarapu
Department of Electrical and Computer Engineering, Iowa State University, Ames, Iowa, USA

***Abstract*—We propose linear operator theoretic framework involving Koopman operator for the data-driven identification of power system dynamics. We explicitly account for noise in the time series measurement data and propose robust approach for data-driven approximation of Koopman operator for the identification of nonlinear power system dynamics. The identified model is used for the prediction of state trajectories in the power system. The application of the framework is illustrated using an IEEE nine bus test system.**

I. Key Concepts

A. Robust approximation of Koopman operator

We have a random dynamic system of form $x_{t+1} = T(x_t, \xi_t)$. For such a discrete dynamical system we can define Koopman linear operator, given any $h \in \mathcal{F}$, $\mathbb{U} : \mathcal{F} \to \mathcal{F}$ is defined by

$$[\mathbb{U}h](x) = \mathbf{E}_\xi[h(T(x,\xi))] = \int_W h(T(x,v))d\vartheta(v)$$

Consider snapshots of state variables subjected to various processes and measurement noises $X = [x_0, x_2, \dots, x_M]$. We define $\mathcal{D} = \{\psi_1, \psi_2, \dots, \psi_K\}$ as the observables on x_k. Define vector valued function $\mathbf{\Psi} : X \to \mathbb{C}^K$ as

$$\mathbf{\Psi}(x) := \begin{bmatrix} \psi_1(x) & \psi_2(x) & \cdots & \psi_K(x) \end{bmatrix} \tag{1}$$

Here, $\mathbf{\Psi}$ lift the system from state space to feature space. Any function $\phi, \hat{\phi} \in \mathcal{G}_\mathcal{D}$ can be written as

$$\phi = \sum_{k=1}^{K} a_k \psi_k = \mathbf{\Psi}\boldsymbol{a}, \quad \hat{\phi} = \sum_{k=1}^{K} \hat{a}_k \psi_k = \mathbf{\Psi}\hat{\boldsymbol{a}} \tag{2}$$

Here the objective is to minimize this residue for all possible pair of data points $\{x_m + \delta, x_{m+1}\}$. Using (2) we have:

$$\mathbf{\Psi}(x_k + \delta x_k)\hat{\boldsymbol{a}} = \mathbf{\Psi}(x_{k+1})\boldsymbol{a} + r.$$

Our aim is to find $\mathbf{K}$, finite approximation of Koopman operator that maps $\boldsymbol{a}$ to $\hat{\boldsymbol{a}}$, i.e., $\mathbf{K}\boldsymbol{a} = \hat{\boldsymbol{a}}$, and minimize the the residue term, r. The robust optimization can be written as a $\min - \max$ convex optimization problem, as follow:

$$\min_{\mathbf{K}} \max_{\delta\mathbf{G} \in \bar{\Delta}} \parallel (\mathbf{G} + \delta\mathbf{G})\mathbf{K} - \mathbf{A} \parallel_F \tag{3}$$

where $\mathbf{K}, \mathbf{G}_\delta, \mathbf{A} \in \mathbb{C}^{K \times K}$ and $\delta\mathbf{G} \in \mathbb{R}^{K \times K}$ is the new perturbation term characterized by uncertainty set $\bar{\Delta}$ which lies in the feature space of dictionary function.

B. Design of robust predictor in power system

Based on the robust optimization formulation (3), we have systematic way of tuning the regularization parameter. Here regularization term implies that the operator framework can fit into data driven predictor design. We first approximate the transfer operator using training data. Let $\bar{x}_0$ be the starting point for trajectory prediction. The initial condition from state space is mapped to the feature space, i.e., $\bar{x}_0 \implies \mathbf{\Psi}(\bar{x}_0)^\top =: \mathbf{z} \in \mathbb{R}^K$. Using Koopman operator system propagates as $\mathbf{z}_n = \mathbf{K}^n\mathbf{z}$. From this we can obtain the trajectory in state space, as $\bar{x}_n = C\mathbf{z}_n$. Here matrix C is obtained as the solution of the following least square problem:

$$\min_C \sum_{i=1}^{M} \parallel x_i - C\mathbf{\Psi}(x_i) \parallel_2^2 \tag{4}$$

II. Results

In order to understand the implications of developed robust prediction and identification algorithm for power system, we consider IEEE 9 bus test case.[1]

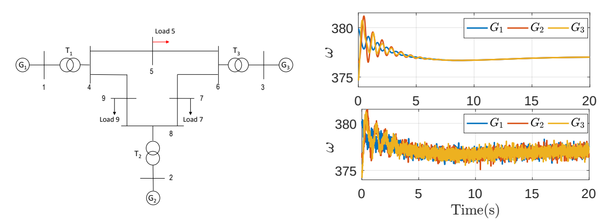

(a) (b)

Fig. 1. (a) IEEE 9 bus system, (b) Post fault frequency measurement for purely deterministic measurement and measurement corrupted with ambient noise of 20 dB

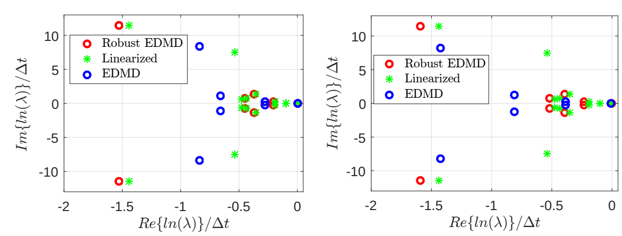

(a) (b)

Fig. 2. System mode identification using Robust EDMD and EDMD (a) For ambient noise of SNR 20 dB (b) For ambient noise of SNR 17 dB

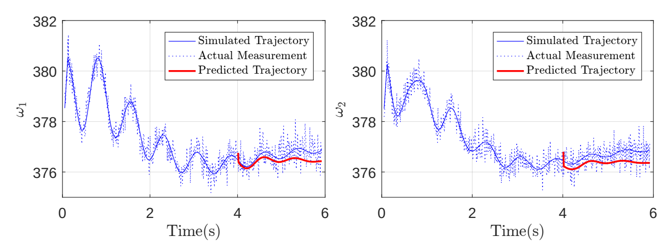

Fig. 3. Generator Angular Speed prediction for noisy measurement

[1]This work is accepted for publication in IEEE PES General Meeting 2019.

ASSESSING AND MITIGATING THE IMPACT OF GEOMAGNETIC DISTURBANCE ON TRANSMISSION SYSTEM RELIABILITY

Rishi Sharma, James D. McCalley

Poster Abstract

GICs induced in the transmission network due to geomagnetic disturbance (GMD) events may lead to large-scale power outages and power system equipment damage. As per the FERC order 830, the two key developmental needs regarding defense against GMD events are; accurate modeling of GICs and GMD impact assessment based on a credible 1-in-100 year GMD benchmark scenario. In this work, we have developed a modeling approach that unifies the 3-D earth conductivity representation and the transmission network representation; this enables computation of the GICs directly using the B-field data. A set of so-called *unified model parameters* are determined using the GIC and B-field data measured during the Dec 2015 GMD event. We also estimate the 1-in-100 year return level of GICs for the transmission network of Iowa, based on extreme value analysis (EVA) of historic GICs calculated using historic (1979-2018) B-field data. The EVA is performed by fitting the historical GIC distribution on a family of distribution models, including power law, lognormal, generalized extreme value and generalized pareto distribution (GPD). The distribution parameter estimation is done by maximizing the log-likelihood function with respect to the extreme historical GIC observations. The 95% confidence interval (CI) of the estimated parameters and the GICs are determined for the 1-in-100 year return level. Finally, the impact assessment for the 1-in-100 year GMD event is done for the transmission network of Iowa, by computing the 1-in-100 year MVAR absorption and voltage drop. Using the 1-in-100 year GICs, the harmonic assessment can be carried out, which in combination with the stability assessment can be used by system planning and operation engineers to allocate appropriate mitigation strategies against GMD event impacts.

Electric Grid Planning with Centralized and Distributed Technologies

Shikha Sharma, Dr. James D. McCalley, Dr. Ian Dobson

Abstract

Today, customers increasingly use the grid as a means to balance their own generation and demand, and want to use grid when their own generation is unavailable. They expect to deliver excess generation back to the grid and to be paid for it - without restrictions on their production. Moreover, they still expect the grid to be there when they need it. To meet these needs, the very architecture of the distribution grid has to change and adopt new technologies, ways of planning, and ways of operating. Consumers are demanding changed business models, and regulators and policy makers are striving to satisfy and even encourage them, sometimes running ahead of the grid's abilities to accommodate the new policies. We consider the costs and trade-offs in planning generation expansion across these scales. To do this, we have developed a multistage expansion planning model to assesses trade-offs between the integration of bulk generation and transmission system expansion with distribution system expansion, considering distributed generation, demand side management, storage, and losses in transmission and distribution network. This approach allows for economic evaluation of distributed and utility-scale generation within the same frame-work, identifying the least-cost investment strategy to address expected demand growth while satisfying EPA CO_2 compliance constraints. The investigation make use of a linear programming model solved with CPLEX to perform long-term, multi-period co-optimized generation, transmission and distribution expansion planning. The method is illustrated on 300 buses WECC system, and results reveals that DSM reduces generation, transmission and distribution infrastructure investments and their utilization. From the study, results reveal that in most of the case investment should be at utility scale, and some mixed of commercial and residential scale and Demand Response and Energy Efficiency are economically attractive.

Modelling and Analysis of a Central Storage Solution for a Municipal Utility to Shave Peak Demand Costs

Authors: S. Siddiqui (ISU), J. McCalley (ISU), R. Amitava (ISU)

Poster Abstract

The penetration of renewable energy resources has been ever increasing in our electric grid, and with the improvements in current technologies and more importantly their cost effectiveness, renewable energy sources combined with a high-capacity, reliable and robust storage system could provide a flexible solution to small municipal utilities, and a path towards reduced energy and demand costs, and in the long run, energy independence. This is especially critical when the utilities have a very uneven, peaking load curve resulting in high peak demand charges. In this work, we review the previous studies on peak shaving strategies, the application of battery storage solutions for such purposes, and the installation and operation of utility scale battery storage systems. We examine a small municipal based utility, and based on the future projections of load and demand charge growth, model a solar PV plus storage solution for the utility. Different scenarios are studied as a resource optimization problem, and their cost benefits and economic merits analyzed. The study concludes with an overall comparison of the feasibility of such storage systems, when compared to the existing system and recommendations are made for our specific case.

Federation based Cyber Physical Security Testbed for Attack Detection Evaluation in Smart Grid

Authors: Vivek Kumar Singh (ISU), Manimaran Govindarasu (ISU), Donald Porschet (ARL), Morris Berman (ARL), Edward Shaffer (ARL)

Posters Abstract

Cyber physical security (CPS) research for smart grid is currently one of the nation's top R&D priorities. The existing vulnerabilities in the legacy grid infrastructure make it particularly susceptible to different cyber attacks. The CPS testbed plays a vital role in developing, evaluating and validating the novel technologies to secure the critical infrastructure like smart grid and to make it attack-resilient. It works as a driving force to accelerate the transition of state-of-the art research works to the industrial products by experimental testing and verification. Most of the published works in the past are based on traditionally isolated CPS testbeds, which do not provide a realistic platform and requires significant investment in money, resources and system modelling. This project aims to go beyond the isolated testbed and develop the sophisticated, federated testbed to provide realistic attack-defense platform by allowing the integration of geographically-dispersed resources in the dynamic cyber-physical environment. Specifically, we present a NASPInet inspired cyber physical federation architecture for CPS security/resiliency experimentation by leveraging the resources available at Iowa State University's Power Cyber (ISU) and the US Army Research Laboratory (ARL). In this work, ISU's testbed is working as multiple substations and the control center is operating at the ISU testbed. We have developed the intelligent anomaly detector to detect possible attacks in the context of wide-area monitoring, protection and control (WAMPAC), which are required to maintain the stability and reliability of smart grid. We also shows the prototype implementation and demonstration, where the control center receives the power system measurements which are further processed by the anomaly detector to identify possible anomalies including cyber attacks in real-time.

Robust Real-Time Modeling of Distribution Systems with Data-Driven Grid-Wise Observability

Authors: Yuxuan Yuan (ISU), Fankun Bu (ISU), Zhaoyu Wang (ISU)

Poster Abstract

Due to financial constraints and cyber-security issues, the number of smart meters (SMs) in many distribution networks is still limited meters compared to the huge size of the network, which hinders the observability of the grid. The lack of knowledge of real-time load behavior inhibits effective monitoring and control of the system. This problem can be further exacerbated due to the common missing sensor data problem. To address these issues, this poster presents a novel data-driven method that determines the daily consumption patterns of customers without smart meters to enhance the observability of distribution systems. This method incorporates data clustering and artificial neural networks for load estimation. A salient advantage of the proposed model compared to previous methods is that it leverages state estimation to ensure the consistency of load inference results with network power flow constraints. Using this method, the daily consumption of unobserved customers is extracted from their monthly billing data. The estimation process takes place at different timescales to improve performance. One challenging issue at the grid-edge is the unavailability of customer context information. Our multi-timescale demand inference model addresses this challenge by only relying on SM data of observed customers and SCADA measurements for model training. The proposed method has been successfully tested and validated using real utility feeders with SM data, and has been able to improve the performance of existing methods in the literature.

Supplementary frequency control of VSC-MTDC for primary frequency support among asynchronous AC systems

Authors: Qian Zhang, James D. McCalley, Venkataramana Ajjarapu

Poster Abstract

Voltage source converter based multi-terminal HVDC (VSC-MTDC) is identified to be a promising technology to facilitate the integration and utilization of large amounts of renewable energy resources in power systems across large geographic areas, and potentially multiple AC systems. One major issue caused by the increased penetration of renewable generation and the decommitment of conventional generators is the decreasing system inertia, which is expected to have adverse impact to the frequency dynamics and pose great challenges to frequency control in power systems. The proposed approach addresses this frequency control challenge by developing supplementary frequency control strategies for the VSC-MTDC to facilitate the exchange of primary frequency reserves among asynchronous AC systems, thus providing frequency support among each other. The proposed frequency control is a droop based global scheme and is shown to be superior to the popularly explored local frequency droop scheme in the literature. The benefits of reduced load shedding, reduced need of total online spinning reserves and reduced impact to the DC voltage profile are illustrated via time domain simulation on an AC-MTDC test system. The VSC-MTDC model and the proposed control are implemented in the commercial grade software PSS/E thus is suitable to study large-scale realistic systems and can be incorporated into the power system planning process at utilities and ISOs.